THE USE OF PARTICULATE MECHANICS IN THE SIMULATION OF STRESS-STRAIN CHARACTERISTICS OF GRANULAR MATERIALS

by

James C. Armstrong
Assistant Research Engineer

and

Wayne A. Dunlap
Assistant Research Engineer

Research Report Number 99-1

Stress Distribution in Granular Masses
Research Project 2-8-65-99

Sponsored by

The Texas Highway Department
In Cooperation with
U. S. Department of Commerce, Bureau of Public Roads

August, 1966

TEXAS TRANSPORTATION INSTITUTE
Texas A&M University
College Station, Texas

ACKNOWLEDGMENTS

The authors gratefully acknowledge the investigations performed by Messrs. Jimmie L. Bratton and F. Lane Lynch, formerly research assistants, Texas Transportation Institute, on the planar arrays of equiradii spheres. Their work formed the basis for much of the information presented in this report.

Mr. Edmund T. Miller contributed valuable suggestions relating to the theoretical approach to the problem. Mr. Frank H. Scrivner also aided in the theoretical part of the research, particularly in the presentation of the theoretical analysis.

Other personnel of the Texas Transportation Institute who contributed to this report include Messrs. Elliot Bray, Jack W. Burke, Chester Michalak, and Tommy L. Snow.

The opinions, findings, and conclusions expressed in this publication are those of the authors and not necessarily those of the Bureau of Public Roads.

TABLE OF CONTENTS

CHAPTER I

INTRODUCTION

General

Among other things, a truly rational flexible pavement design method requires the accurate determination of traffic induced stresses. In flexible pavement design methods, these stresses are often calculated theoretically -- generally using the theory of elasticity applied to continuous media -- and then modified based on experience. Apparently the modifications are necessary because the traffic stresses cannot be accurately calculated in a layered system composed of soils and granular materials.

Tests conducted at Texas A&M University and a limited number of reports by others (1, 2, 3)[1], suggest that granular materials of the kind used in road construction are not linearly elastic (i.e., strains are not linear functions of the stresses), especially when subjected to rapid loading conditions. This indicates that classical elasticity methods for calculating stresses in these materials need revision.

Deformation Hypothesis for Granular Materials

As a result of tests conducted on Project 2-8-62-27, "Distribution of Stresses in Layered Systems Composed of Granular Materials," a new deformation hypothesis for granular materials analogous to Hooke's Law for metals was proposed (10). This hypothesis is expressed mathematically below:

$$\epsilon_z = \frac{\sigma_z - K_1 \ (\sigma_r + \sigma_\theta)}{K_2 + K_3 \ (\sigma_r + \sigma_\theta)} \qquad \text{Equation (1.1)}$$

where: ϵ_z = Strain in the vertical direction

σ_z = Stress in the vertical direction

---

1. Refers to References Cited.

σ_r, σ_θ = Radical and tangential stresses, respectively

K_1, K_2, K_3 = constants which must be determined experimentally for each material.

Two other equations can be written for ϵ_r and ϵ_θ by a cyclical interchange of the subscripts in Equation 1.1. Figure 1.1 illustrates graphically the meaning of the parameters K_z and K_s.

Basically, the new hypothesis means this: the modulus of deformation of granular materials, instead of being constant as assumed in elasticity theory, varies when the stresses vary. Thus, within a pavement subjected to a moving load, the modulus varies from instant to instant and from point to point; and in addition, its value depends upon the direction in which it is measured.

Based on this hypothesis, a set of six partial nonlinear differential equations were developed for describing the stresses and displacements in a layered system of granular materials. Unfortunately, attempts to solve the equations to obtain stresses induced by traffic on a flexible pavement have been unsuccessful owing to the complexity of the mathematics.

The initial deformation hypothesis was based on observations from static triaxial tests and from rapid repetitive triaxial loading tests. A linear stress-strain relationship was used in developing the hypothesis. With the advent of more sophisticated recording equipment, it was observed that the stress-strain curves actually had a reverse S-shape under rapid repetitive loading. This does not completely invalidate the original deformation hypothesis because tests have shown that the stress-strain characteristics are still greatly dependent on the state of stress existing in the material regardless of the loading rate. However, the fact that the stress-strain curves under rapid repetitive loading were curvilinear and that the deformation equations could not be readily solved, led a search for new methods of describing the deformation characteristics of granular materials.

Particulate Nature of Granular Materials

A granular soil mass is composed of a number of discrete particles which are relatively nonplastic; it may or may not contain water in its voids. By way of an analogy, suppose a steel cylinder, considered to be closely elastic in its behavior, was machined into spheres and the mass of spheres was then stressed. The particulate mass need not exhibit the same modulus of elasticity and Poisson's ratio as the orginal cylinder. In fact, there is no reason to believe that the two elastic constants would even exist for the mass although the separate spheres would still retain the original constants.

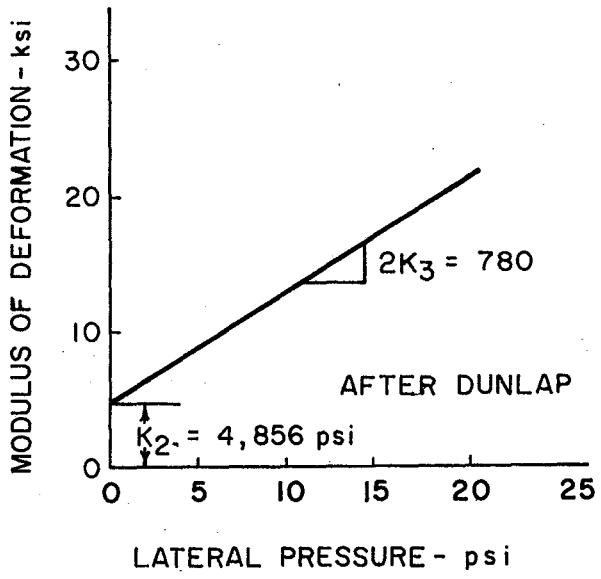

Figure 1.1 Experimental modulus of deformation versus lateral pressure for Texas triaxial material.

Investigations in the relatively new field of particulate mechanics have shown considerable promise in explaining the stress-strain characteristics of masses of discrete particles and the theory may be capable of describing the stress-strain behavior of granular soils.

Particulate mechanics considers the forces and deformations at contact points between individual particles. The deformation equations can be developed for a given array or mass of particles provided the geometry of the array is known. Using the deformation equations, the strain within the array can be calculated if the particle parameters (coefficient of friction between particles, Poisson's ratio, and modulus of elasticity of the particles) are known.

Objections of the Research Program

The objectives of this research were:

A) To develop expressions relating stress and strain for various arrays of elastic equiradii spheres.

B) To compute the stress-strain curves of the arrays using the equations developed in A) above for a range of parameters (elastic constants and coefficient of friction), encompassing those which might be expected for actual granular materials.

C) To compare the computed or theoretical stress-strain curves to the curves of an actual soil subjected to rapid repetitive loading.

For this program, three different arrays were analyzed. They were a) a loose planar array (Figure 1.2) b) a dense planar array (Figure 1.3) and c) a loose three dimensional array (Figure 1.4). The arrays were examined for both triaxial and one dimensional compression. It was believed that if the theoretical and actual curves agreed closely, then the equations could be expanded to a semi-infinite mass composed of layers of granular materials, and by applying appropriate boundary conditions, stresses and displacements in the mass could be calculated.

Principal Conclusions

While this exploratory study did not demonstrate a generally acceptable agreement between particulate theory and experimental results, it did show that:

1. The theoretical stress-strain curves for the three arrays exhibited a tendency for the secant modulus to increase with increase in lateral pressure. (This tendency, so frequently observed in the testing of granular

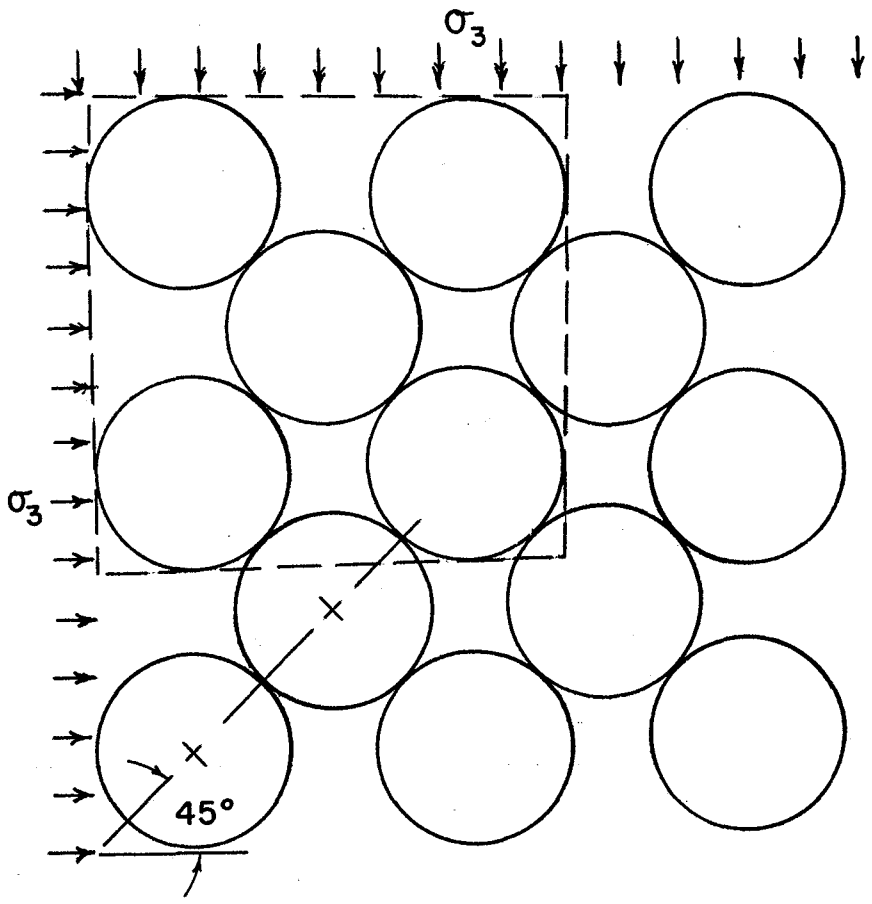

Figure 1.2 Geometry of the loose planar array showing diagonal angle 45 degrees (Bratton). The dashed portion indicates a unit cell.

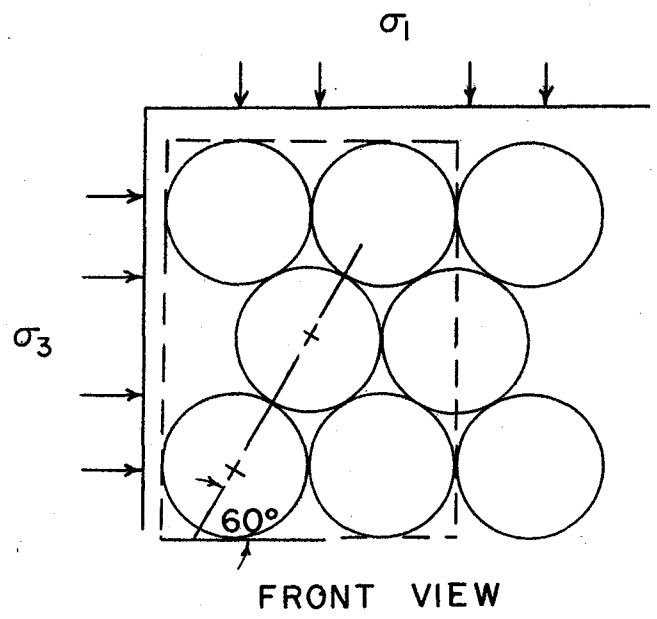

Figure 1.3 The dense packed planar array acted on by external stresses σ_1 and σ_3. Note 60^o diagonal angles. The dashed portion indicates a unit cell.

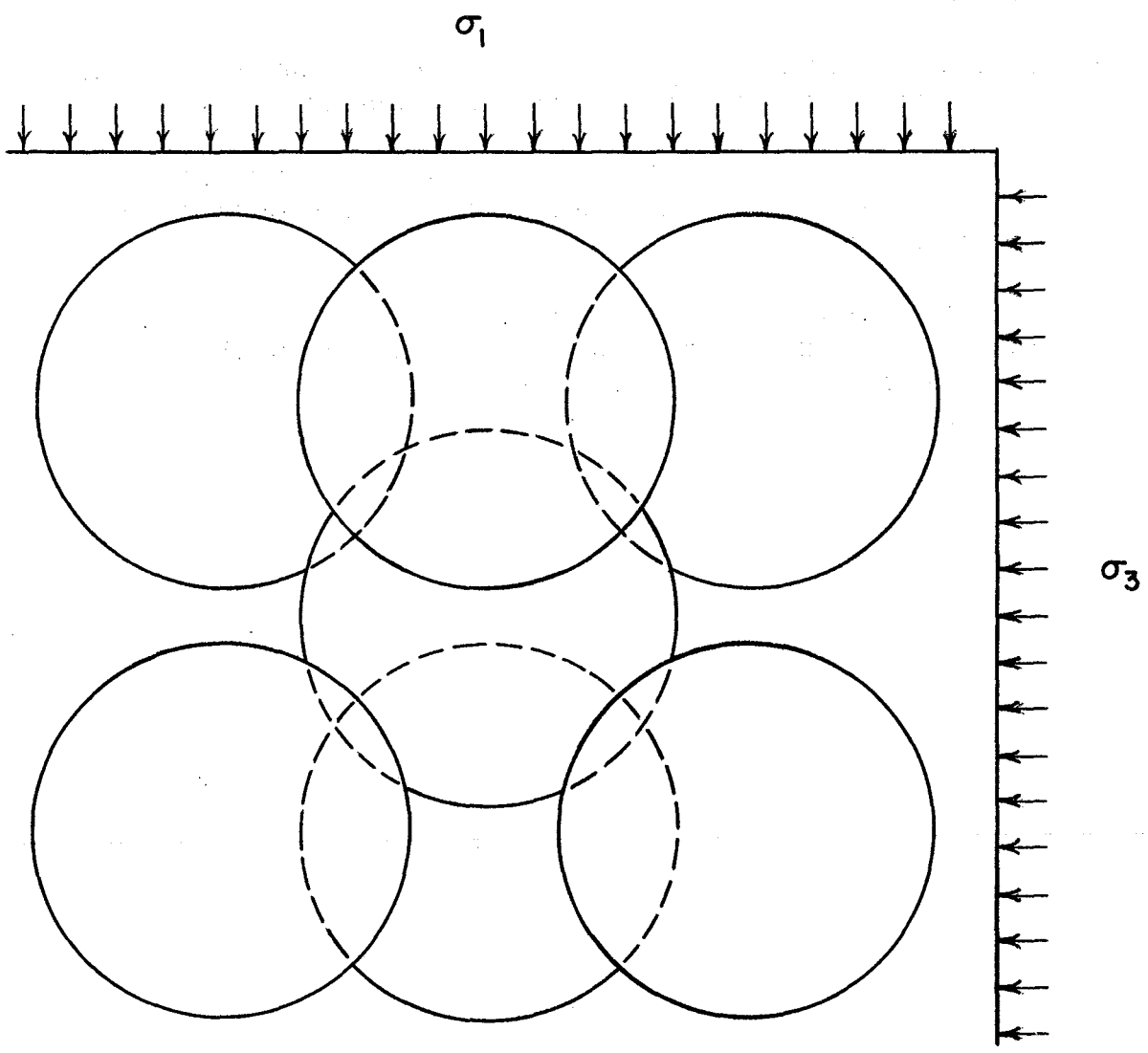

Figure 1.4 The unit cell of the three dimensional loose array showing stresses acting.

materials, cannot be explained by the usual assumption of an elastic, continuous medium).

2. For two of the arrays studied the computed stress-strain curves exhibited the typical reverse-S shape observed in triaxial tests conducted at constant lateral pressure.

3. The study, which was limited to arrays of equiradii spheres and to stresses below those capable of producing sliding, also indicated that

before acceptable agreement between theory and experiment can be expected, the theory must be extended to include some or all of the following features:

(a) Arrays of spheres of varying diameter
(b) Arrays that include particle shapes other than spherical
(c) Slide and counter-slide between particles
(d) Pore pressures.

CHAPTER II

REVIEW OF LITERATURE

Research on Equiradii Spheres

Owing to the complexity of the mathematics, the use of particulate mechanics in soil simulation studies has been confined to the investigation of equiradii elastic spheres. When the spheres are subjected to normal and tangential forces, they deform elastically at their points of contact until the tangential forces become large enough to overcome Coulomb's friction. After which the spheres slide past one another until they reach more favorable positions to resist the applied forces.

The mathematical study of the effects produced by mutual compression of elastic bodies was initiated by Hertz (4), who examined the case in which bodies are acted on by forces normal to their contact surfaces. According to Hertz, the radius, a, of the contact area between two spheres acted on by a force normal to the contact surface is:

$$a = [\, 3 (1 - \mu^2) Nr/4E \,]^{1/3} \qquad \text{Equation (2.1)}$$

where: E = the modulus of elasticity

r = the radius of the sphere

μ = Poisson's ratio

N = normal force.

The vertical displacement of the sphere centers due to the normal force is [see Figures 2.1 (a) and 2.1 (b)]:

$$\alpha = 2[\, 3 (1 - \mu^2) N/4E \,]^{2/3} r^{-1/3} = 2a^2/r \qquad \text{Equation (2.2)}$$

Later, Cataneo (5) and Mindlin (6, 7) extended the contact theory by including the effect of tangential forces acting on the spheres [see Figure 2.1 (c)]. When a monotonically increasing tangential force, T, is applied to a contact surface acted on by a constant normal force, slip[1] is initiated on the circumference of the surface of

---

[1] At this point it is well to distinguish between slip and slide. Slip is relative movement between two contiguous points on the contact surface, while slide is gross movement over the entire surface of contact.

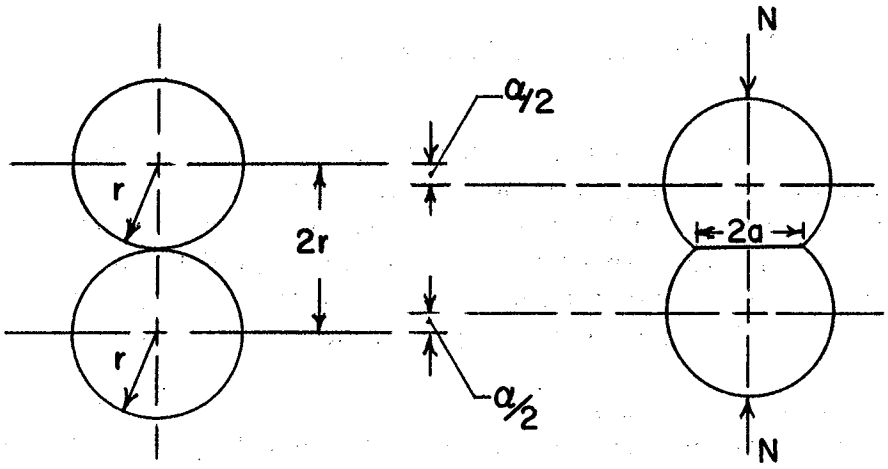

TWO SPHERES IN CONTACT
UNDER ZERO STRESS
(a)

TWO SPHERES COMPRESSED
UNDER NORMAL FORCE
(b)

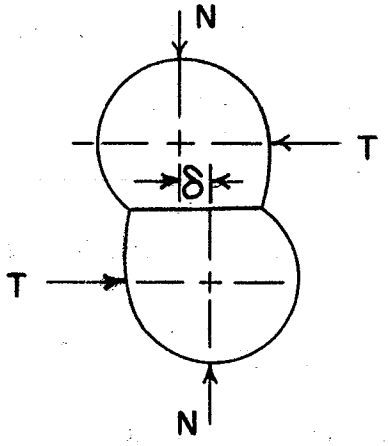

TWO SPHERES SUBJECTED TO BOTH
NORMAL AND TANGENTIAL FORCES
(c)

Figure 2.1 Spheres under various loading condition.

contact and progresses radially inward. The portion of the surface of contact on which slip occurs lies between the outer annulus of radius, a, and inner annulus of radius, c, where:

$$c = a\,(1 - T/FN)^{1/3} \qquad \text{Equation (2.3)}$$

where: N = the normal force

T = the tangential force

F = the coefficient of friction.

From Equation (2.3) it may be noted that as the value of the tangential force approaches the value of FN (static friction force), c approaches zero and slip progresses over the whole contact surface. Figure 2.2 shows the distribution of tangential stresses, T, on the contact area during loading. When c = O, rigid body sliding occurs between the particles and the geometry of the array changes.

The tangential displacement, δ, resulting from the tangential and normal force is:

$$\delta = [3\,(2 - \mu)\,FN/8Ga\,[1 - (1 - T/FN)^{2/3}] \qquad \text{Equation (2.4)}$$

where: $G = E/2\,(1 + \mu)$ = the shear modulus.

Whitman (8) first utilized the principles and equations of particulate mechanics to develop the deformation characteristics of a loose packed two dimensional array of equiradii spheres subjected to one dimensional compression. The determination of the stress-strain relationships of this array was simplified by 45^{o} symmetry of the spheres. Whitman indicated that the resulting stress-strain curves were nonlinear and had a reverse S-shape configuration. In subsequent research, Whitman et al. (3) noted that dry sand tested under conditions of one dimensional compression also displayed reverse S-shape stress-strain curves (see Figure 2.3). This phenomenon was explained as follows:

> As the load is initially applied, deformations in the sand grains occur resulting in a steep stress-strain curve concave to the strain axis.
>
> The load is further increased causing the grains to start sliding relative to each other. At this stage the stress-strain curve becomes more concave to the strain axis indicating an increase in strain rate.
>
> As the particles are rearranged into a denser state, sliding becomes more difficult, the strain rate decreases resulting in a stress-strain curve concave to the stress axis.

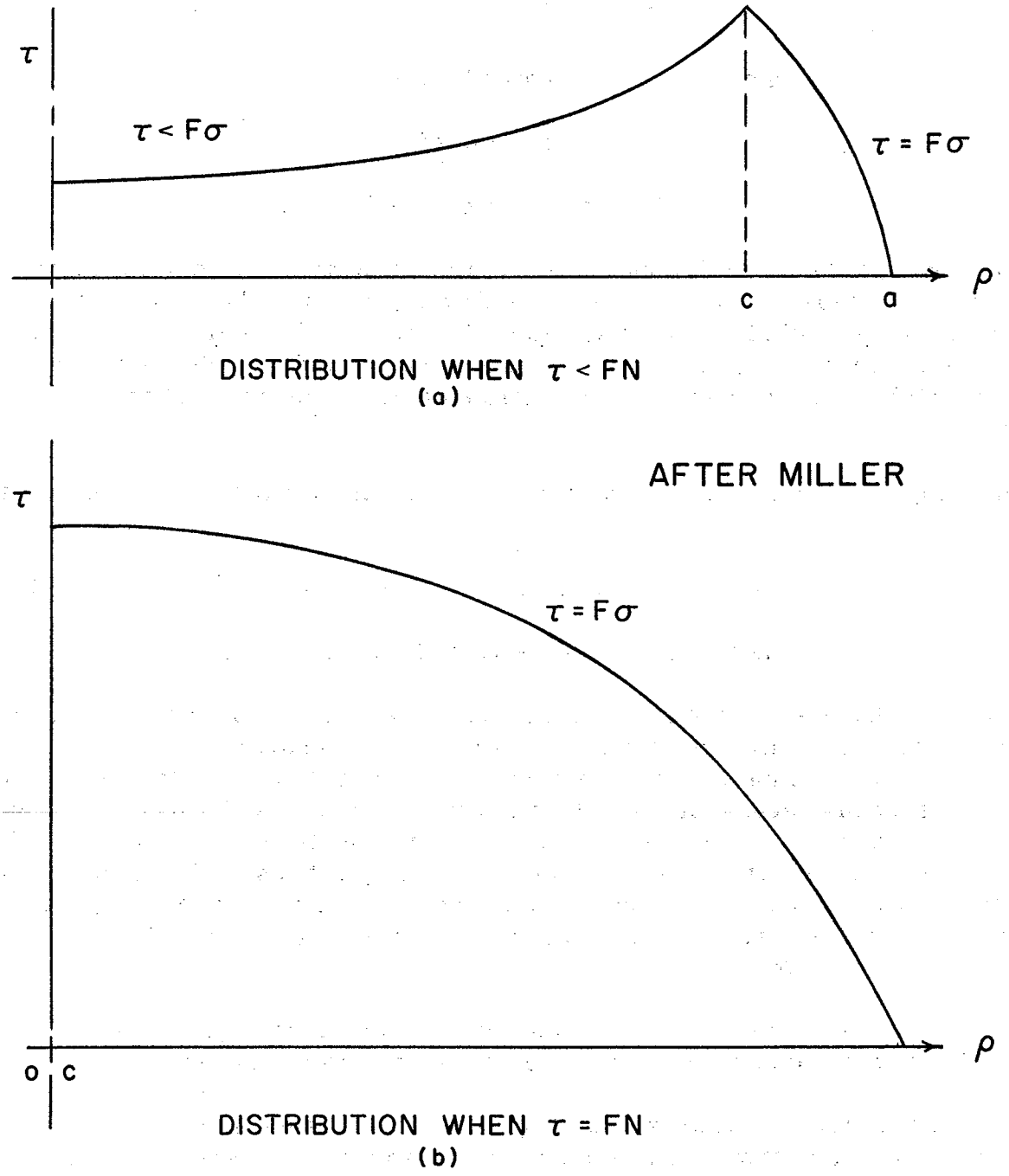

Figure 2.2 Distribution of tangential stresses during loading.

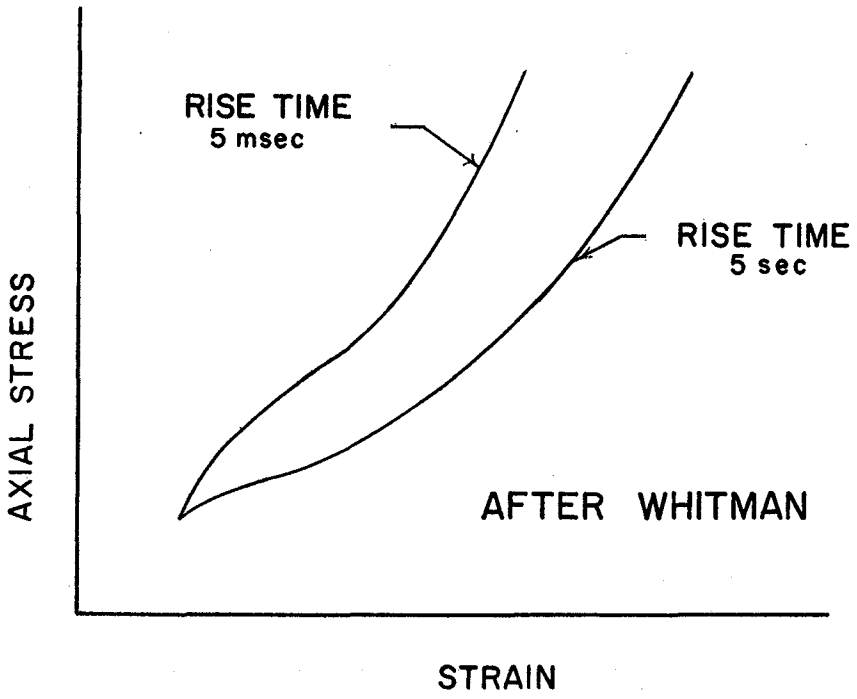

Figure 2.3 Typical observed stress-strain behavior for dry sand.

Miller at M.I.T. (9) examined the loose planar array[2] (Figure 2.1) subjected to both triaxial and one dimensional compression. He indicated that the theoretical curves differed somewhat from those of actual soils, and concluded this was probably due to the fact that a) the soil particles were not spherical, b) the packing was not regular, c) the particles were not equiradii, and d) the soil array was three dimensional which could tend to accentuate small differences.

There has been only a limited amount of research conducted on three dimensional systems of spheres. One investigator, Deresiewicz (12), derived the equations to explain the deformation characteristics of a simple cubic array of equiradii spheres (Figure 2.4); however, his orientation consisted of a series of planar arrays stacked side by side which has no apparent advantage over a planar array. He did not compare his results with experimental data from real soils.

Hendron (13) investigated a face centered array[3] of equiradii spheres subjected to one dimensional compression. He stated that this array closely approximated the energy absorption loss exhibited in actual soils. Hendron tested four different sands under one dimensional compression using high pressures and found that:

A) The secant modulus increased as the relative density increased.

B) The secant modulus increased as the pressure increased up to a point. Beyond this, the higher pressures significantly crushed the grains causing the stress-strain curve to become concave downward.

C) The constrained tangent modulus varied by a factor of eight or nine for different sands.

It was concluded that factors such as angularity and grain size distribution significantly influenced the stress-strain behavior over a wide range of pressures. This conclusion is well taken: since angularity and grain size distribution play a major role in particle interlocking, they evidently have a definite effect on the behavior of the stress-strain curves.

Hendron's results did not exhibit reverse S-shape stress-strain curves (see Figures 2.5 through 2.8). This was probably due to the rather slow rates of strain that he used in his testing program (0.01 and 0.005 inches per minute).

---

[2] A two dimensional array and a planar array are synonymous. Such an array is only one sphere-diameter in thickness.

[3] A face centered array is a three dimensional dense array.

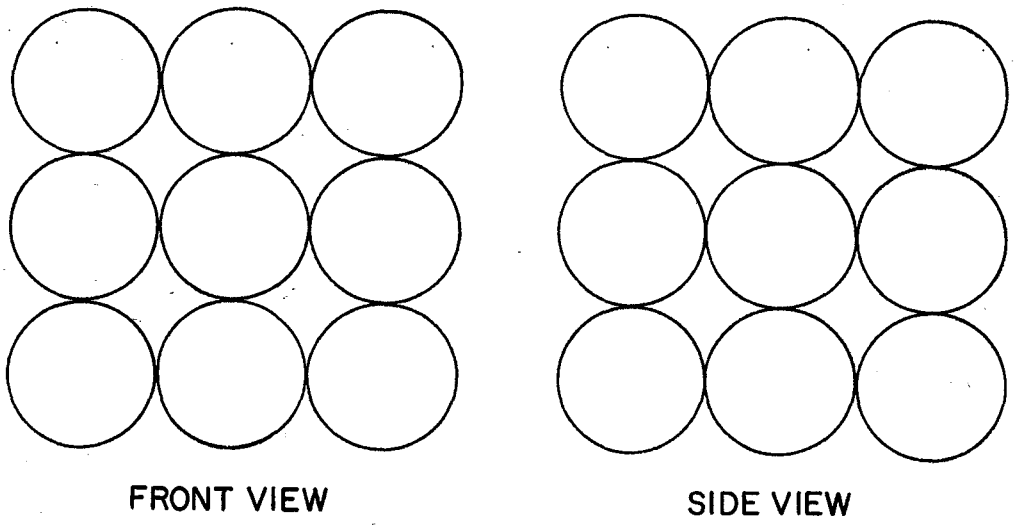

Figure 2.4 The front and side views of the simple cubic array.

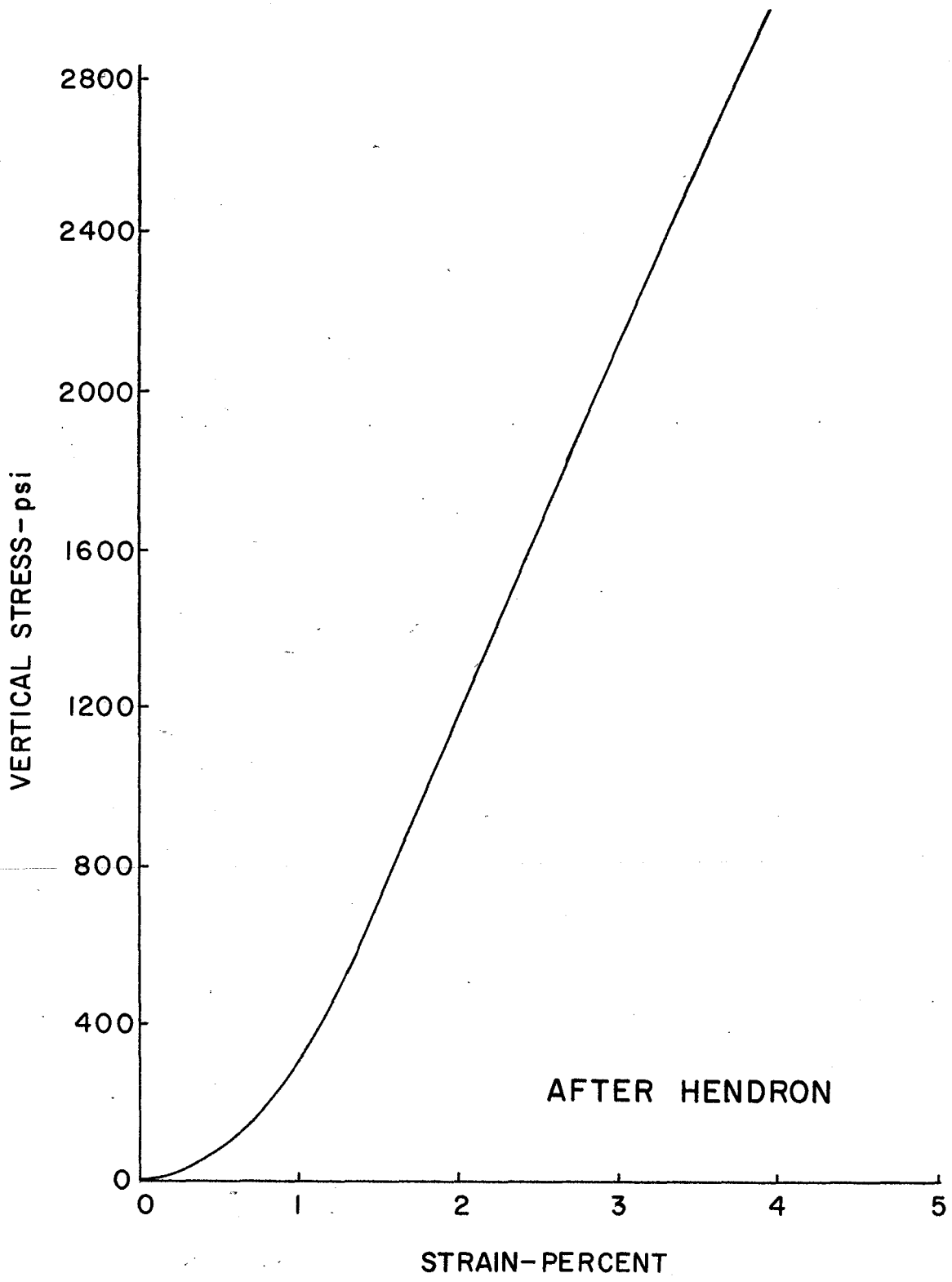

Figure 2.5 Stress-strain curve for Sangamon River sand in one dimensional compression.

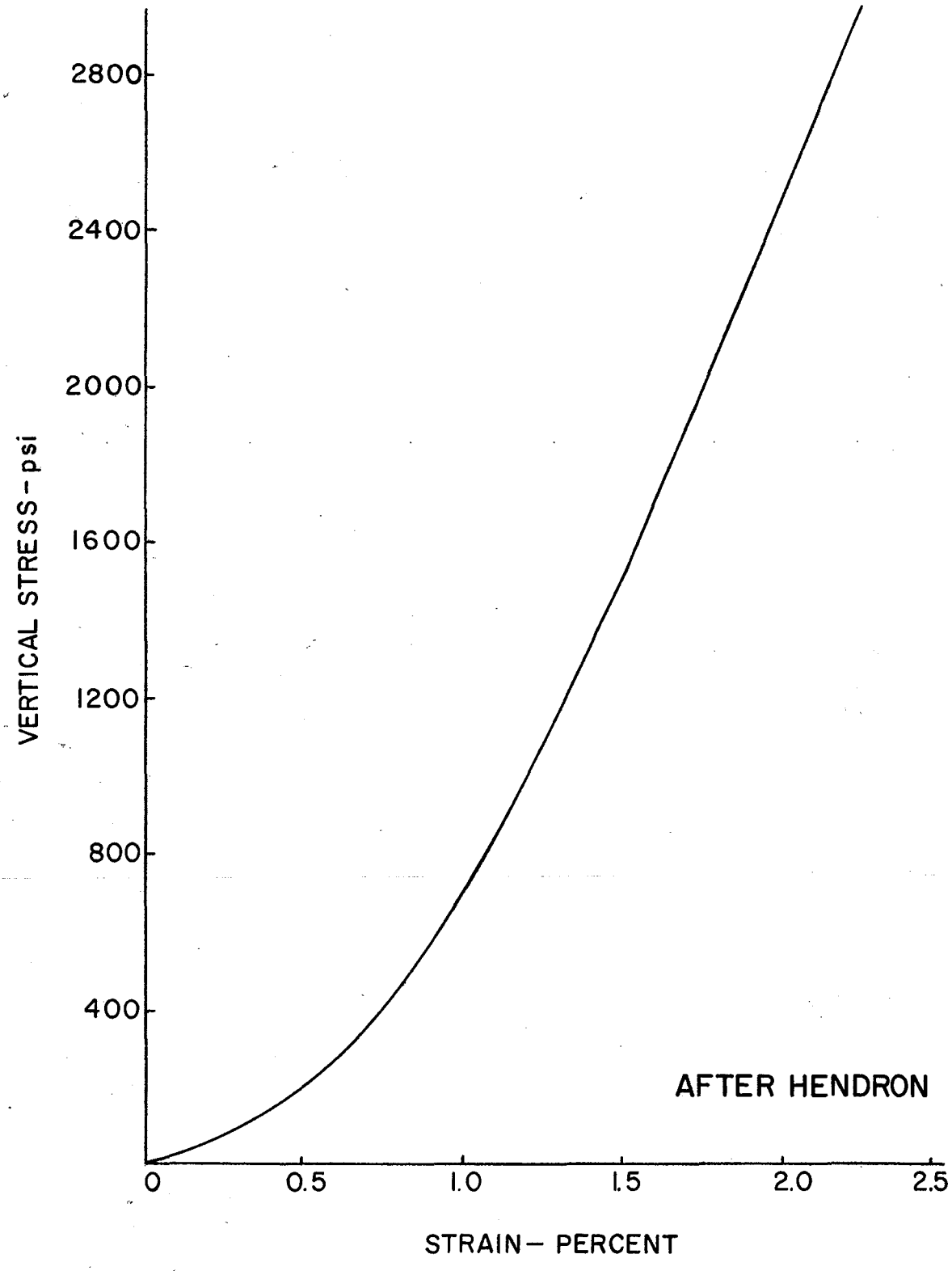

Figure 2.6 Stress-strain curve for Minnesota sand in one dimensional compression.

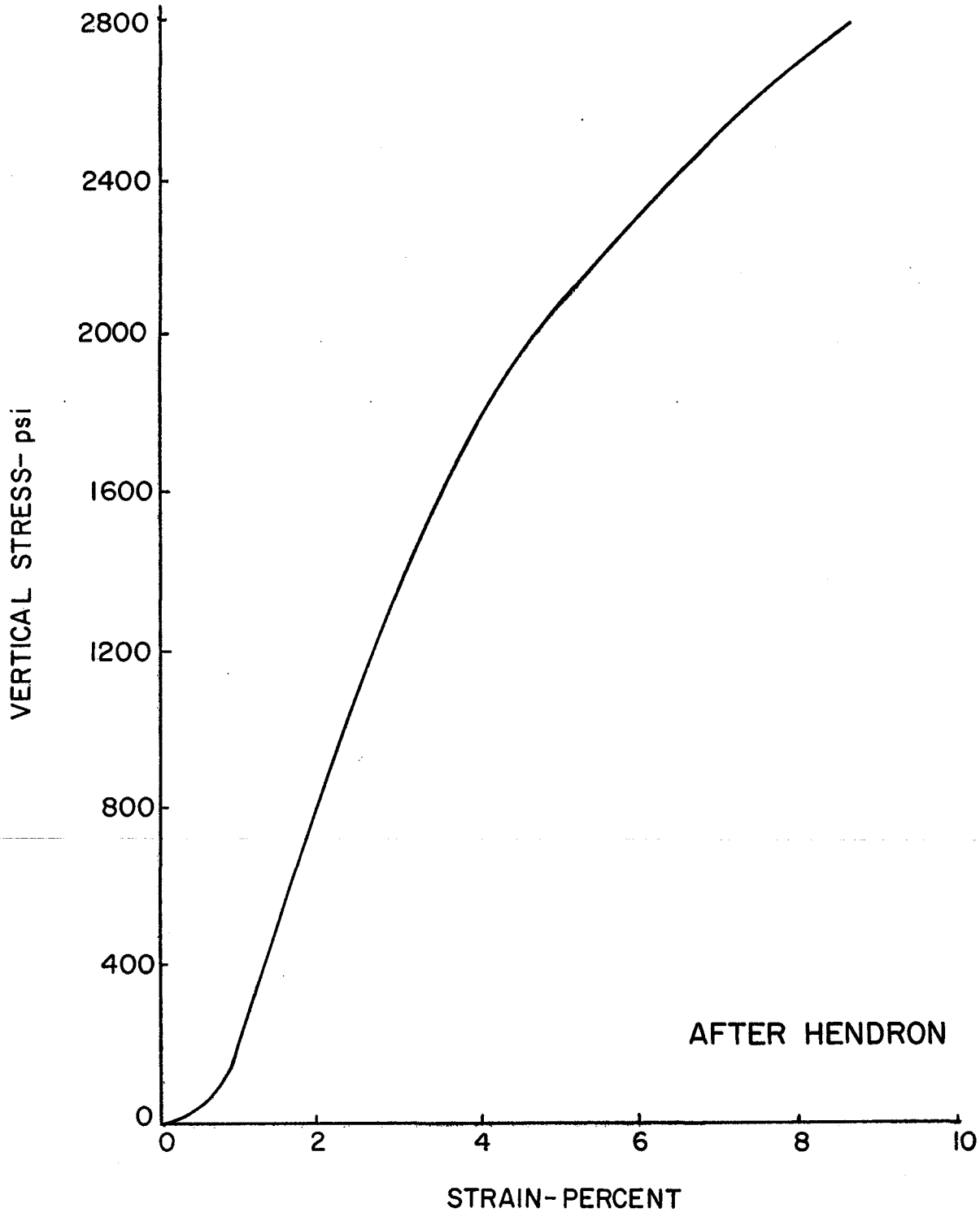

Figure 2.7 Stress-strain curve for Pennsylvania sand in one dimensional compression.

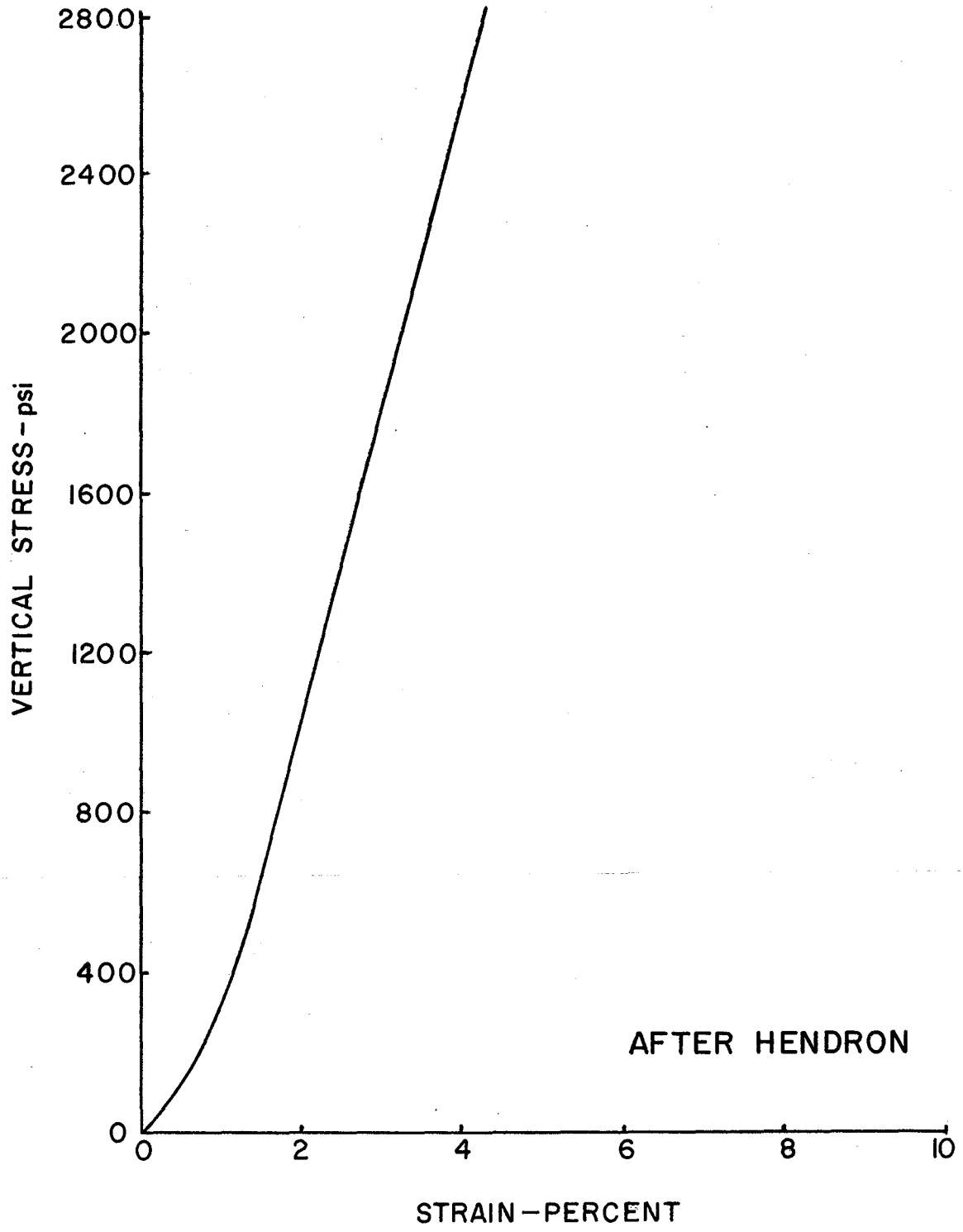

Figure 2.8 Stress-strain curve for Wabash River sand in one dimensional compression.

Contact Points Between Particles

One of the major contributing factors of stress-deformation relationships is that of the area of contact between mineral grains. Research has indicated that the theoretical computations of this area may be in error.

Bowden and Tabor (33) found that the real area of contact between two bodies acted on by normal force was much smaller than the apparent or gross area, and that adhesion takes place between adjacent surfaces at contact between irregularities. To cause slide between the bodies in contact, sufficient tangential force must be applied to shear essentially solid material at the real contact points. The total tangential force is then proportional to the area of real contact, and since this area is a function of the applied load, the tangential force is also a function of the applied load.

Scott (34) indicates that when the interface between the two particles is contaminated by a film of foreign material, the shear strength of the film plays a definite part in determining the frictional coeffieient between the two surfaces. He adds that the contact film is absent only in special tests where extreme care is used to prevent its presence.

Influence of Variable Confining Pressure on Stress-Strain Characteristics

In many cases standard triaxial compression tests do not duplicate field stress conditions. For example, in a flexible pavement the radial, tangential, and vertical stresses at a point change simultaneously as a vehicle approaches, whereas in a triaxial test the confining pressure generally remains constant as the vertical stress is increased.

In the development of the deformation hypothesis described in Chapter I, the condition of a variable confining pressure was considered. It was assumed that the radial stress varied linearly with the vertical stress such that

$$m = \sigma_r / \sigma_z = \text{constant} \qquad \text{Equation (2.5)}$$

If Equation (2.5) is combined with Equation (1.1), it results in:

$$\epsilon_z = \frac{(1 - 2K_1 m)\,\sigma_z}{K_2 + 2K_3\, m\, \sigma_z} \qquad \text{Equation (2.6)}$$

By means of Equation (2.6), a hypothetical case was solved using typical values for K_1, K_2 and K_3. Figure 2.9 presents these results and compares them to the strict elastic case for which K_3 is assumed to be zero, K_1 is Poisson's ratio and K_2 is the modulus of elasticity.

O'Brien (20) subsequently performed variable confining pressure tests to examine the validity of Equation 2.6. He had considerable difficulty with equipment and had to reduce his rate of loading to 0.005 inches per minute which is rather unrealistic compared to field conditions. Based on his findings, he concluded that laboratory tested samples of granular materials can be made to duplicate field stress-strain curves. He also noted that the proposed deformation hypothesis -- Equation (2.6) -- appeared to be correct.

O'Brien indicated a need for refinement in equipment and techniques before accurate experimental results could be obtained. He especially noted that a better method for recording load and deformation was needed.

Effect of Rapid Loading

It has been observed that the rate or time of loading has a definite effect on the shearing strength and modulus of deformation of soils. Casagrande and Shannon (31) found that if specimens of soil and soft rock are subjected to a single rapidly applied load, their ultimate strengths are significantly greater than those observed for specimens using loading rates common in conventional testing procedures. Furthermore, rapid loading produces a definite increase in the modulus of deformation.

Whiteman and Healy (32) concluded that the strengths of dry sands and very dense saturated sands are not time dependent, i.e., the compressive strengths of the sands they tested were little affected by changes in the loading time. However, they found that the compressive strengths of loose saturated sands were dependent upon failure time. For loose saturated Ottawa sand, the compressive strength increased by 40 percent between failure times of five seconds and 0.025 second. This increase amounted to about 100 percent for Camp Cook sand when the failure time was reduced from three minutes to 0.2 second. Whitman and Healy pointed out, however, that the observed increases could have been affected by the laboratory apparatus and that the same strength changes may not develop in natural deposits of these same materials.

Whitman's conclusions at first appear to contradict Casagrande's. However, Casagrande worked on the basis of total stresses while Whitman based his findings on effective stresses. If Casagrande had measured pore pressures, his conclusions may have been similar to Whitman's.

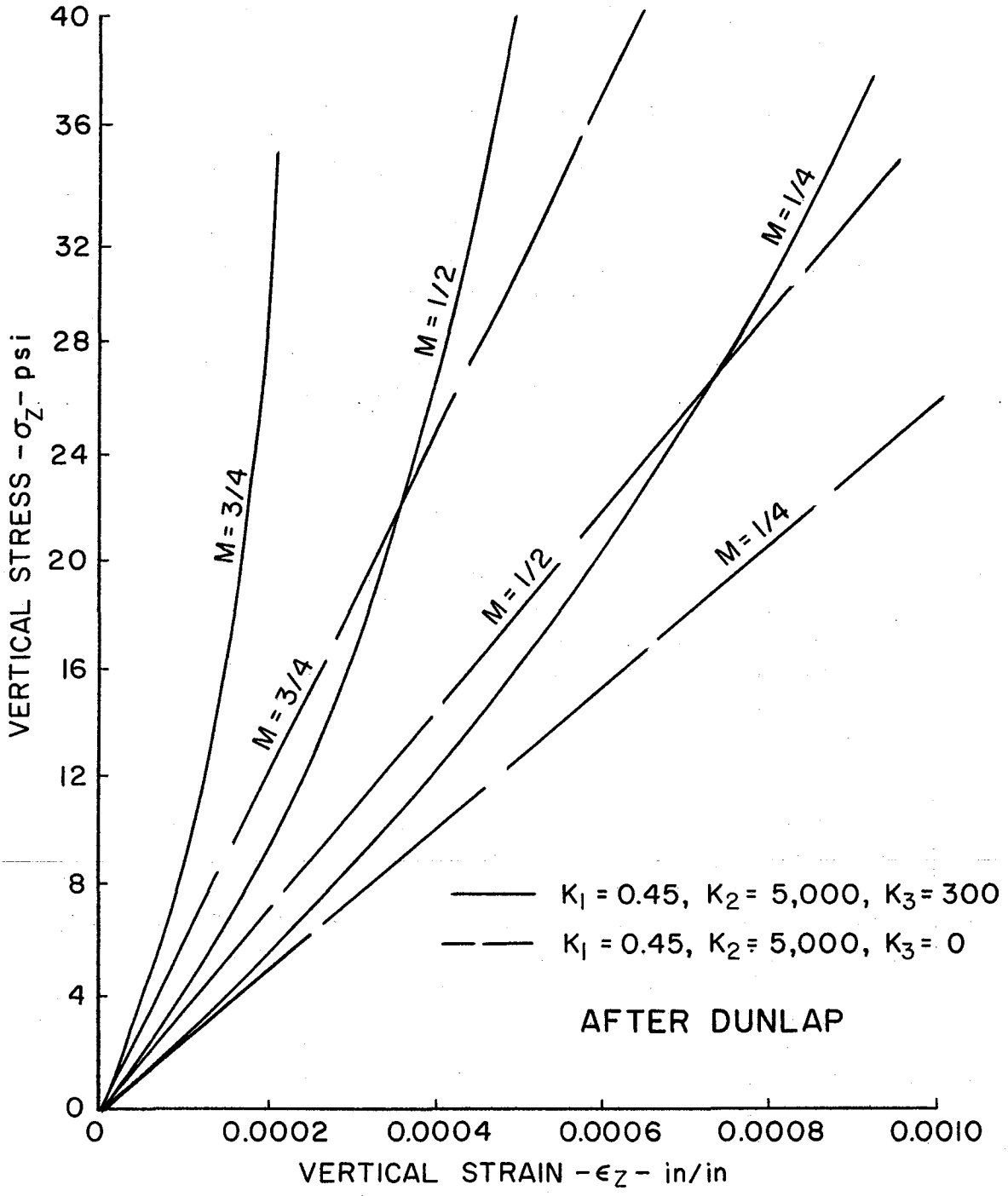

Figure 2.9 Hypothetical stress-strain conditions of variable confining pressure test. Solid lines are for the proposed deformation law while the dashed lines are for the elastic case.

Wilson and Sibley (26) indicated that the shape of the stress-strain curve is greatly influenced by the rate at which the load is applied. They found that generally the stress-strain curves from dynamic confined compression tests are reversed S-shaped, starting with a high modulus for axial loads slightly above the hydrostatic pressure, then decreasing with increased axial stress until some point well beyond the confining pressure, and then increasing again with further increase in the axial stress.

They noted that for most materials the constrained modulus of deformation increased as the loading rate increased. However, it was also mentioned that some completely saturated materials and some weakly cemented sands appeared to have moduli which were more or less independent of the magnitude of the stress increase.

Summary of Previous Research

It has been observed that the deformation characteristics of actual soils differ markedly from those of the elastic materials usually assumed in pavement design methods. Particulate mechanics, which considers forces and deformation between individual particles, may come closer than other methods to simulating stress-strain relationships, particularly of granular soils.

At present, particulate theory is restricted to equiradii spheres owing to the mathematical complexity involved when dealing with other shapes or with spheres of unequal radii. And there are other complicating factors which must be considered. The heterogeneous nature of real soils causes the number of contacts between particles to vary within the materials, and the surfaces of the contacts are contaminated with five grained materials and moisture. In addition, it is difficult to conceive of a real soil in which the coefficient of friction, Poisson's ratio and modulus of elasticity would remain constant from particle to particle.

Nevertheless, the little amount of information available on particulate mechanics theory indicates that it has potential and should be investigated in greater detail. If it does nothing else, it should serve to delineate those particle parameters which have the greatest influence on stress-strain behavior of granular materials.

Since arrays of particles in real soils bear little resemeblance to the simple arrays which can be presently investigated with particulate mechanics theory, it appears that the best approach is to select a few different arrays and compare their stress-strain characteristics to those of real soils. In addition, the particle parameters should be investigated for each array. Those parameter values which result in the best fit to actual stress-strain curves may not be the actual values for the particles, but they should represent average or perhaps synthetic values suitable for design applications.

CHAPTER III

THEORETICAL DEVELOPMENT

Loose Planar Array

Figure 3.1 is a front and side view of the loose planar array of equiradii spheres showing the geometry. The area on which the vertical σ_1, and lateral, σ_3, stresses are assumed to act is $4\sqrt{2}r^2$. Forces F_1 and F_3 are the vertical lateral reactions due to the loads imposed by the respective stresses. Therefore:

$$F_1 = 2\sqrt{2}\, r^2 \sigma_1 \qquad \text{Equation (3.1)}$$

$$F_3 = 2\sqrt{2}\, r^2 \sigma_3 \qquad \text{Equation (3.2)}$$

where: r = the radius of the spheres.

The normal, N, and tangential, T, components of these forces are:

$$N = 4r^2 (\sigma_1 + \sigma_3)/2 \qquad \text{Equation (3.3)}$$

$$T = 4r^2 (\sigma_1 + \sigma_3)/2 \qquad \text{Equation (3.4).}$$

The normal and tangential displacements, α and δ, can be calculated as indicated in Equation (2.2) and Equation (2.4), respectively. However, if T = FN, sliding takes place between particles and the corresponding equation for δ is:

$$\delta = \left[{}^{3}(2-\mu)\, FN/_{8Ga} \right] + S_L \qquad \text{Equation (3.5)}$$

where: S_L = displacement by sliding.

Equations 2.4 and 3.5 explain the tangential displacement during the first load cycle. When the array is unloaded the tangential displacement, δu, can be calculated from the equation given below:

$$\delta u = \frac{3(2-\mu)\, FN}{8Ga} \left\{ 2 \left[1 - \frac{T^* - T}{2FN} + N^* - N \right]^{2/3} - \left(1 - \frac{T^*}{FN^*}\right)^{2/3} \left(\frac{N^*}{N}\right)^{2/3} - 1 \right\} + S_L$$

Equation (3.6)

where: T* = Maximum tangential force during loading,

N* = Maximum normal force during loading.

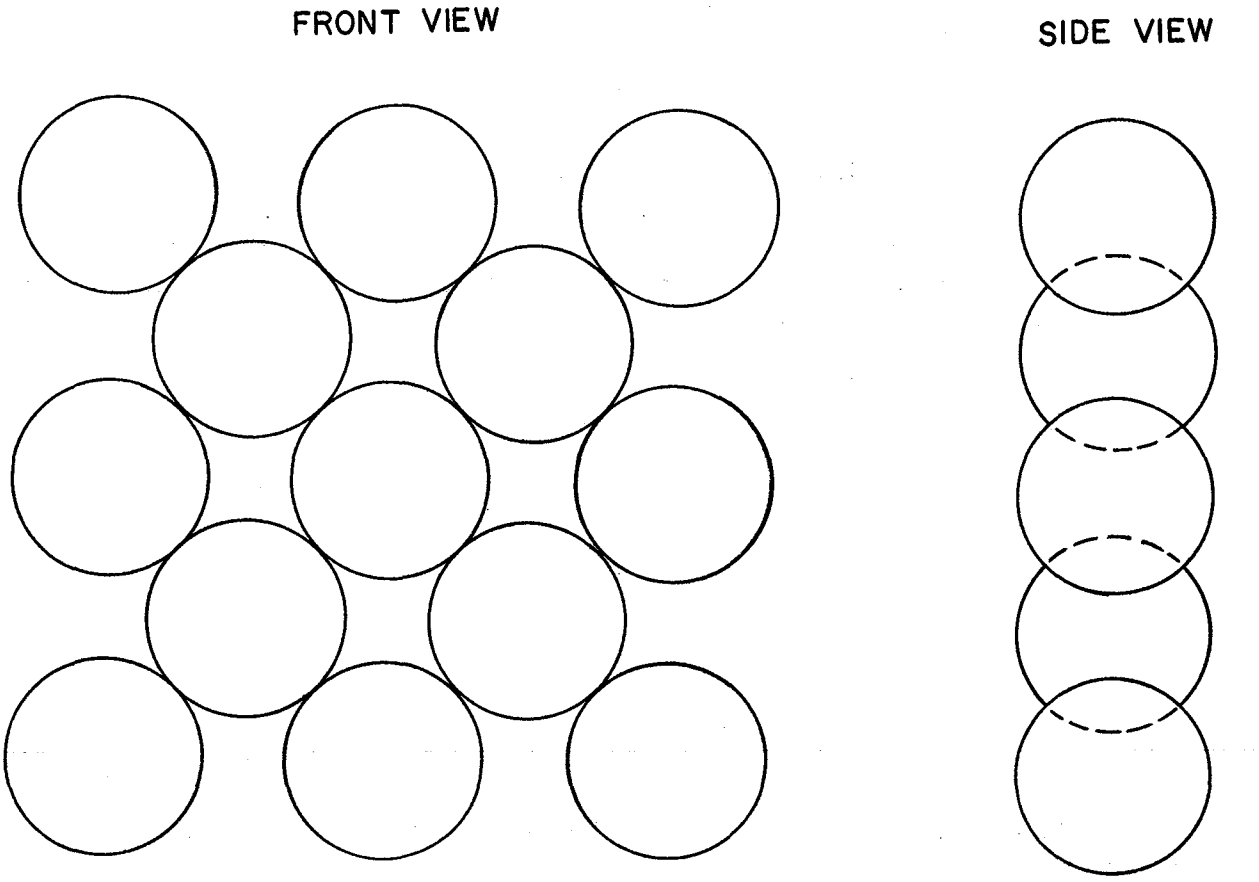

Figure 3.1 The loose planar array of elastic equiradii spheres.

The equation for the tangential displacement upon reloading, δr, has the following form:

$$\delta r = \frac{3(2-\mu)F}{8G}\left\{\frac{N_L}{a}\left[2\left(1-\frac{T^*-T}{2FN_L}\left(\frac{N^*N_L}{2N_L}\right)^{2/3}-\left(1-\frac{T^*}{FN^*}\right)^{2/3}\left(\frac{N^*}{N}\right)^{2/3}\right.\right.\right.$$
$$\left.\left.\left.+2\left(1-\frac{T-T_L}{2FN_L}+\frac{N-N_L}{2N_L}\right)^{2/3}+1\right]+\frac{N}{a}\left[1-\left(\frac{N_L}{N}\right)^{2/3}\right]\right\}+Su$$

Equation (3.7)

where: N_L = lowest normal force

T_L = lowest tangential force

Su = slide developed during unloading.

From the preceding equations, it is possible to describe the strain for a given set of stresses provided the geometry of the array is known. For the loose planar array the following equations can be developed:

$$\epsilon_1 = \frac{1}{2r}(\alpha+\delta) \qquad \text{Equation (3.8)}$$

$$\epsilon_3 = \frac{1}{2r}(\alpha+\delta) \qquad \text{Equation (3.9)}$$

where: ϵ_1 = vertical strain

$\sim\epsilon_3$ = lateral strain.

With these equations both the vertical and lateral strain can be calculated for any given system of stresses if the boundary conditions are known.

Dense Planar Array

Figure 3.2 is a front and side view of the dense planar array showing the geometry. The surface acted on by the vertical and lateral stresses are $4r^2$ and $4\sqrt{3}r^2$, respectively. The contact force $F_1 = 2r^2\sigma_1$. Since the dense array also has two contact points with spheres at its equator (see Figure 3.2), there is an additional force F_o; thus the system is indeterminate. However, if the assumption $F_o = 0$[1] is made then the system becomes determinate and $F_3 = 2\sqrt{3}r^2\sigma_3$. The normal and tangential components of these contact forces are:

$$N = \sqrt{3}r^2(\sigma_1+\sigma_3) \qquad \text{Equation (3.10)}$$

$$T = r^2(\sigma_1-3\sigma_3) \qquad \text{Equation (3.11)}.$$

[1]A basis for the assumption $F_o = 0$ is contained in Appendix A.

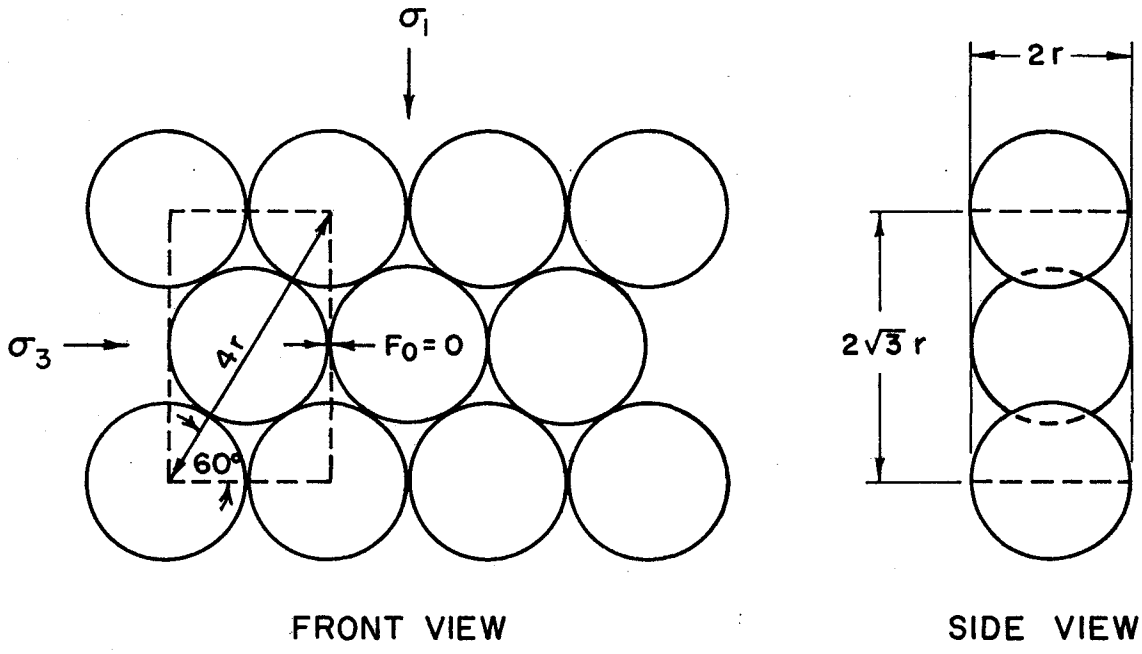

Figure 3.2 The dense packed planar array acted on by external stresses σ_1 and σ_3. Note 60° diagonal angles. The dashed portion indicates a unit cell.

For the dense array the tangential displacement as derived by Lynch (11) is:

$$\delta = \frac{3\,(2-\mu)}{8\,Ga_1}\left[2\left(1-\frac{T_L - T}{2FN}\right)^{2/3} - \left(1-\frac{T_L}{FN}\right)^{2/3}\right]$$

Equation (3.12)

where: $a_1 = \left[\frac{3\,(1-M^2)}{4E}\,(N+\Delta N)r\right]^{1/3}$

ΔN = increment of normal force.

Equations 2.2 and 3.12 express the normal and tangential displacements within the sphere unit and, knowing the geometry of the array, the strain equations can be developed. They are:

$$\epsilon_1 = \frac{\delta + \sqrt{3}\,\alpha}{2\sqrt{3}\,r}$$

Equation (3.13)

and

$$\epsilon_3 = \frac{\alpha - \sqrt{3}\,\delta}{2r}$$

Equation (3.14)

With these equations the vertical and lateral strain can be determined for a given system of stresses provided the boundary conditions are known.

Loose Three Dimensional Array

Examination of the three dimensional loose array of equiradii spheres shown in Figure 3.3 revealed that it was symmetrical about axes which intersect at 60° angles.

Figure 3.3 is a top view of a unit cell consisting of seven spheres. The points labelled A through G represent the centers of the spheres designated by the same letters. If point D is considered to be in the plane of the paper, then points A, B and C are in a plane parallel to and above the paper; and points, E, F and G are in a plane parallel to and below the paper. The plane of the paper is midway between planes ABC and EFG. The lines connect the centers of the outer spheres, and delineate the triangular areas on which the vertical and confining pressures are assumed to act.

Figure 3.4 is the same view as before, but the spheres have been removed. The geometrical configuration represented by this line drawing is a cubic octahedron[1]. The

[1] A cubic octahedron is a double pyramid with four equilateral triangles on each pyramid.

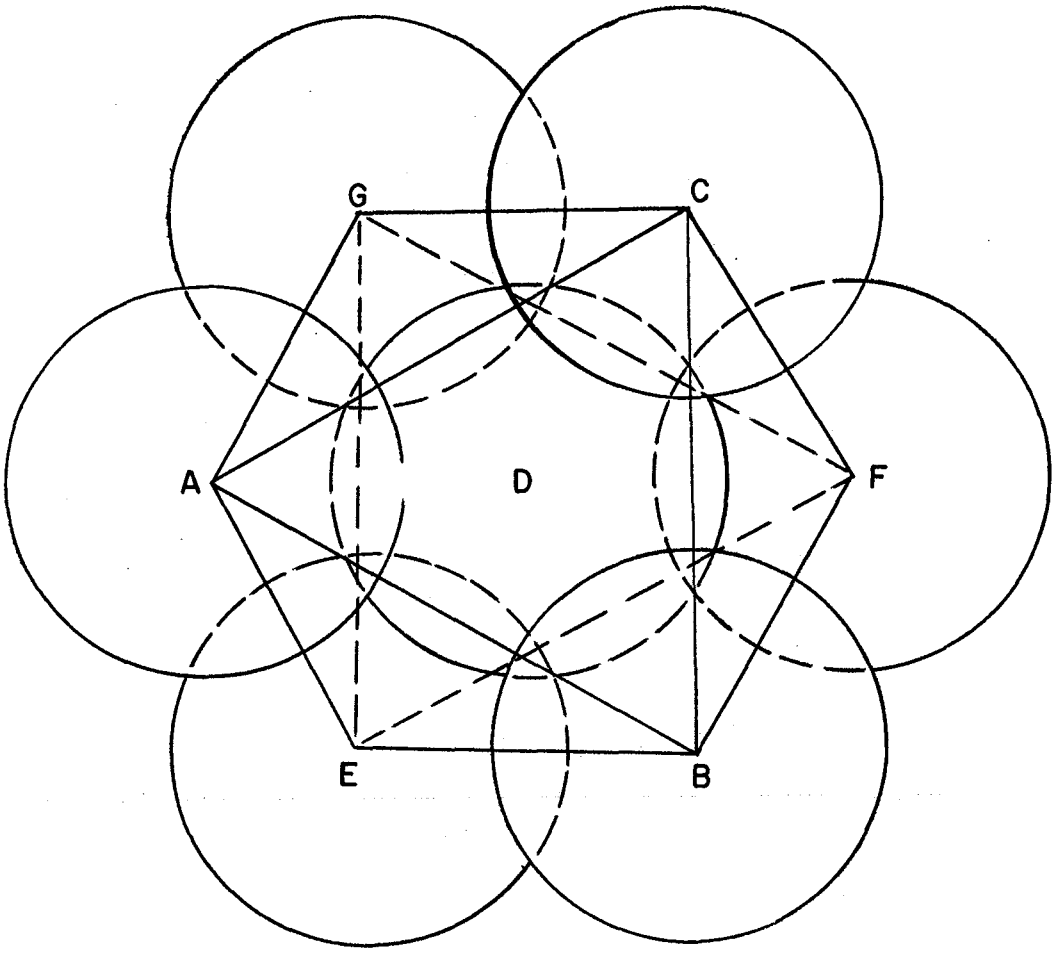

Figure 3.3 Top view of the loose array of equiradii spheres showing the lines connecting sphere centers which delineate the stress triangles.

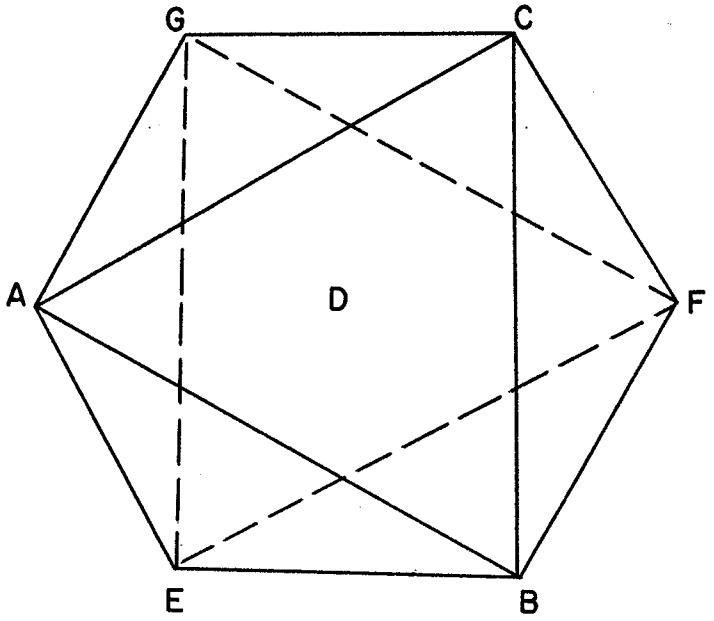

Figure 3.4 The top view with the spheres removed exemplifying the line drawing of Figure 3.1.

octahedron is lying on one of its triangular faces. This geometric figure, due to symmetry, consists of four pairs of triangular parallel planes. The two triangles composing each pair have the same relationship to each other as ABC and EFG. The other pairs are AGE and BCF, BEF and ACG, and ABE and CFG. The area of each triangular surface is equal to $3.46r^2$.

The loading of the unit cell may be described as a two step process: (1) a fluid pressure is applied and is considered to act normal to each of the eight triangular surfaces; (2) a vertical stress is applied normal to surface ABC.

As the vertical load is applied to sphere D through spheres A, B and C, it is transferred to the three bottom spheres as shown in Figure 3.5. The vertical reaction, F_1, at each of the six points of contact resulting from this load transfer is $1.15r^2\sigma_1$, where σ_1 is the vertical stress applied including the fluid pressure acting on ABC. The normal and tangential components of F_1 on the contact surfaces are $0.665r^2\sigma_1$ and $0.940r^2\sigma_1$, respectively.

The normal and tangential components on the contact surfaces resulting from the fluid pressure acting on triangles other than ABC and EFG are $1.771r^2\sigma_3$ and $-0.940r^2\sigma_3$, respectively. The minus sign is used in this case to denote the tangential force acting opposite to the tangential force resulting from σ_1. The triangles are inclined at 19.4° with the vertical.

The total normal force is:

$$N_t = 0.665\, r^2\sigma_1 + 1.771\, r^2\sigma_3 \qquad \text{Equation (3.13)}$$

while the total tangential force is:

$$T_t = 0.940\, r^2\sigma_1 - 0.940\, r^2\sigma_3 \qquad \text{Equation (3.14)}$$

For purposes of computer programming, let $N_t = P$ and $T_t = Q$. Alpha (α) was determined by substituting the values of N_t and T_t in Equation (2.2).

$$\alpha = 2\left[\, 3\,(1 - \mu^2)\, P/4E \,\right]^{2/3} r^{-1/3} \qquad \text{Equation (3.15)}$$

Likewise delta (σ) was calculated by substituting the values of N_t and T_t in Equation (2.4).

$$= \left[\, 3\,(2 - \mu)\, FP/8Ga \,\right]\left[\, 1 - (1 - Q/FP)^{2/3} \,\right] \qquad \text{Equation (3.16)}$$

where: $G = E/2\,(1 + \mu)$ = the shear modulus.

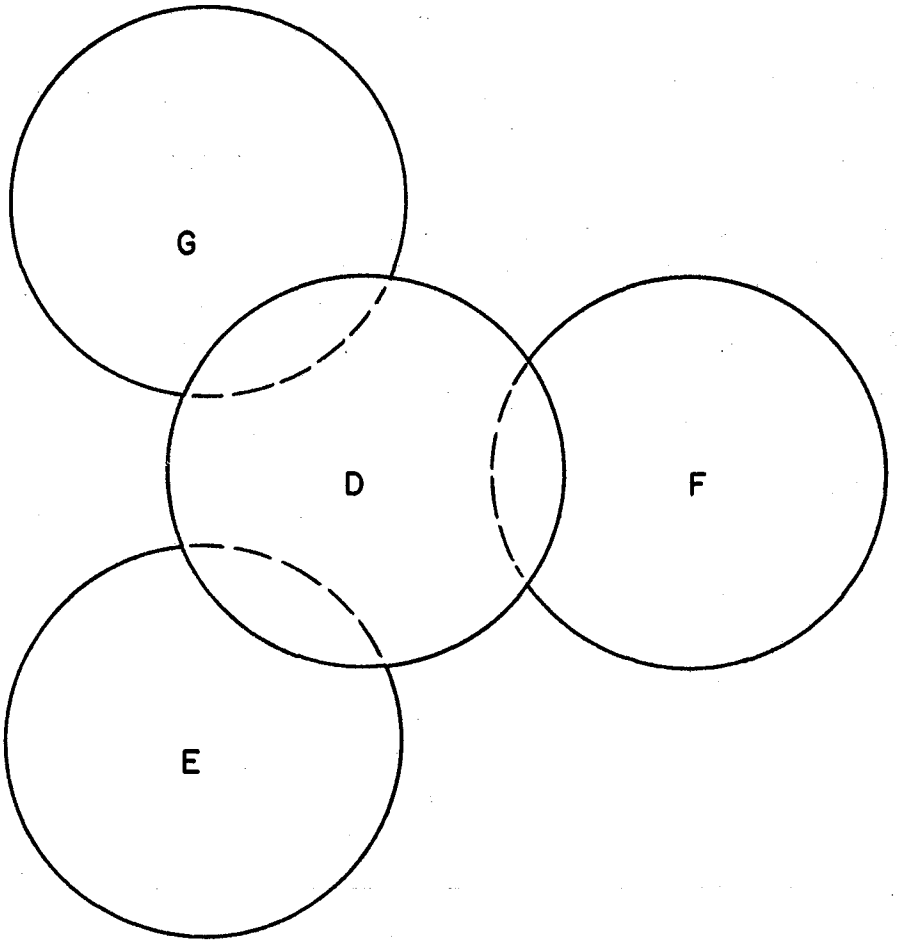

Figure 3.5 Top view of the loose array of equiradii spheres with the three upper spheres removed. This indicates how the center sphere is in contact with three bottom spheres. The load on the center sphere is transferred through these contact points to the bottom spheres.

The displacements are calculated in two steps: 1) the alpha and delta equations (3.15 and 3.16) are solved for hydrostatic conditions which yield initial values (α_o and δ_o); 2) the stress (σ_1) is incremented, and new alpha (α) and delta (δ) values are calculated.

Since the alpha and delta relationships of the sphere unit are known, it is possible to calculate the strains induced by a given system of stresses. The vertical strain, ϵ_1, resulting from the relative displacement of adjacent spheres due to vertical and horizontal stresses was calculated as shown below:

$$\epsilon_1 = \frac{\text{relative vertical displacement within the unit}}{\text{thickness of the unit}}$$

$$\epsilon_1 = \frac{3\Delta\delta\,(\cos 35.3^\circ) + 3\Delta\alpha\,(\sin 35.3^\circ)}{3.46r}$$

$$\epsilon_1 = (0.706\,\Delta\delta + 0.5\,\Delta\alpha)/r \qquad \text{Equation (3.17)}$$

where: $\Delta\delta = \delta - \delta_o$

$\Delta\alpha = \alpha - \alpha_o$.

The radial strain, ϵ_3, due to vertical and horizontal stresses was calculated by considering relative radial displacement of spheres.

$$\epsilon_3 = \frac{\text{relative radial displacement of the spheres}}{\text{width of the unit}}$$

$$\epsilon_3 = \frac{3\Delta\alpha\,(\cos 35.3^\circ) - 3\Delta\delta\,(\sin 35.3^\circ)}{3.68r}$$

$$\epsilon_3 = (0.66\,\Delta\alpha - 0.47\,\Delta\delta)/r \qquad \text{Equation (3.18)}$$

The above equations completely define the deformation -- both laterally and vertically -- for the loose array of equiradii spheres with the orientation described. In order to apply triaxial compression conditions to the equations, the confining pressure must be held constant, and computations of ϵ_1 and ϵ_3 can be easily made. One dimensional compression, on the other hand, requires that the radial strain be

equal to zero. When these boundary conditions are applied to the array either condition may be calculated.

The deformation equations for all the arrays were programmed for the University's 7094 computer.

CHAPTER IV

THE RESEARCH PROGRAM

General

The purpose of the experimental phase of the research project was to determine the stress-strain characteristics of certain base course materials subjected to repetitive triaxial loading. The purpose of the theoretical phase was to use particulate mechanics to explain the observed shapes of dynamic stress-strain curves.

To do this specimens were repetitively loaded and typical stress-strain curves developed from the data. (Much of this information was gathered as a by-product of research conducted on Project 2-8-62-27). The deformation equations for three arrays of elastic equiradii spheres were developed for triaxial compression and one dimensional compression conditions (Chapter III). A parametric study was made to determine the effect of the various parameters (μ, E, F and σ_3) on the stress-strain characteristics of the array. Ultimately, a comparison was made between theoretical and actual results to determine the applicability of the theoretical approach.

The Research Material

The material was obtained from a borrow pit near Seguin, Texas. The local classification -- caliche gravel -- is a bit misleading since the particles larger than about one-quarter of an inch consist of a cherty of flinty core with a porous appearing limestone ($CaCO_3$) rind surrounding it, or hard calcium carbonate covered by the rind. The limestone rind ranged from molecular thickness to a maximum of about one-quarter inch (see Figure 4.1).

The gravel is the result of weathering and erosion of the limestone beds of the Edwards Plateau Region of Texas. As flooding developed along the Guadalupe River, the boulders and finer material were swept downstream. The chert and hard calcite, being more resistant to weathering, survived to be redeposited in gravel beds similar to the one where the research material was excavated. The limestone film which actually gives the material its name resulted from alternating wet and dry seasons. In wet seasons insoluble calcium carbonate was changed in the upper layers to soluble calcium bicarbonate by the action of weak carbonic acid. This solution leached into the lower layers. During dry seasons water evaporated from the lower layers and insoluble calcium carbonate was once again formed and precipitated as a film on the larger particles.

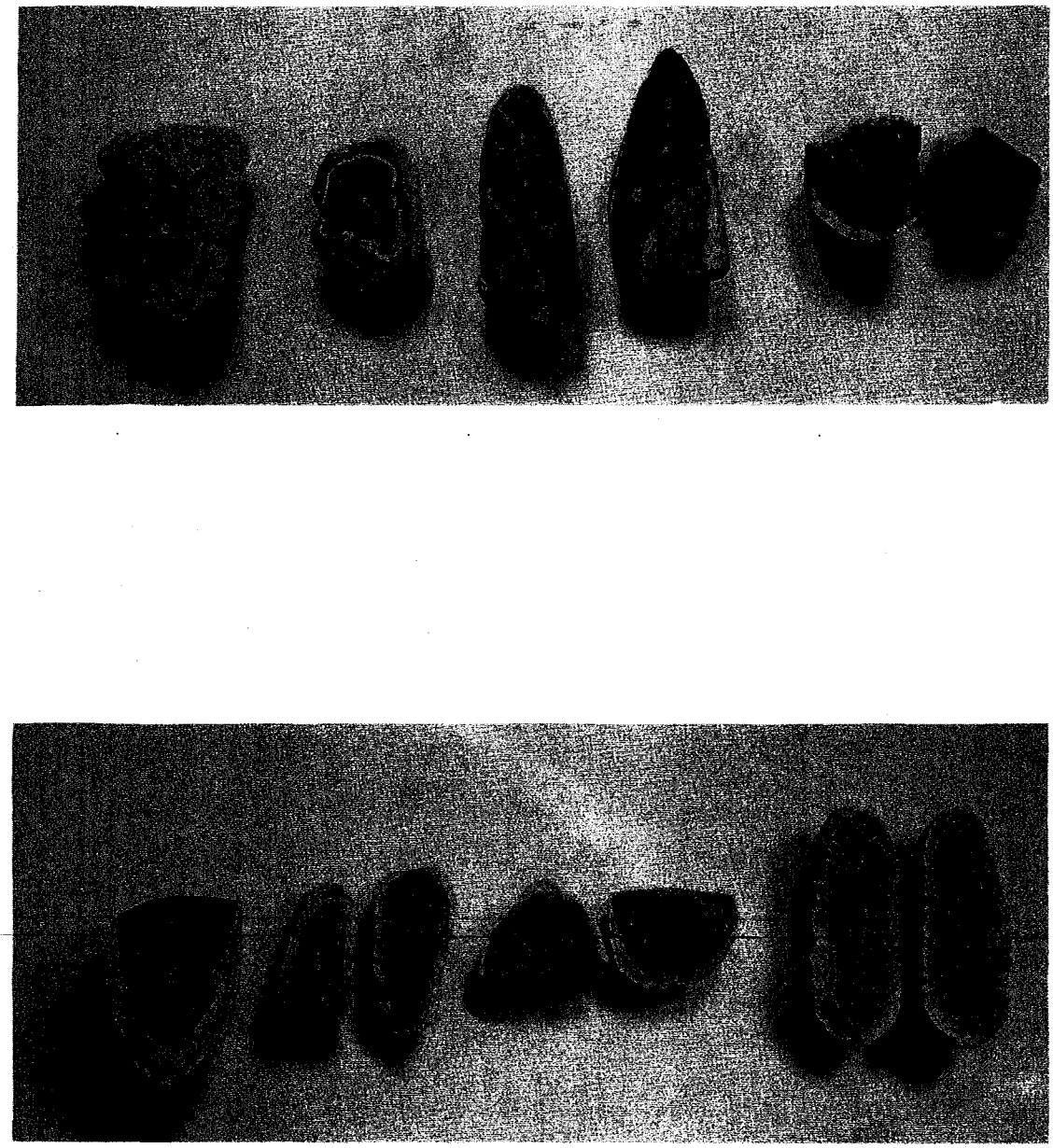

Figure 4.1 Typical particles of the caliche gravel split open to show the calcium carbonate rind on this material. Top picture shows particles with chert centers while those in bottom picture are carbonate centers. Note variation in thickness of the rind and the presence of annular rings in the thicker rind.

Engineering Characteristics of the Material

Engineering characteristics of the material were determined by physical tests performed on the desired gradations. The results of some of the more important tests are as follows:

A. Compaction Characteristics. (Test Method Tex-113-E) (14)
The compaction characteristics were determined for a compactive effort of 13.26 ft. lbs. per cu. in. The referenced procedure was revised somewhat to facilitate fabrication of replicate specimens (15).

The optimum moisture content using the revised procedure was 6.8 percent and the maximum dry unit weight was 135.4 pcf.

B. Specific gravity. (Test Method Tex-201-F) (14) Gs = 2.653

C. Atterberg Limits. (ASTM Designation D423-S4T and D424-S4T) (16)

1. Liquid Limit. $W_l = 21.3$

2. Plastic Limit. $W_p = 13.9$

3. Plasticity Index. $I_p = 7.4$

D. Los Angeles Abrasion. (ASTM Designation D131-116-E) (16)
Wear = 27.3 percent

E. Wet Ball Mill. (Test Method Tex-116-E) (14)
Wear = 36.2 percent

F. Permeability. (17)
$k = 0.02 \times 10^{-4}$ cm/sec

G. Texas Triaxial Classification. Test Method Tex-117-E) (14)
Class = 2.8 (See Figure 4.2)

H. Soil Classification.

1. Unified - GM

2. Texas - Type B, Grade 3.

Figure 4.3 is a pictorial representation of the research material indicating the shape of the various particle sizes. The upper picture shows particle sizes

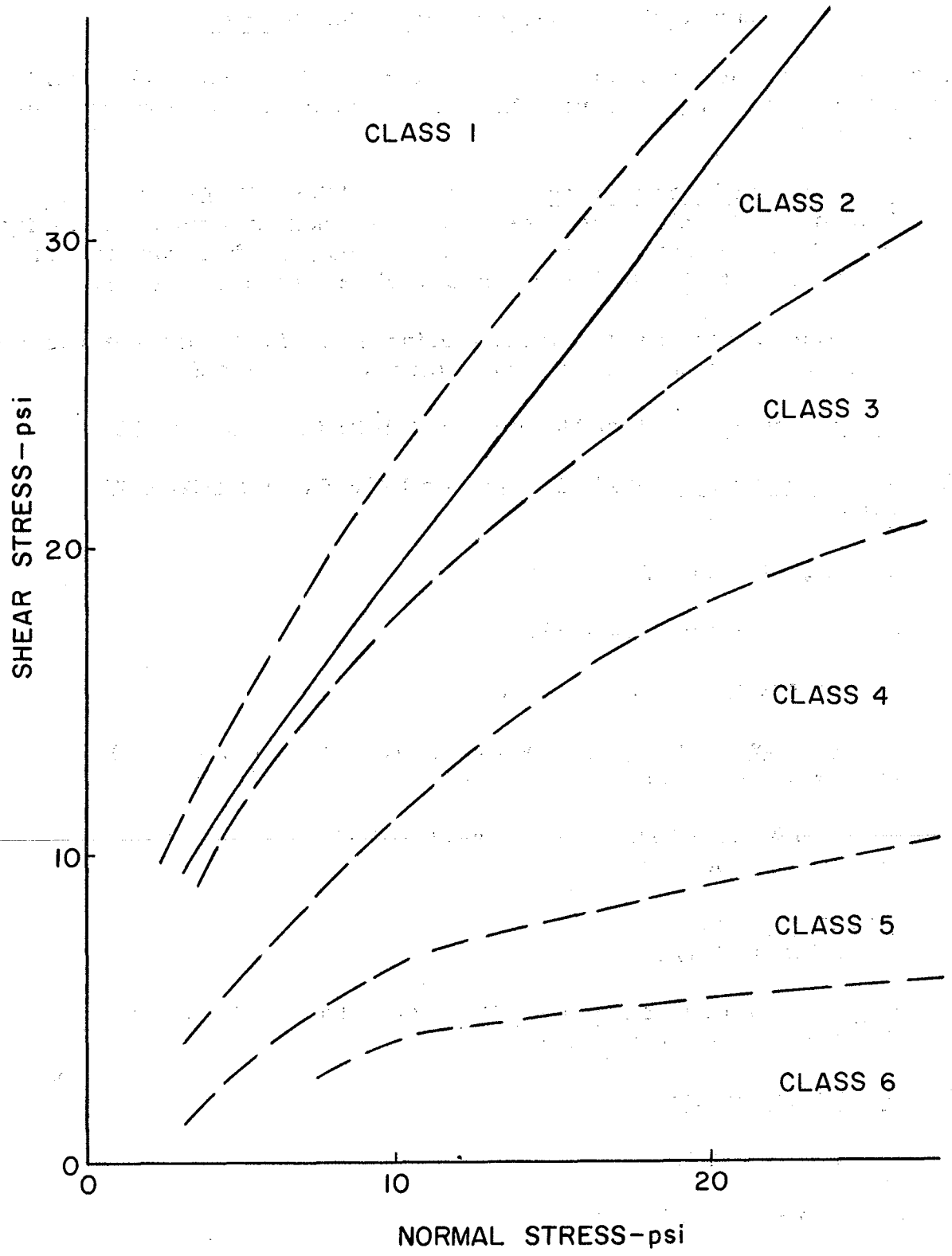

Figure 4.2 Chart for classification of experimental material.

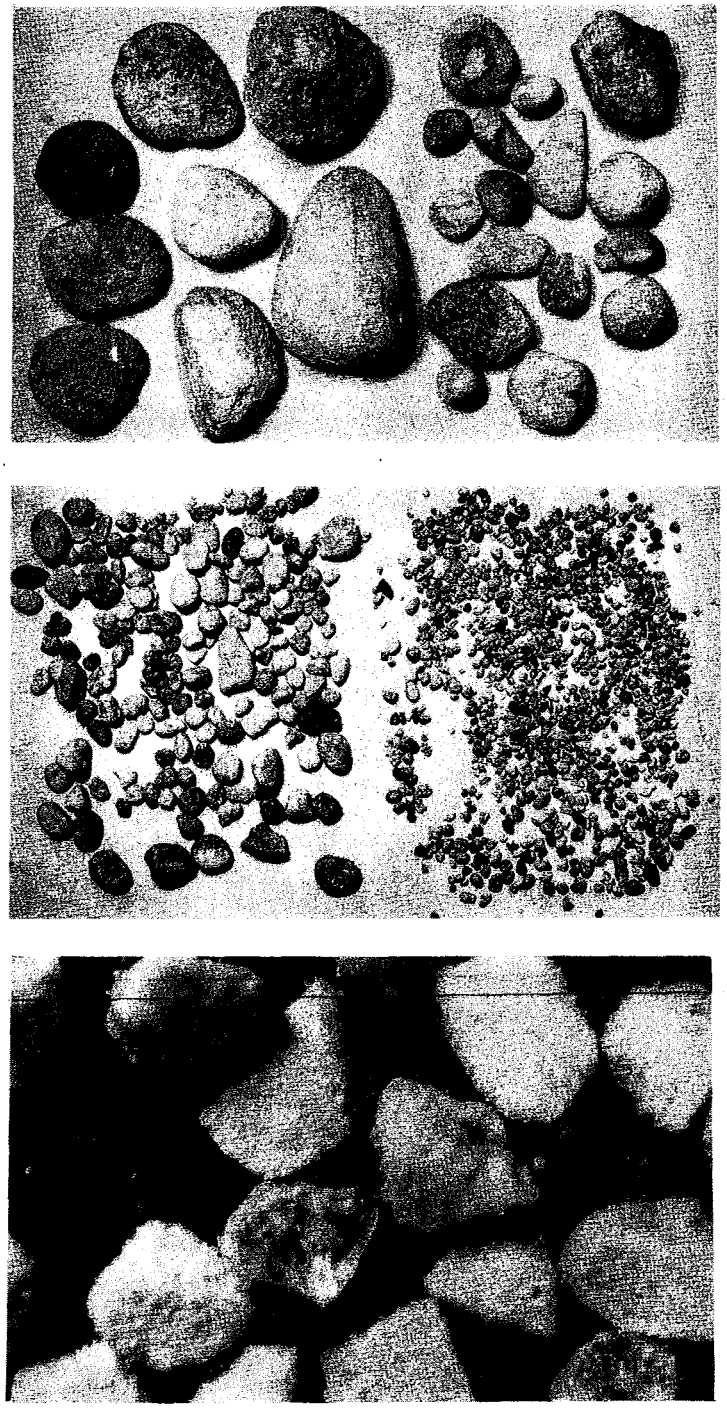

Figure 4.3 A pictorial representation of the research material.

of 1-3/4 - 1/2 inches, middle picture is 1/2 inch - #10 mesh particles; lower picture #40 - #50 mesh particles, magnified 30X. The lower picture shows quartz particles (glass like) and calcium carbonate (powder like). It can be noted from the lower picture that dust covers the particles and therefore contaminates the contact points between particles.

Preparation for Repetitive Loading Specimens

Approximately four cubic yards of the material were dried for twenty-four hours in a 140° F oven, and then separated on a Gilson shaker into seven size groups. These various sizes were stored in 55-gallon drums to be recombined later into the gradation shown in Figure 4.4. Twelve-inch high by six-inch diameter specimens were then compacted using the revised procedure (15) for fabricating compaction specimens.

After compaction the specimen was extruded and then encased in a rubber membrane which was, in turn, sealed to the head and pedestal of a triaxial cell with "silicone rubber" (Dow Corning Silastic RTV) and a one-inch wide rubber band made from motorcycle innertubes. This method of sealing proved to be quite effective after numerous other methods had failed to stop water leakage. The cell was assembled, filled with tap water and allowed to sit overnight. The following morning 3.0 psi confining pressure was applied to the chamber, and the drainage ports to the head and pedestal were opened to allow entrapped air to escape. A volume change device (Figure 4.5) was connected to the two ports and initial readings recorded for water and air. The confining pressure was increased to the desired level and the volume change device was observed for possible leaks in the membrane.

Testing Equipment

The repetitive testing equipment has been previously described (18), however a brief description will be included to promote an understanding of the test results.

Repetitive loading unit. The repetitive loading unit is essentially a hydraulic operated testing machine capable of applying repetitive loads to four specimens simultaneously (see Figure 4.6). The loads are applied by interchangeable hydraulic rams. Each of the four testing stations has a restrictor valve and an adjustable pressure regulator to control the line pressure to that desired for each individual ram.

The speed and frequency of loading is dependent on timer actuated solenoid valves. Each timer is essentially a synchronous motor, turning a shaft mounted

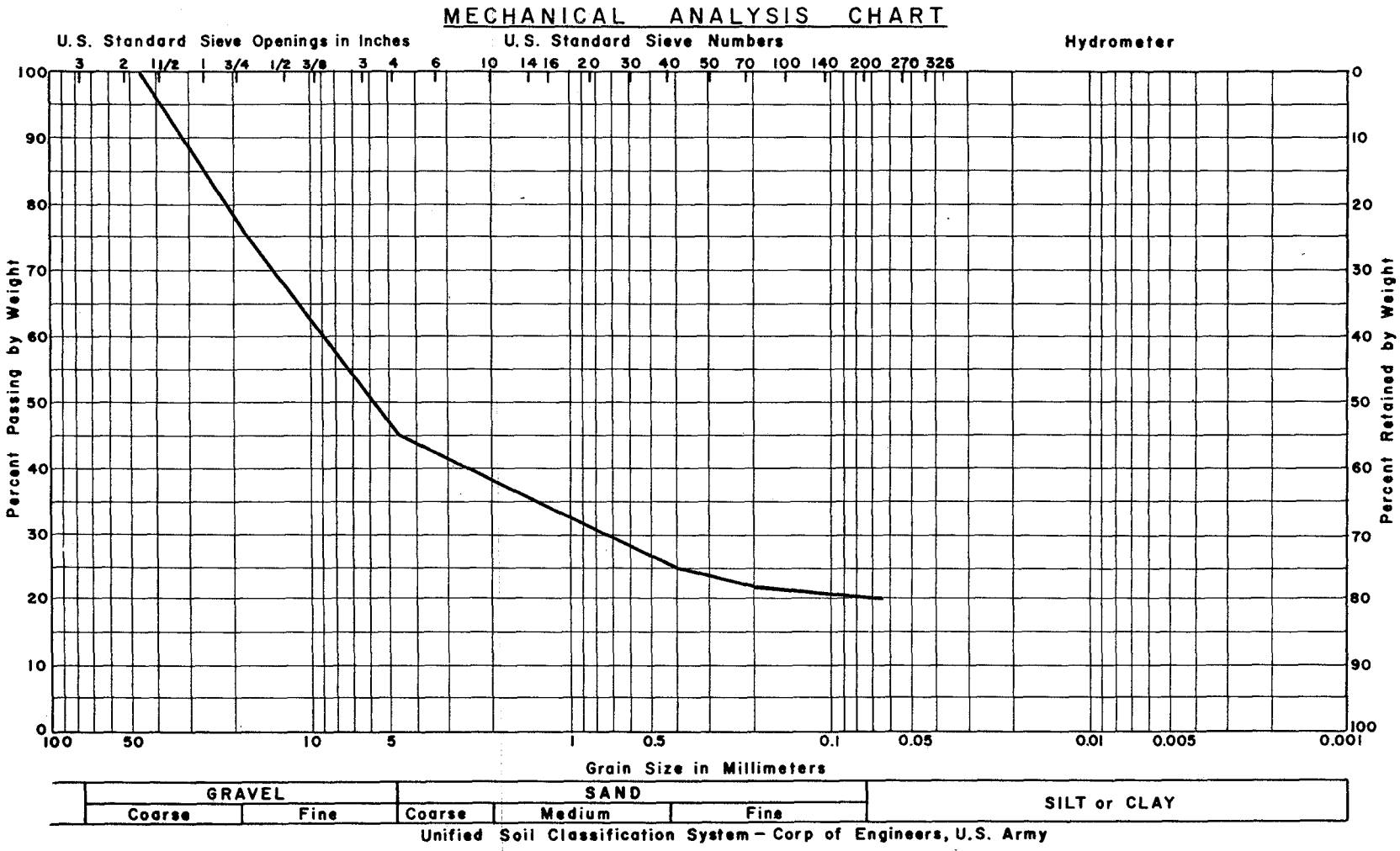

Figure 4.4 Gradation of the research material.

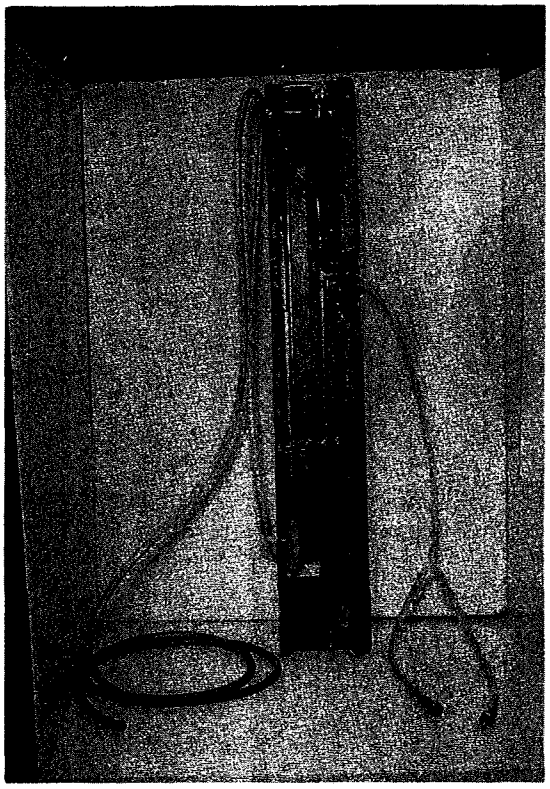

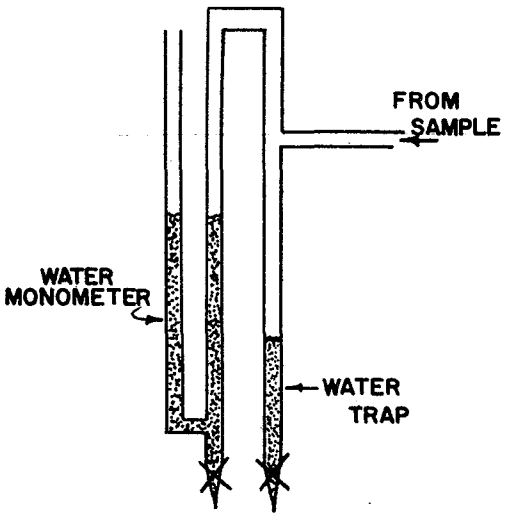

Figure 4.5 Photograph and schematic diagram of volume change device.

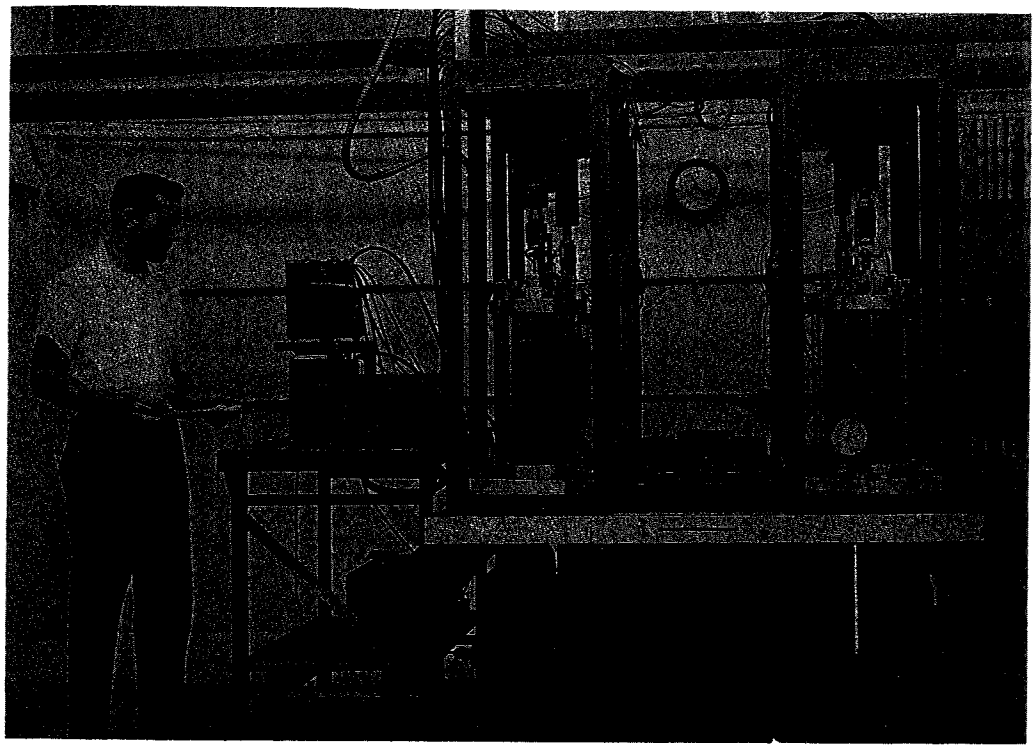

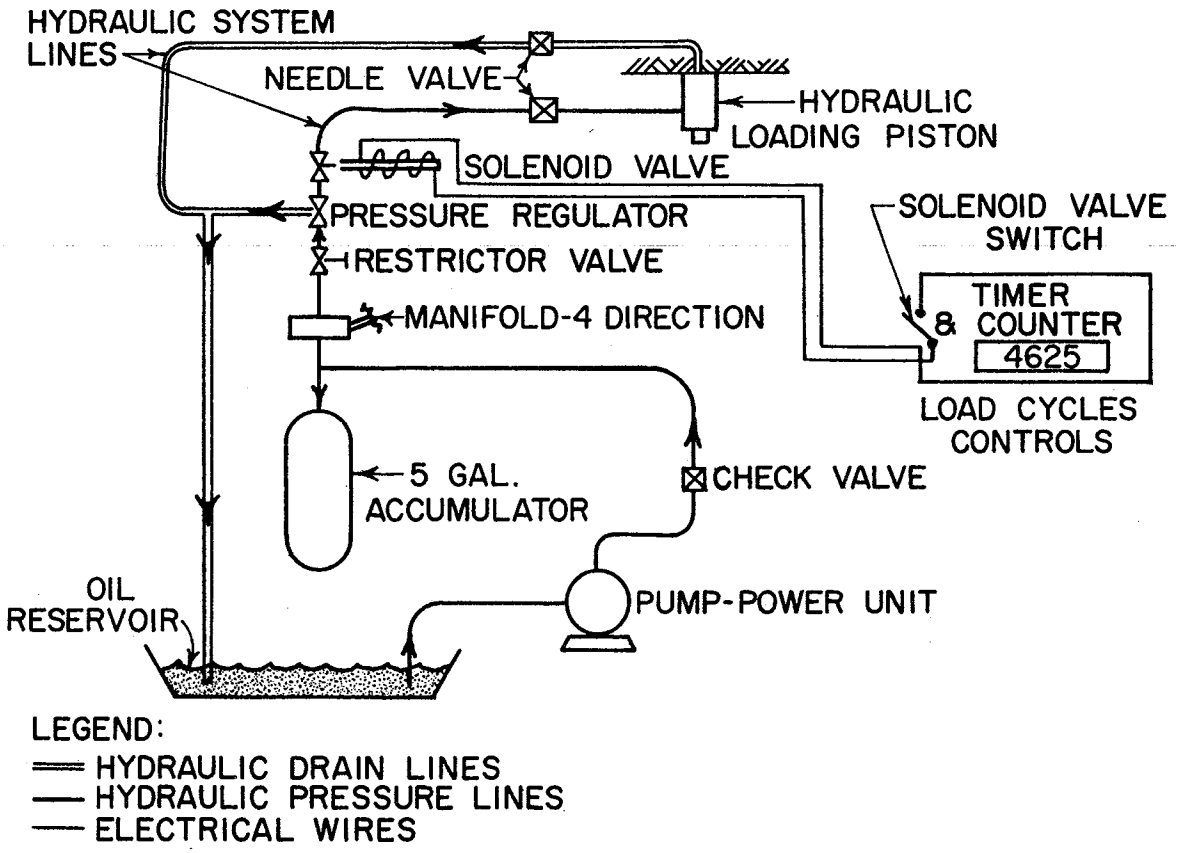

Figure 4.6 Photograph and diagram of the repetitive loading apparatus.

cam, which alternately opens and closes a microswitch connected to the solenoid valve. By alternating motors with different speeds and gear arrangements, a wide assortment of time cycles is available. The shaft mounted cam can be adjusted so that the microswitch remains on from two to 98 percent of the total cycle time.

Triaxial compression cells. The triaxial compression cells (Figure 4.7) were designed by personnel of the Texas Transportation Institute and constructed locally. They were made for 6-inch diameter by 12-inch high specimens and are conventional except for the loading piston arrangement. The piston is one-inch diameter hardened stainless steel and it travels through two linear ball bushings. The ball bushings minimize friction and insure full loading on the specimen.

Protective membranes. The membranes used in this research were 1/32-inch thick butyl rubber. These were substituted for the standard latex membranes when it was discovered that practically all of the commercial latex membranes had very small holes in them, were very easily punctured and were exceedingly permeable to air.

Measuring system. Transducers for measuring vertical load were attached directly to the pistons of the hydraulic rams. They were hollow cylinders of seamless aluminum tubing onto which were mounted four temperature compensated strain gages in a full bridge arrangement (see Figure 4.8).

The vertical deflection transducers were composed of two cantilever beryllium copper blades with strain gages mounted so that a full bridge was again formed (see Figure 4.8).

Two Model 82-6 Honeywell Bridge Balance units were used to regulate voltage and balance the transducers, and a 24-channel Model 1508 Honeywell Visicorder oscillograph (Figure 4.9) recorded transducer output.

Measurements from the load-deformation recordings were used to calculate dynamic stress-strain curves. To facilitate computations, an I.B.M. 7094 computer was used to calculate and plot the stress-strain data.

Repetitive Testing Procedures

While the specimen was being observed for possible leaks, a dummy cell consisting of a piece of steel pipe was placed in the triaxial station to be used. The dummy cell was loaded repetitively and whatever adjustments deemed necessary to gain the desired magnitude and shape of loading curve were made. Loading was allowed to continue until the system "warmed up" and until no significant variation was noticed in the magnitude or shape of the loading curve. At this point, the triaxial cell containing the specimen was quickly inserted in the station, the initial height

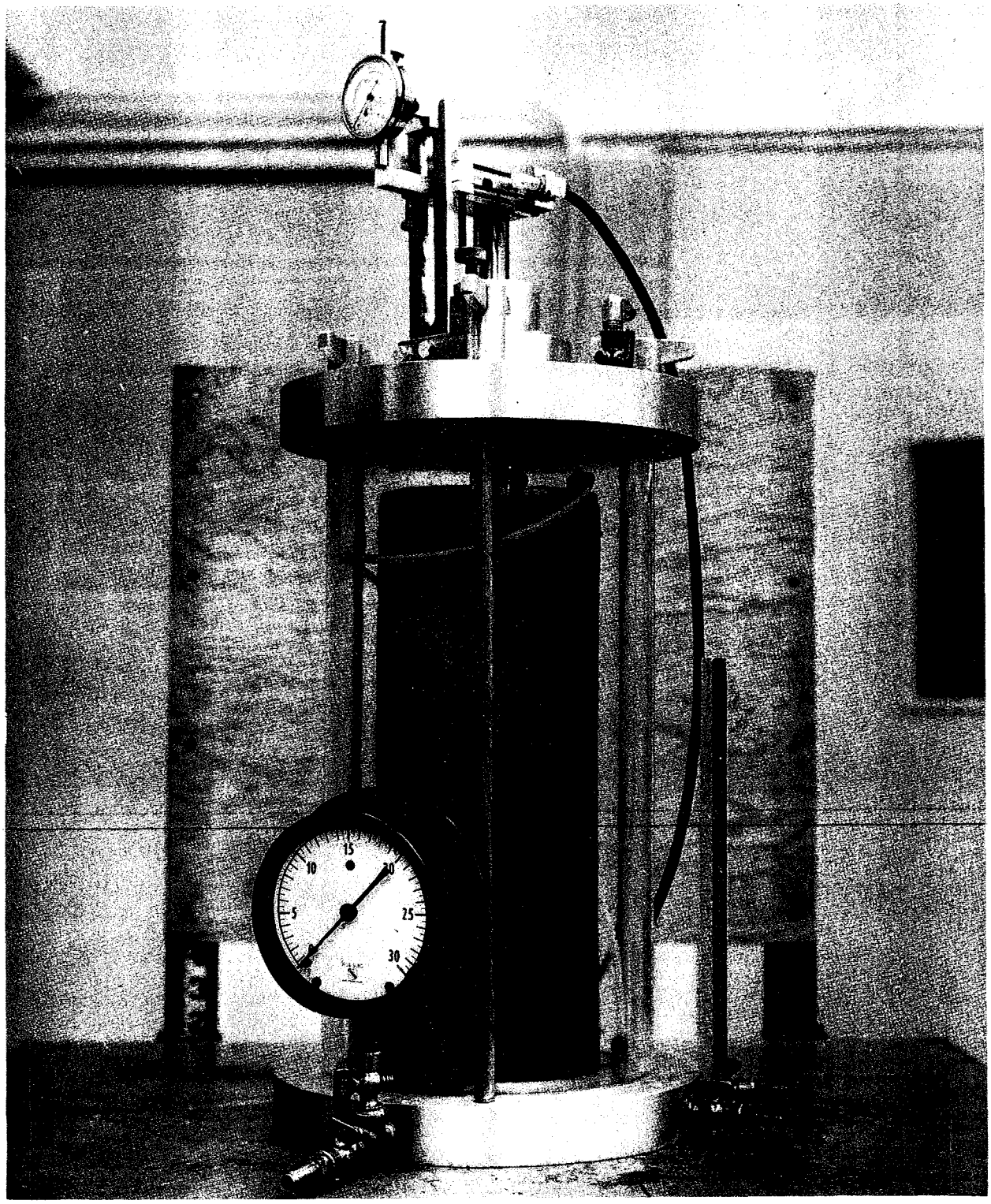

FIGURE 4.7 Picture and schematic diagram of specimen volume change apparatus.

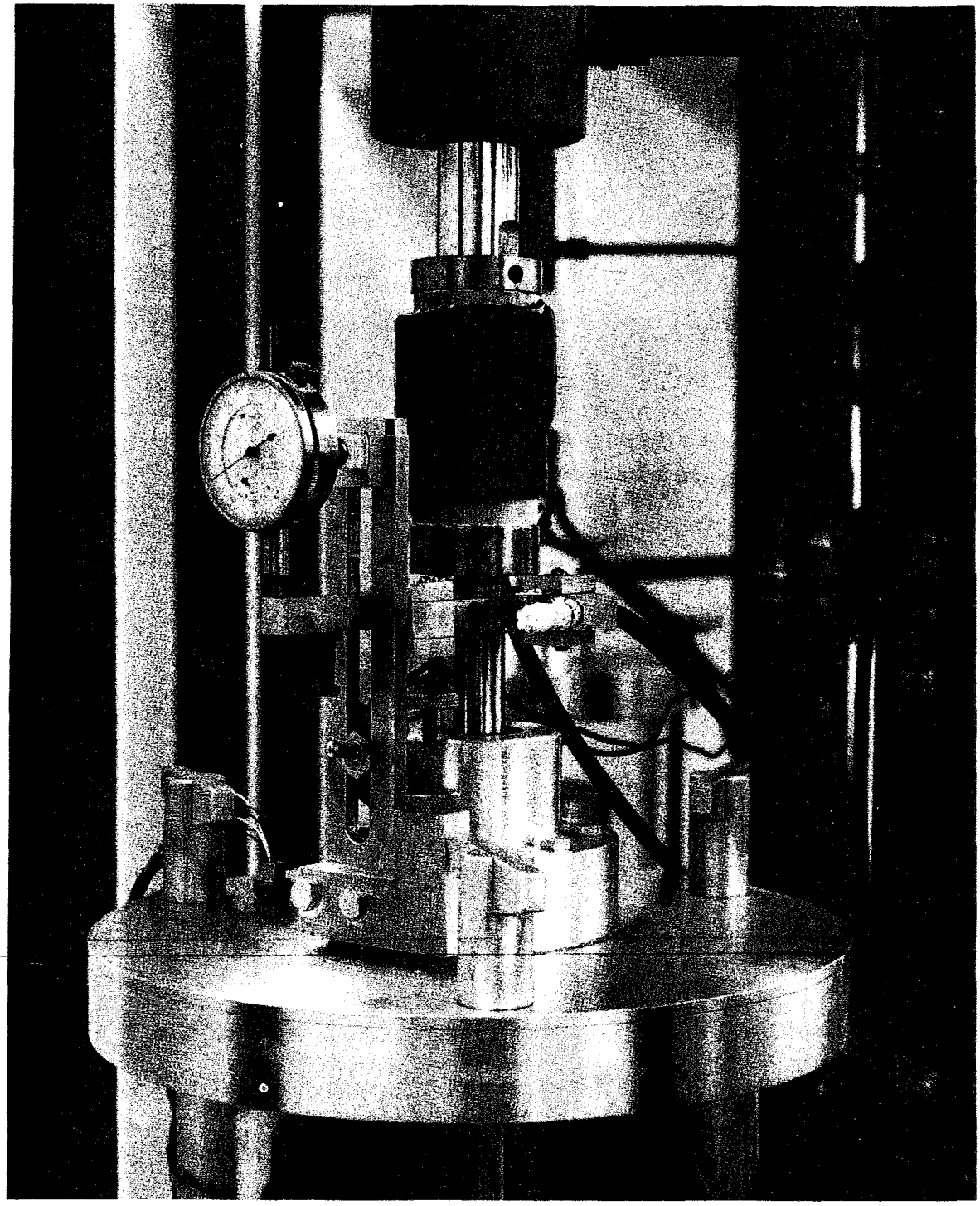

Figure 4.8 Close-up of head of triaxial cell showing mounting arrangement of dial indicator, force and deformation transducers. Note position of safety switch on piston clamp guide.

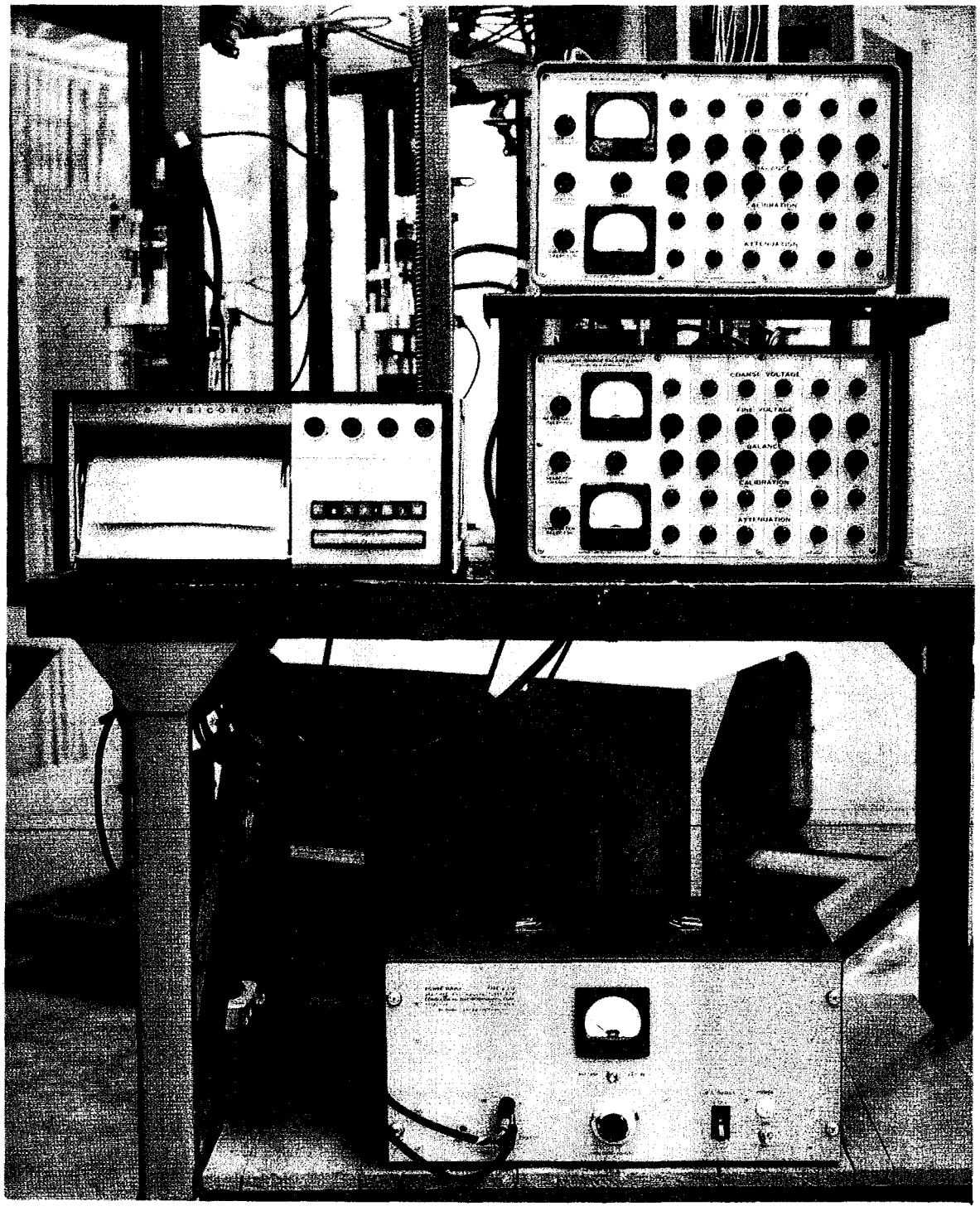

Figure 4.9 Honeywell visicorder and related instrumentation.

of sample and zero readings on the volume change device were recorded and repetitive loading was begun.

The load was applied to the specimen for 0.2 second and released for 1.8 seconds. This loading cycle had been found to be one of the more destructive (19), and simulates traffic moving at approximately 30 to 35 miles per hour. A typical load and deflection pattern is shown in Figure 4.10. Specimen height and volume change measurements were recorded throughout the life of the specimen at 1, 5, 10, 20, 40, 80, 160, 325, 650, 1300, 2500, 5000, 10,000 repetitions, etc. to plot progressive failure. Knowing the volume of the specimen, its unit weight and degree of saturation could be plotted throughout its life. Dynamic load and deformation recordings were made starting at 325 repetitions. In general the recordings were continued until arbitrary failure (5 percent strain) occurred or until it became evident that failure would not occur within a reasonable length of time (three weeks to one month).

At the conclusion of regular testing, the confining pressure was increased from its initial value to 30 psi and a load-deformation recording was made. The radial stress was then reduced in 5 psi decrements, and the recording process repeated after a stabilization period of approximately 50 repetitions.

After completion of the test, the cell was removed from its station, drained and disassembled. The sample was weighed, photographed, broken into approximately the original 2-inch layers and dried.

The Parametric Study

The deformation equations developed in Chapter III contain several parameters of the material which affect the shape of the stress-strain curves. To facilitate choosing a range of values for these parameters, four fragments of the research material were cored. One core was dark chert, another light chert, another nearly pure quartzite and the fourth a piece of hard limestone, indicating the variable nature of the material. The dynamic modulus of elasticity and Poisson's ratio, determined sonically, varied from 9.8×10^6 psi to 17.1×10^6 psi and from 0.05 to 0.24, respectively. Additional information, shown in Table IV.1, was obtained from various publications. From these sources it was indicated that the modulus of elasticity could be expected to be within 5 to 20 million psi, Poisson's ratio within 0.1 to 0.3 and the coefficient of friction between 0.1 and 0.5. Factorial arrangements encompassing these ranges were developed for each of the three arrays considered (see Figures 4.11 through 4.13). For each box in the factorials, stress-strain curves were computed for confining pressures of 5, 10, 20 and 30 psi.

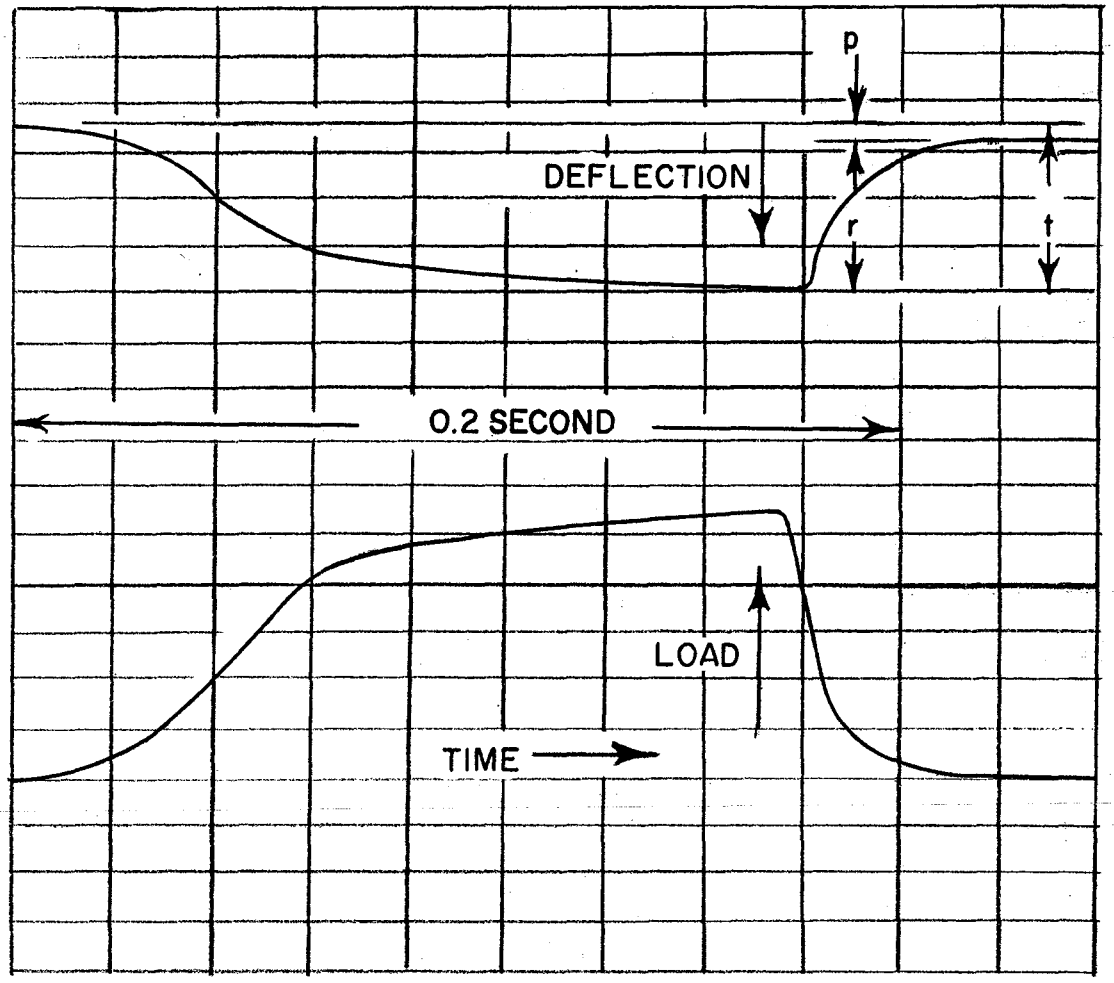

Figure 4.10 A typical load-deflection oscillograph.

TABLE IV.1

Summary of Reported Values for Modulus of Elasticity, Poisson's Ratio, and Coefficient of Friction of Rocks and Minerals.

Reference	Rock	$Ex10^6$	μ	F Oven Dry	F Saturated
Reynolds (21)	Quartzite	4.5-8.3			
	Limestone	4.8-5.4	0.16-0.23		
	Granite	4.5-8.3	0.15-0.24		
	Sandstone	4.8-5.4	0.17		
Willis and De Reus (22)	Chert	3.1-18.0			
	Quartzite	3.8-10.2			
	Sandstone	2.9- 4.0			
	Basalt	11.4-13.9			
	Granite	7.6- 9.8			
	Limestone	5.1-12.6			
	Dolomite	2.5-10.0			
Hirsch (23)	Calcareous-Siliceous Gravel	8.6			
	Crushed Limestone	4.5			
Mantell (24)	Flint	5.6			
	Sandstone	5.2			
	Moline Limestone	4.5			
	Soft Limestone	3.7			
Horn and Deere (25)	Clear Quartz			0.11	0.42
	Rose Quartz			0.13	0.45
	Feldspar			0.11	0.76
	Calcite			0.14	0.68
Balmer (28)	Limestone chalcedonic	8.0-8.8	0.18-0.22		
	Limestone med. grained	4.9-5.2	0.17-0.23		
	Subgraywacke med. grained	1.7-1.9	0.03-0.09		
	Schist	9.4-9.9	0.15-0.20		

F	μ	E x10^6	σ_3 = 5, 10, 20, and 30 psi					
		5	7	8	9	10	13
0.05	0.10	X	X	X	X	X	X
	0.15	X	X	X	X	X	X
	0.20	X	X	X	X	X	X
	0.25	X	X	X	X	X	X
	0.30	X	X	X	X	X	X
0.10	0.10	X	X	X	X	X	X
	0.15	X	X	X	X	X	X
	0.20	X	X	X	X	X	X
	0.25	X	X	X	X	X	X
	0.30	X	X	X	X	X	X
0.15	0.10	X	X	X	X	X	X
	0.15	X	X	X	X	X	X
	0.20	X	X	X	X	X	X
	0.25	X	X	X	X	X	X
	0.30	X	X	X	X	X	X
0.20	0.10	X	X	X	X	X	X
	0.15	X	X	X	X	X	X
	0.20	X	X	X	X	X	X
	0.25	X	X	X	X	X	X
	0.30	X	X	X	X	X	X

Figure 4.11 The factorial arrangement for the loose planar array.

F	μ	Ex 10^6	σ_3 = 5, 10, 20 and 30 psi					
		5	8	8.5	13	15	20
0.2	0.2	X	X	X	X	X	X
	0.3	X	X	X	X	X	X
	0.4	X	X	X	X	X	X
	0.5	X	X	X	X	X	X
0.3	0.2	X	X	X	X	X	X
	0.3	X	X	X	X	X	X
	0.4	X	X	X	X	X	X
	0.5	X	X	X	X	X	X
0.4	0.2	X	X	X	X	X	X
	0.3	X	X	X	X	X	X
	0.4	X	X	X	X	X	X
	0.5	X	X	X	X	X	X
0.5	0.2	X	X	X	X	X	X
	0.3	X	X	X	X	X	X
	0.4	X	X	X	X	X	X
	0.5	X	X	X	X	X	X

Figure 4.12 The factorial arrangement for the Dense planar array.

F	μ	E $\times 10^6$	σ_3 = 5, 10, 20 and 30 psi		
		5	10	15	20
0.2	0.2	X	X	X	X
	0.4	X	X	X	X
0.4	0.2	X	X	X	X
	0.4	X	X	X	X

Figure 4.13 The factorial arrangement for the loose three dimensional array

CHAPTER V

DISCUSSION OF TEST RESULTS

Results for the Loose Planar Array

The results of the parametric study for the loose planar array were analyzed to ascertain the influence of the various particle parameters (Poisson's ratio, coefficient of friction and modulus of elasticity) on the shape and distribution of the theoretical stress-strain curves. Also, a comparison was made between the theoretical stress-strain curves and actual stress-strain curves for a cherty limestone gravel subjected to rapid repetitive loading. It was found that the theoretical curves possessed the correct shape, but the effect was not as pronounced as the effect indicated by the actual stress-strain curves. This is illustrated in Figure 5.1, which shows theoretical stress-strain curves for the elastic constants and friction factor which best fit the actual stress-strain curves.

The effect of varying E, μ, F, and the confining pressure[1] is shown in Figures 5.2 through 5.5. It was found that:

A) As E increased there was a significant increase in the secant modulus. Changing E had no effect on the position of the inflection point (Figure 5.2).

B) As μ increased, the secant modulus increased slightly, and the coordinates of the inflection point increased significantly (Figure 5.3).

C) As F increased the secant modulus increased. It also influenced the position on the curve at which inflection occurred, i.e., as F increased the stress at which inflection occurred also increased.

D) As the confining pressure increased the secant modulus increased (Figure 5.5).

In summary it can be said that the position of the inflection point was affected by μ and F while the secant modulus was affected to some extent by all parameters.

Results for the Dense Planar Array

The parametric study showed that the theoretical stress-strain curves did not exhibit a reverse S-shape (see Figure 5.6). Also the range of strain values was not great enough to compare well with experimental results.

---

[1]In the one dimensional compression case, PO is the initial confining pressure and the change in vertical stress is termed delta sigma.

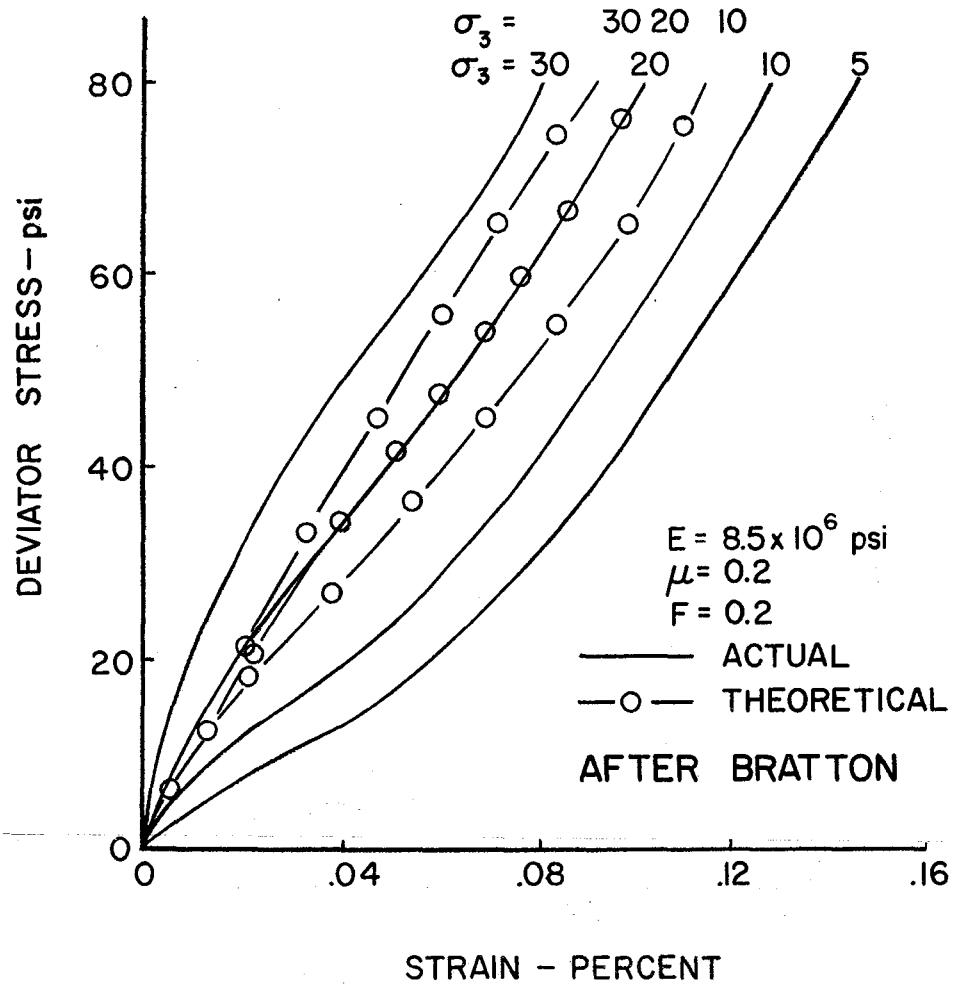

Figure 5.1 A comparison of a theoretical two dimensional loose array under one dimensional compression with experimental curves.

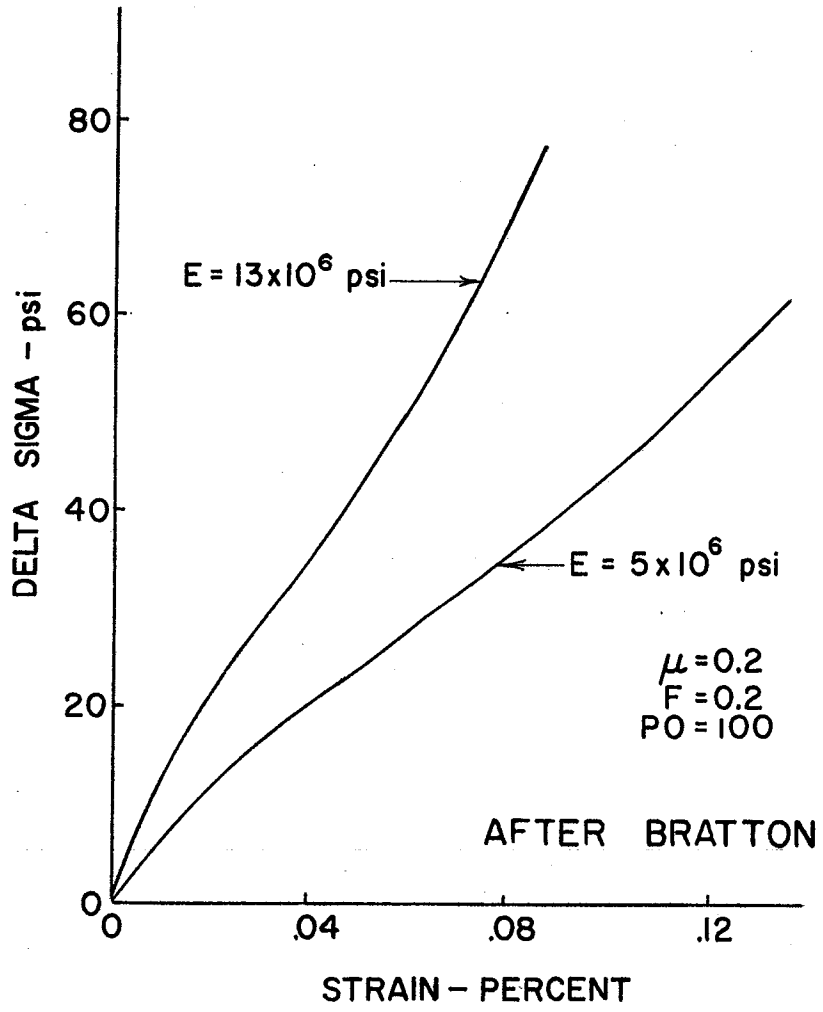

Figure 5.2 Effect of E on shape of stress-strain curves (two dimensional loose array under one dimensional compression).

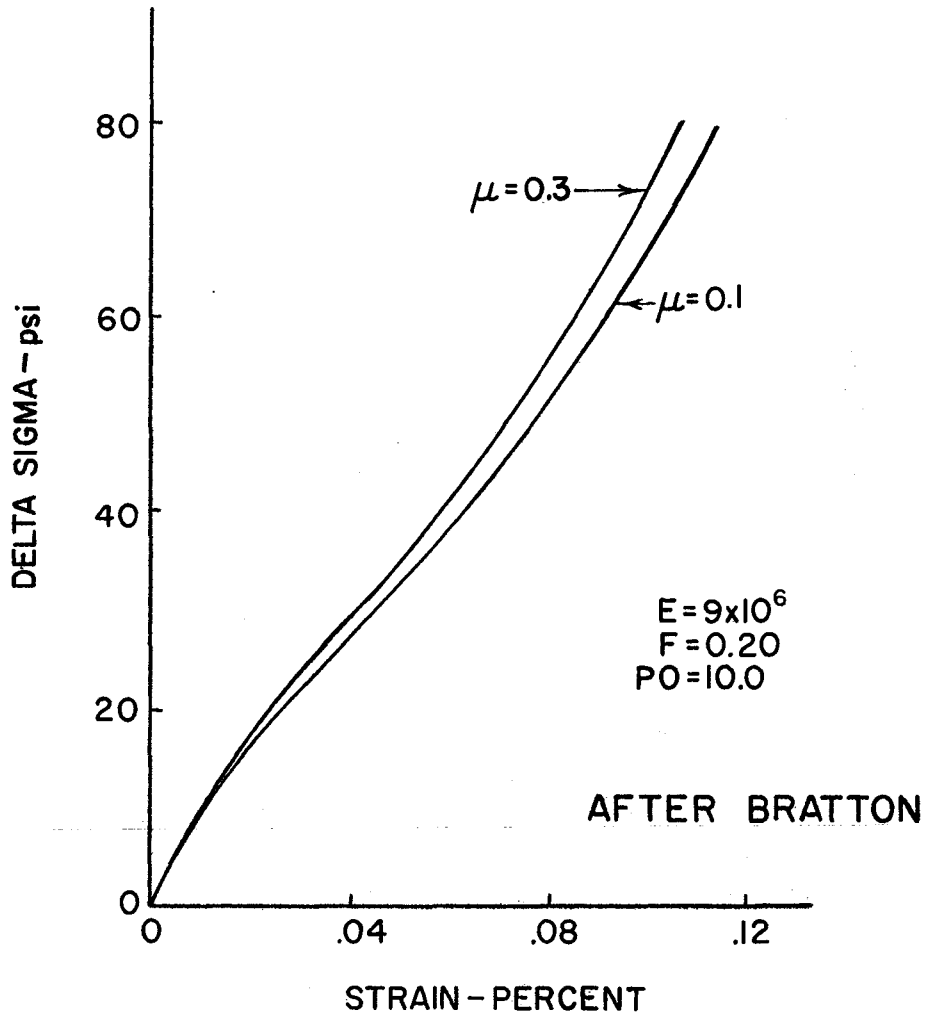

Figure 5.3 The effect of varying μ on the shape of stress-strain curves (two dimensional loose array under one dimensional compression).

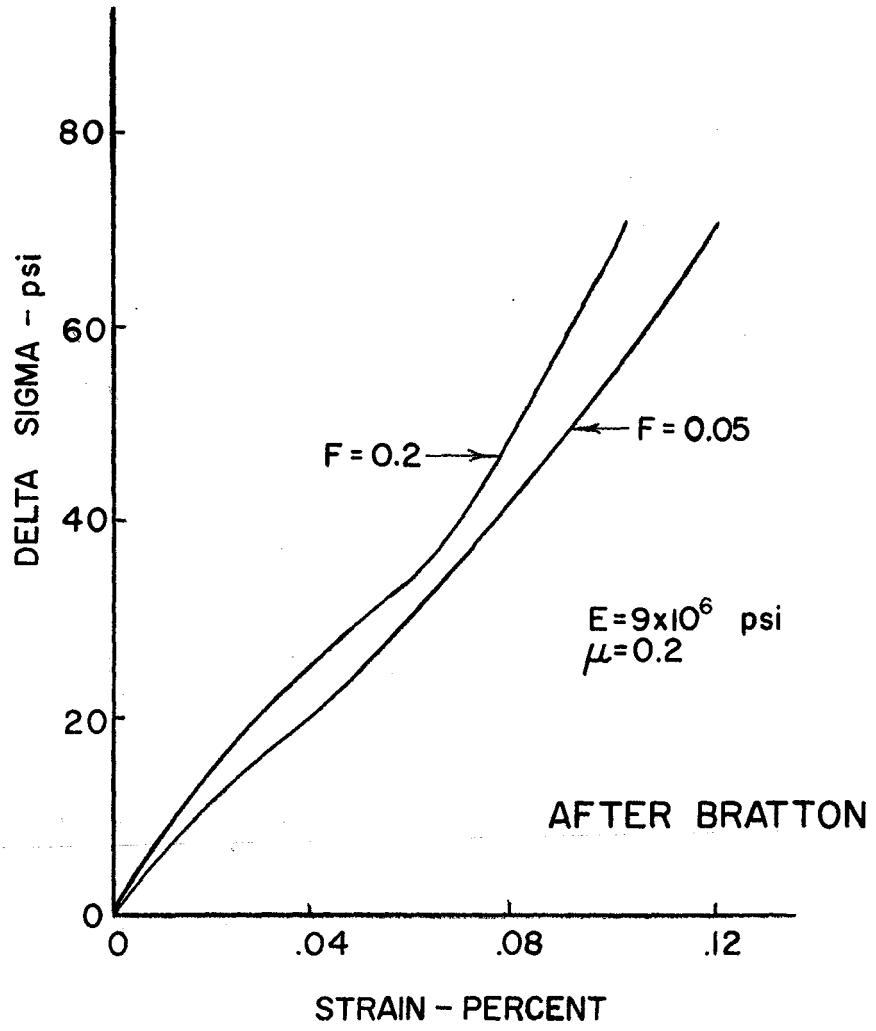

Figure 5.4 The effect of F on the shape of stress-strain curves (two dimensional loose array under one dimensional compression).

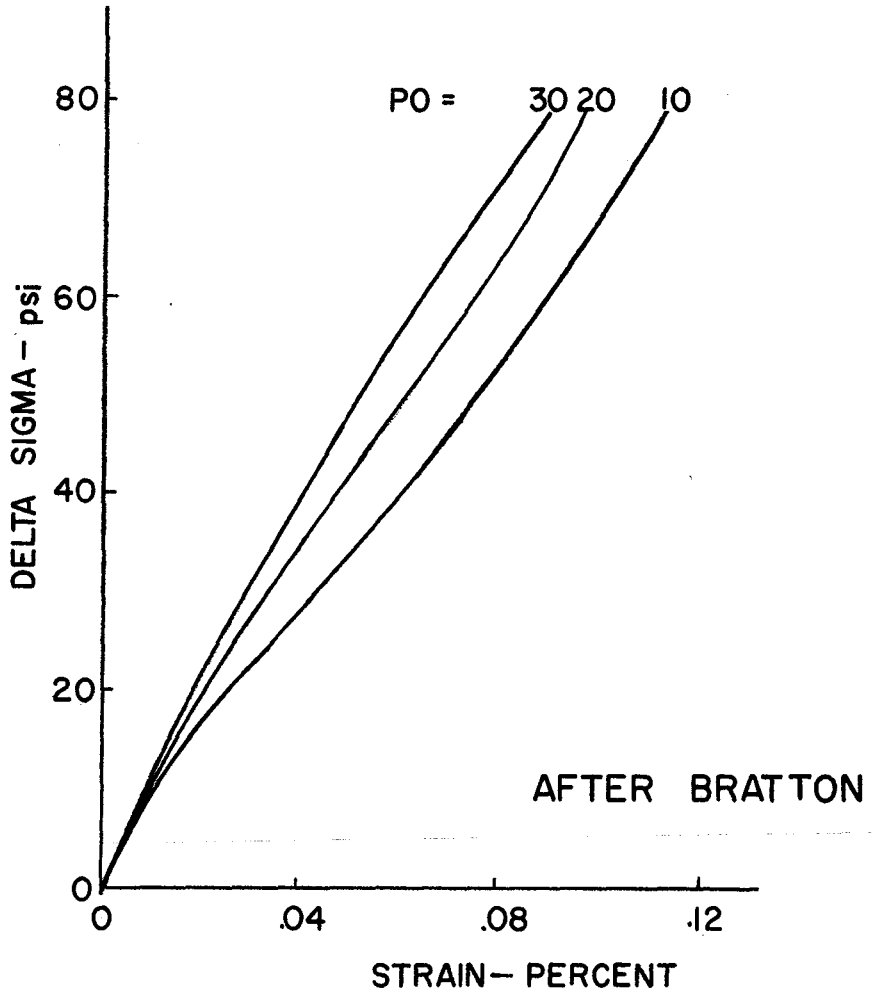

Figure 5.5 The effect of initial confining pressure on the shape of stress-strain curves (two dimensional loose array under one dimensional compression).

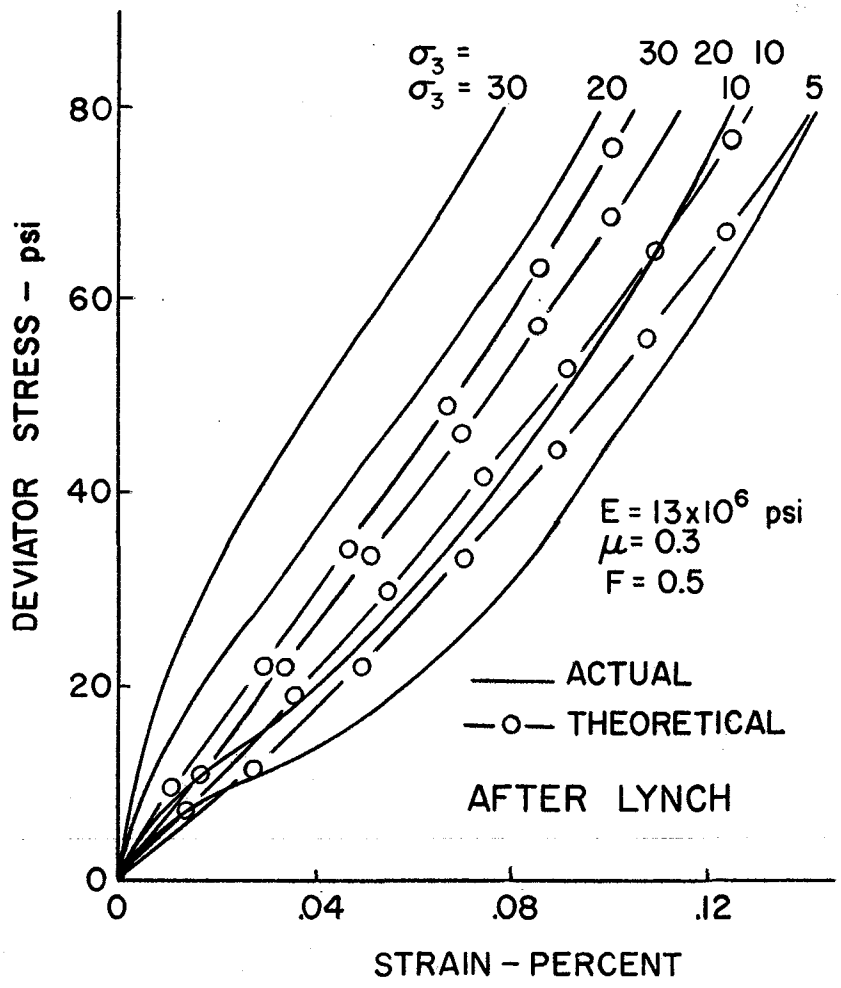

Figure 5.6 Stress-strain curves for two dimensional dense array under triaxial compression, compared with a set of actual stress-strain curves. (Speciman compacted at 50 blows per layer.)

It was believed that the stress-strain curves of the same soil compacted to a denser state would compare more favorably. However, this proved not to be the case: the theoretical stress-strain curves still did not compare well with the actual curves (see Figure 5.7). These results indicated that the dense planar array was too rigid to use in soil simulation studies.

It was also observed that:

(A) Increasing the modulus of elasticity while holding all other parameters constant increased the secant modulus, but the general shape of the curve did not change (see Figure 5.8).

(B) Increasing F while the other factors remained constant had little effect on the shape of the stress-strain curves produced from the dense array (see Figure 5.9), but it did increase the stress at which failure occurred.

(C) Increasing μ or Poisson's ratio had less effect on the stress-strain curves than any of the other parameters. The slope of the stress-strain curves was increased slightly (Figure 5.10).

(D) Increasing the confining pressure resulted in an increase in the secant modulus. (Figures 5.6 and 5.7).

To summarize: The modulus of elasticity, Poisson's ratio, and coefficient of friction had little effect on the shape of the stress-strain curves; however, increasing the coefficient of friction markedly increased the stress at which failure occurred. An increase in confining pressure was accompanied by an increase in the secant modulus.

Results for the Three-Dimensional Array Subjected to Triaxial Compression

The results of the parametric study were analyzed with the thought of comparing them to past research concerning deformation hypotheses for granular soils. Figure 5.11 shows the theoretical curves determined by triaxial compression conditions which best compare with the experimental curves used by Bratton (10) and Lynch (11). It may be noted that the spread of strain is less than that obtained from the actual soil. This indicates the actual soil is not as stable as the array of equiradii spheres up to the point where sliding begins to occur. This is reasonable since the uniform contact area utilized in the theoretical array would be much more stable than that found in the random packing of non-uniform particles of actual soils (see Figure 5.12). Many of the contact points in the actual soil are more likely to slide than those found in the theoretical array, thus indicating one other possibility for getting

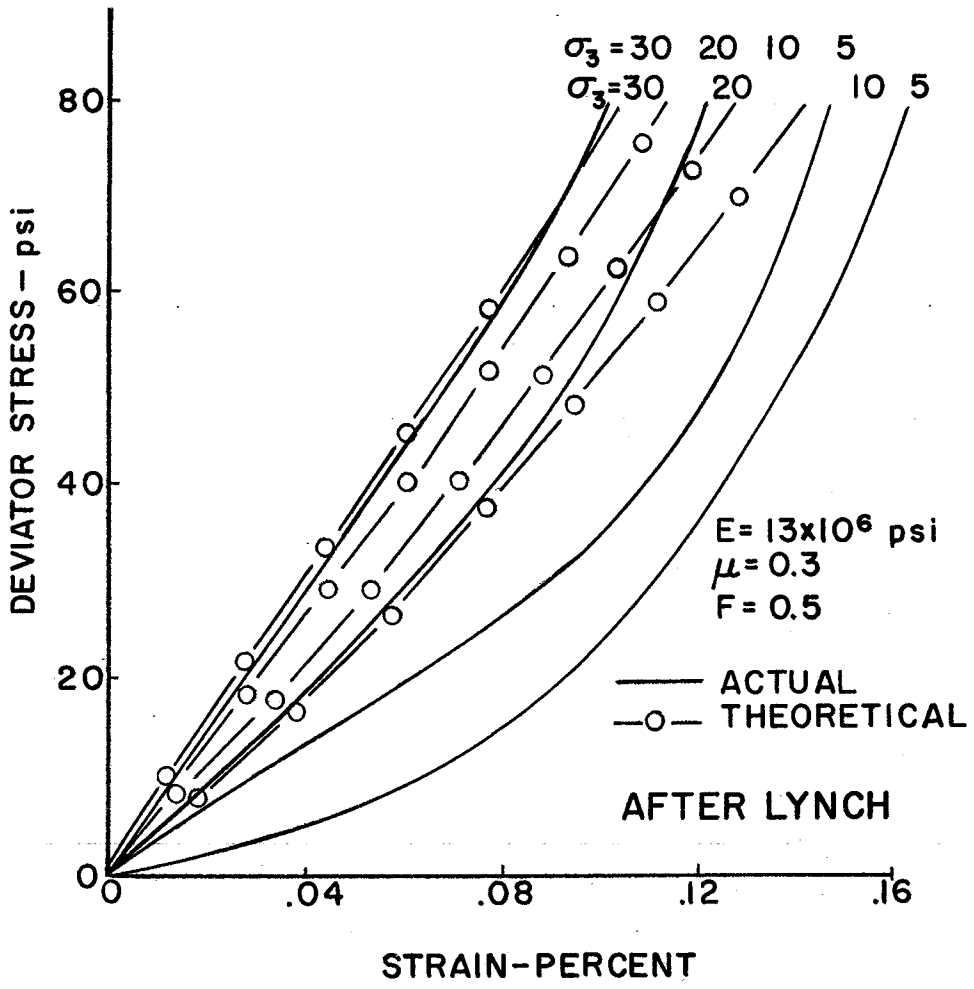

Figure 5.7 Stress-strain curves for a two dimensional dense array under triaxial compression, compared with a set of actual stress-strain curves for a dense soil (specimen compacted at 125 blows per layer).

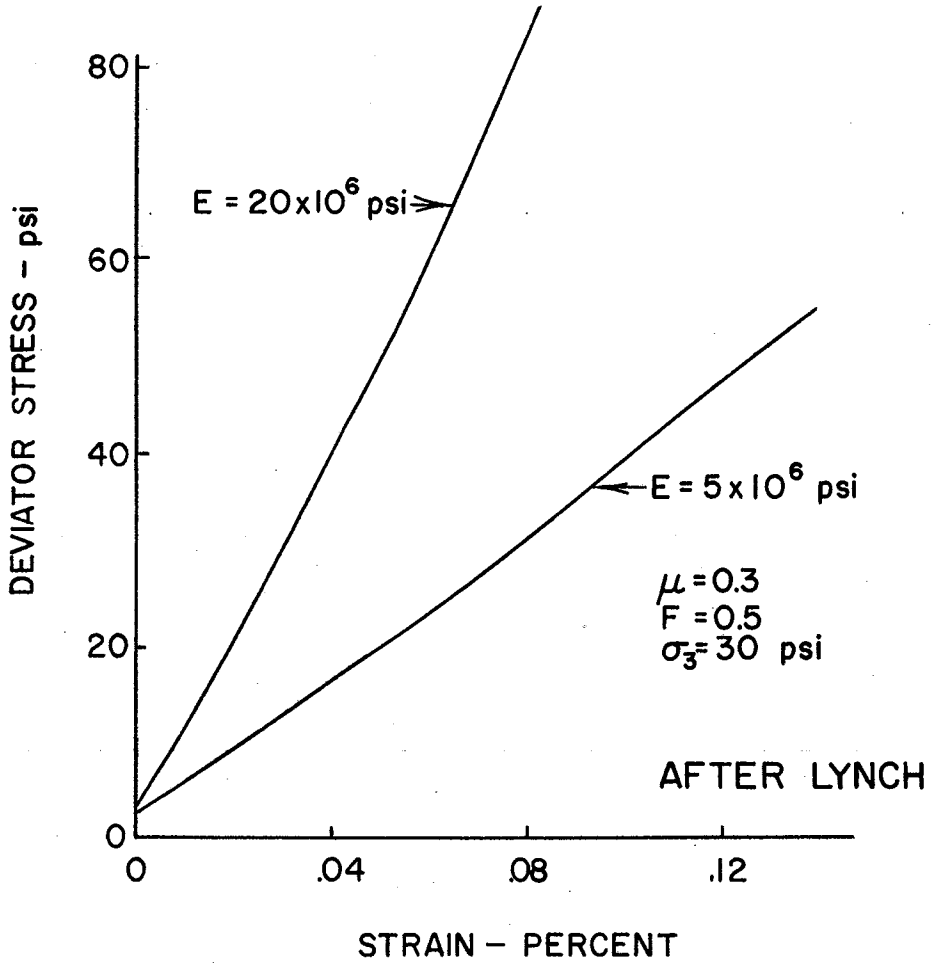

Figure 5.8 The effect of varying E on the shape of stress-strain curves (two dimensional dense array under triaxial compression).

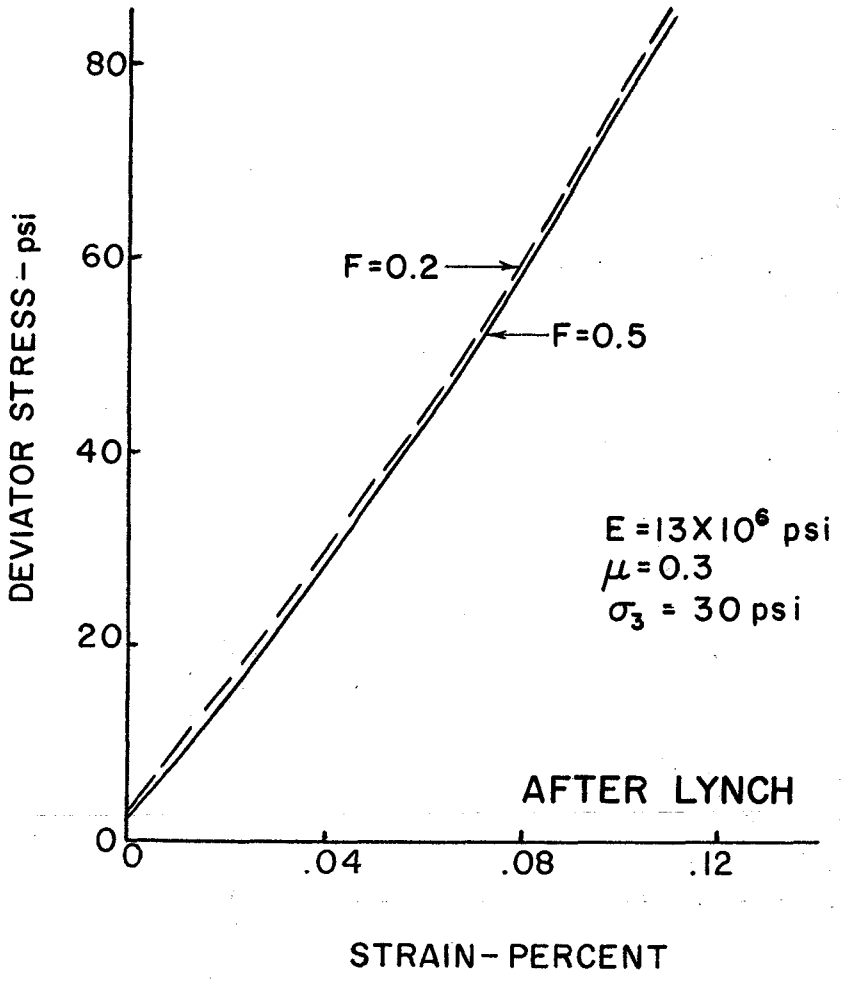

Figure 5.9 The effect of varying F on the shape of stress-strain curves (two dimensional dense array under triaxial compression).

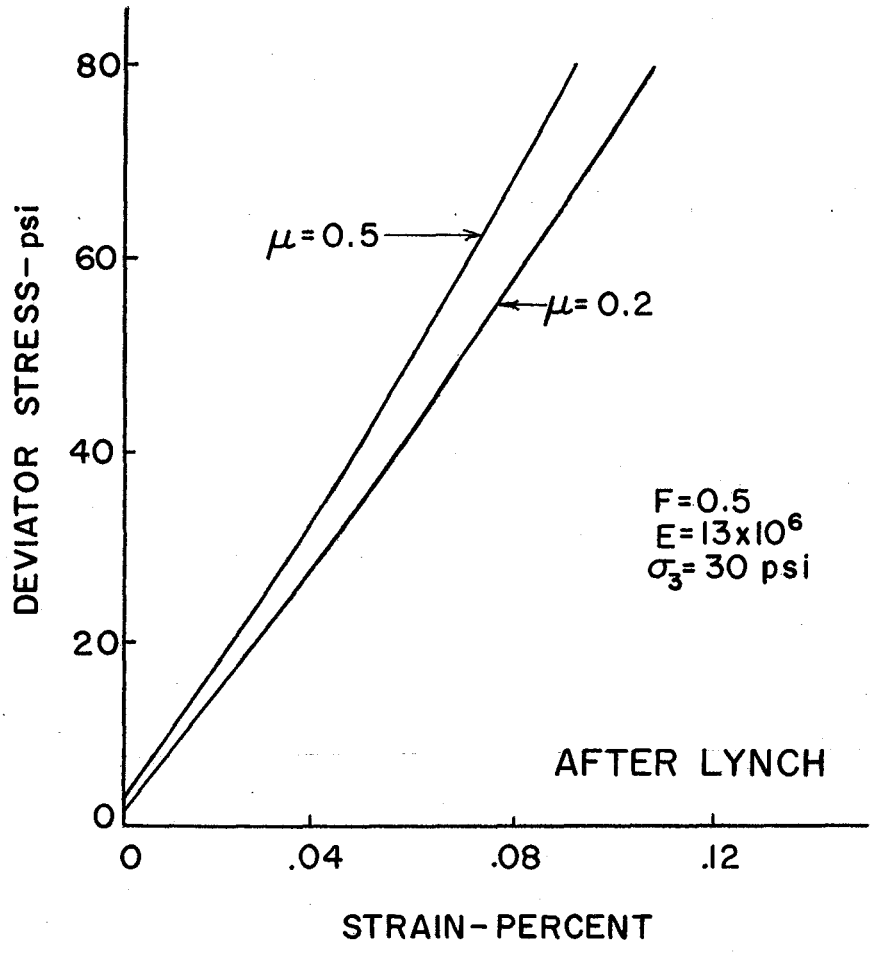

Figure 5.10 The effect of varying μ on the shape of stress-strain curves (two dimensional dense array under triaxial compression).

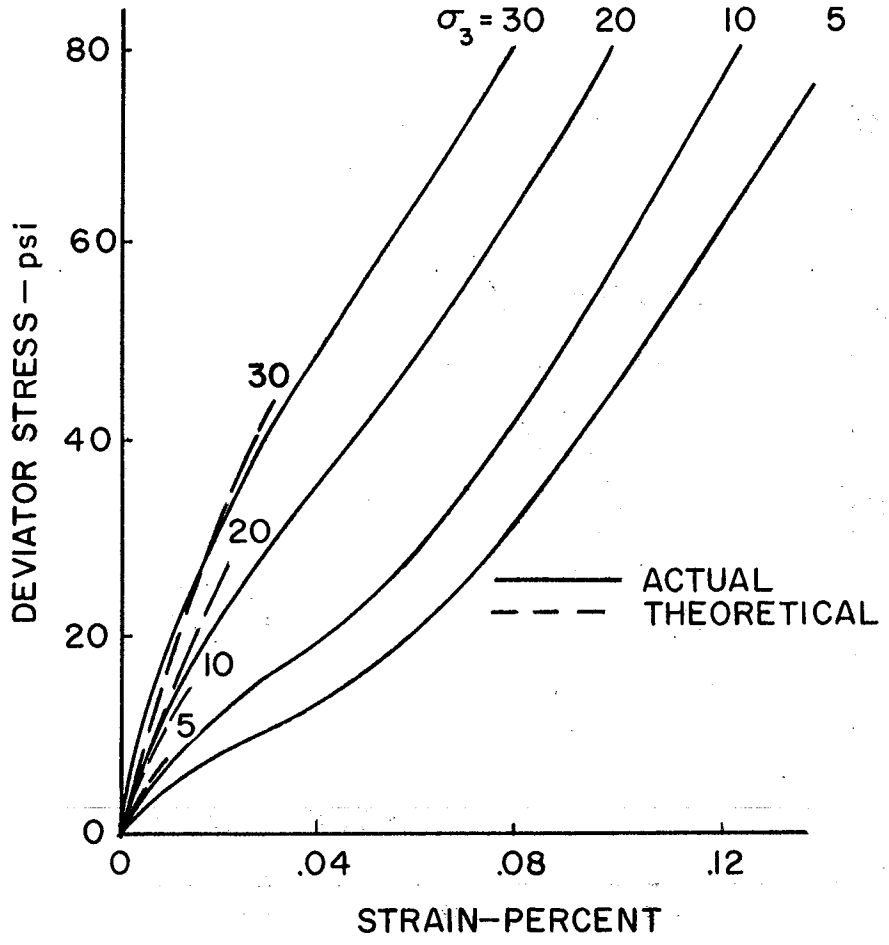

Figure 5.11 The comparison of actual stress-strain curves with theoretical curves for a three dimensional loose array under triaxial compression.

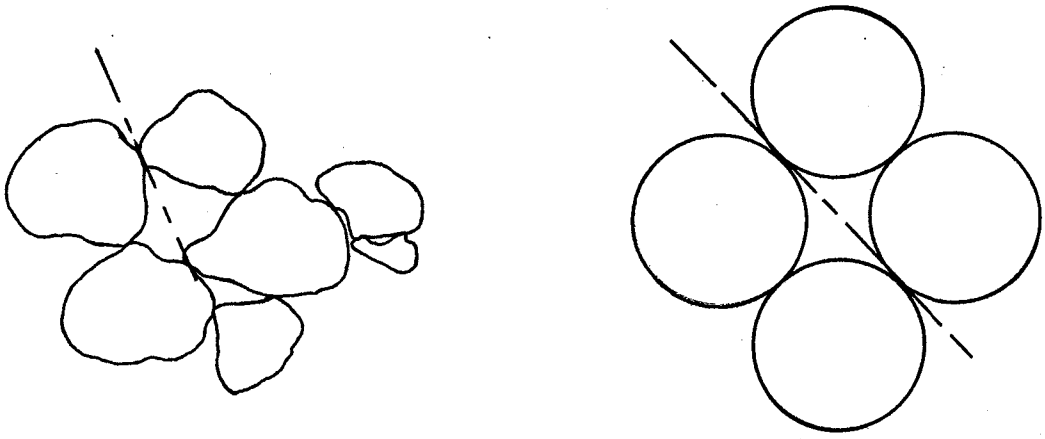

Figure 5.12 Actual soil compared with a theoretical array.

more strain. Also, the theoretical curves are based on smooth contact surfaces, thus modilizing complete friction, while according to Bowden and Tabor (33), the actual soil does not meet this assumption.

Failure of Three Dimensional Loose Array Under Triaxial Loading

It is seen from Figure 5.11 that under low confining pressures, sliding begins almost immediately in the spherical array. Once sliding occurs between the spheres, the deformation equations become indeterminate and there is no way of examining the stress-strain properties of the array subjected to greater loads. Thereafter, the strain is strictly a function of the changing geometry of the sphere array. The actual soil, on the other hand, was allowed to continue well past the point where sliding occurred, and a reorientation of particles allowed further increases in stress and strain.

There is a definite need for some type of computer technique that can predict the location of each sphere at any particular instant of time. With this available, strains which occur due to sliding of particles could be predicted and incorporated in subsequent deformation equations.

Results of Changing Parameters Under Triaxial Loading Conditions for the Three Dimensional Loose Array

When Poisson's ratio was the only parameter varied, there was no appreciable effect on the shape or load carrying capacity of the stress-strain curves as exemplified in Figure 5.13.

When F was increased, then a) the load carrying capacity of the array increased, and b) the secant modulus increased, i.e., the slope of the stress-strain curve became steeper (see Figure 5.14).

When the modulus of elasticity of the spheres was increased a) the tangent modulus increased, and b) the load carrying capacity of the array increased (see Figure 5.15).

As the confining pressure was increased then a) the load carrying capacity of the array increased; b) the secant modulus increased considerably (see Figure 5.16).

It is interesting to note the behavior of the strain ratio, $\Delta\epsilon_3/\Delta\epsilon_1$, shown in Table V.1. In every case the values are negative. They increase algebraically at the beginning of testing, but at some point the trend is reversed and they begin to decrease for the remainder of the test, indicating that the array is expanding radially.

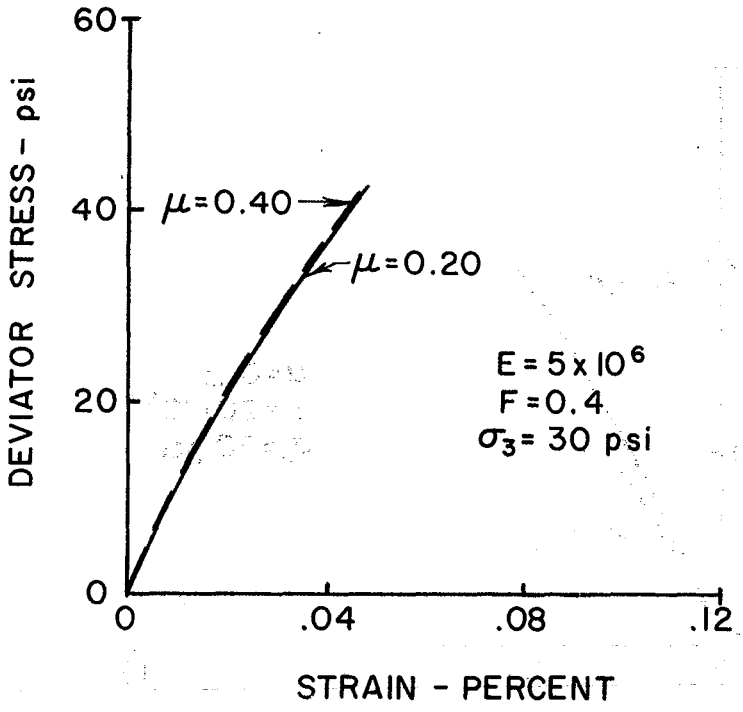

Figure 5.13 The effect of changing Poisson's ratio on a stress-strain curve (three dimensional loose array under triaxial compression).

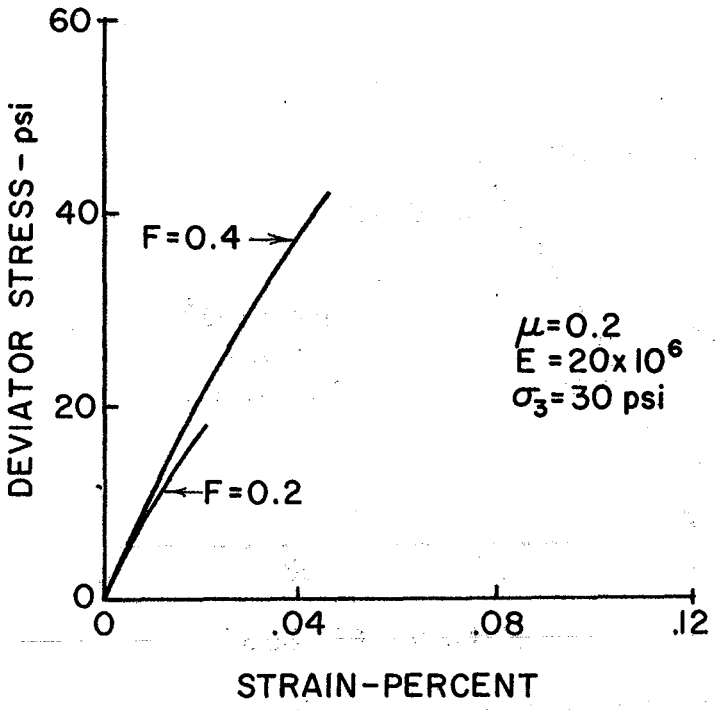

Figure 5.14 The effect of increasing the coefficient of friction on the shape of stress-strain curves (three dimensional loose array under triaxial compression).

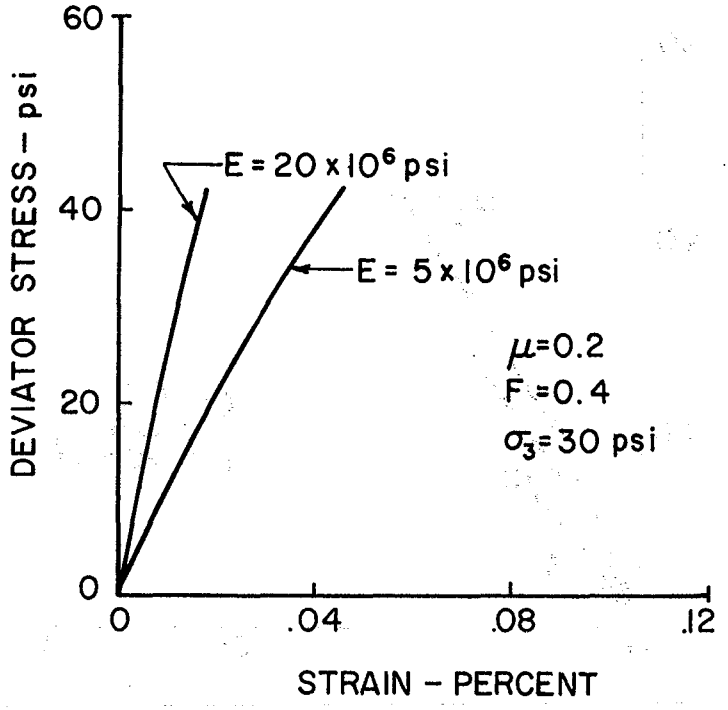

Figure 5.15 The effect of increasing the modulus of elasticity on the shape of a stress-strain curve (three dimensional loose array under triaxial compression).

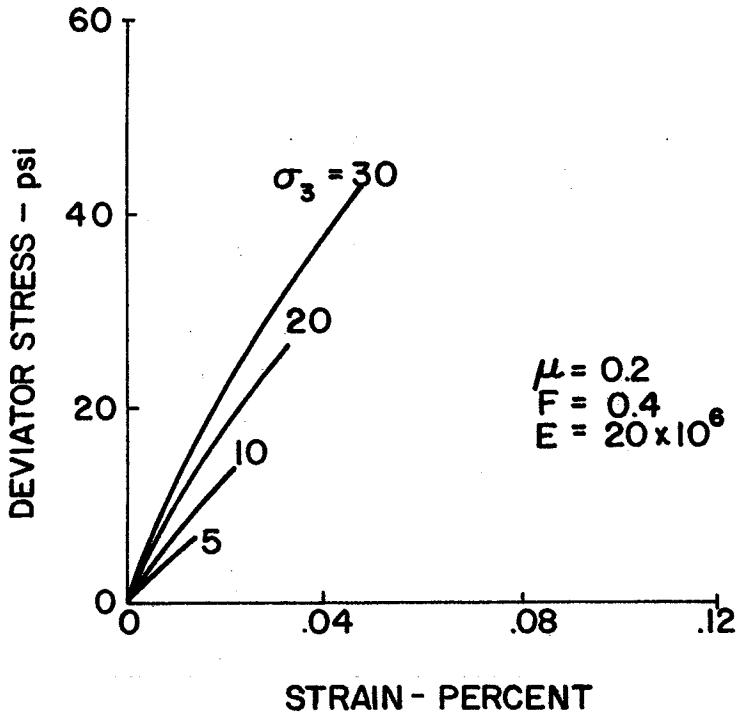

Figure 5.16 The effect of increasing the confining pressure on the shape of a stress-strain curve (three dimensional loose array under triaxial compression).

TABLE V.1

Strain Ratio Results for Triaxial Conditions

μ	F	E	SIGMA 3
0.2	0.2	10×10^6 psi	30 psi

DELTA SIGMA 1 (psi)	DELTA EPSILON 1 (in/in)	STRAIN RATIO
2.00	0.1816×10^{-4}	-0.0357
4.00	0.2435×10^{-4}	-0.0231
6.00	0.3701×10^{-4}	-0.0194
8.00	0.5008×10^{-4}	-0.0182
10.00	0.6370×10^{-4}	-0.0181
12.00	0.7807×10^{-4}	-0.0190
14.00	0.9356×10^{-4}	-0.0211
16.00	0.1111×10^{-3}	-0.0259
18.00	0.1356×10^{-3}	-0.0496

This bulging effect was actually observed in the soil specimens. The author has observed that Ottawa sand specimens which are initially in a rather loose state, bulge during triaxial testing.

In summary, the load carrying capacity of the array was affected little by changes in Poisson's ratio and the modulus of elasticity of the particles, but was notably influenced by the coefficient of friction and the radial stress. This is in agreement with the behavior of the dense planar array.

The strain, on the other hand, was affected by the modulus of elasticity, the coefficient of friction and the confining pressure. Poisson's ratio had no apparent effect on strain.

Comparison of Triaxial Compression Loading of the Three Dimensional Array with Deformation Hypotheses

When the results of the triaxial compression loading were compared with the deformation hypothesis described in Chapter I, it was noted that the curves exhibited a remarkable resemblance as far as shape was concerned to Dunlap's data from Texas triaxial tests (Figure 5.17). However, the magnitude of the theoretical modulus of deformation was ten times as great as those of actual soils (compare Figure 5.18 and 1.1), indicating a much greater stiffness than actually occurred in the test specimens. This is probably due to assumption of perfect contacts between spheres which is unrealistic in actual soils. The data for the curve in Figure 5.18 are shown in Table V.2.

Results of the One Dimensional Compression of the Three Dimensional Array

Unlike the triaxial loading, the one dimensional compression conditions did not produce early failures since slide could not generally occur for the range of parameters studied. The slope of the curves continued to increase throughout their entirety. Therefore, instead of automatically terminating the calculations when slide occurred -- as in the triaxial loading condition -- the one dimensional compression curves were stopped when the vertical stress reached 100 psi.

When compared to the actual stress-strain curves used for evaluating the loose planar array (Figure 5.1) and the dense planar array (Figure 5.6), the one dimensional compression of the three dimensional array did not produce a good fit (Figure 5.19). The range of strain was too small, and the shape of the curves did not resemble those of the actual soil. In general, the slopes of the stress-strain curves were concave to the stress axis and much too steep.

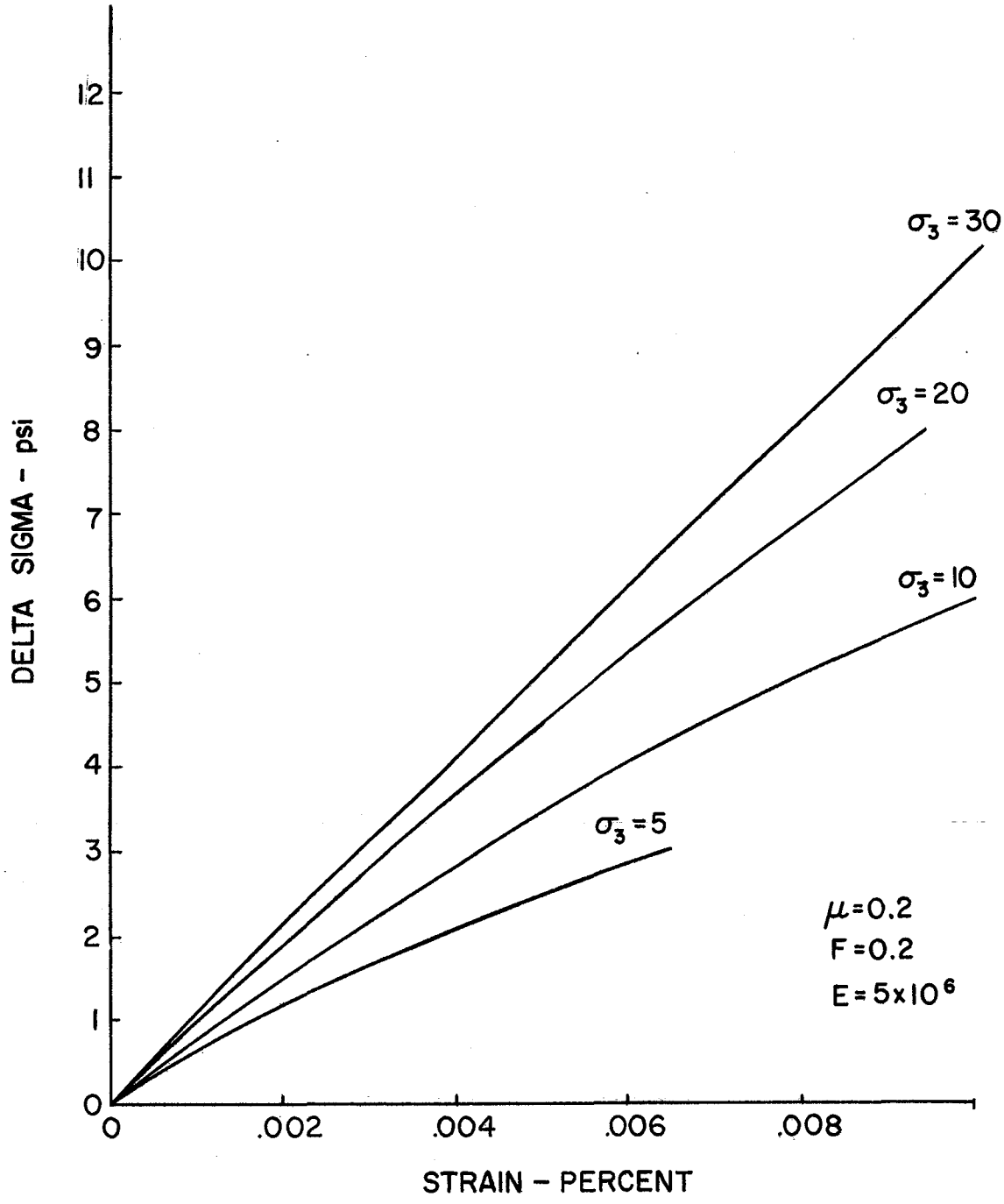

Figure 5.17 A typical fan-shaped array of curves from which M_Z values were calculated.

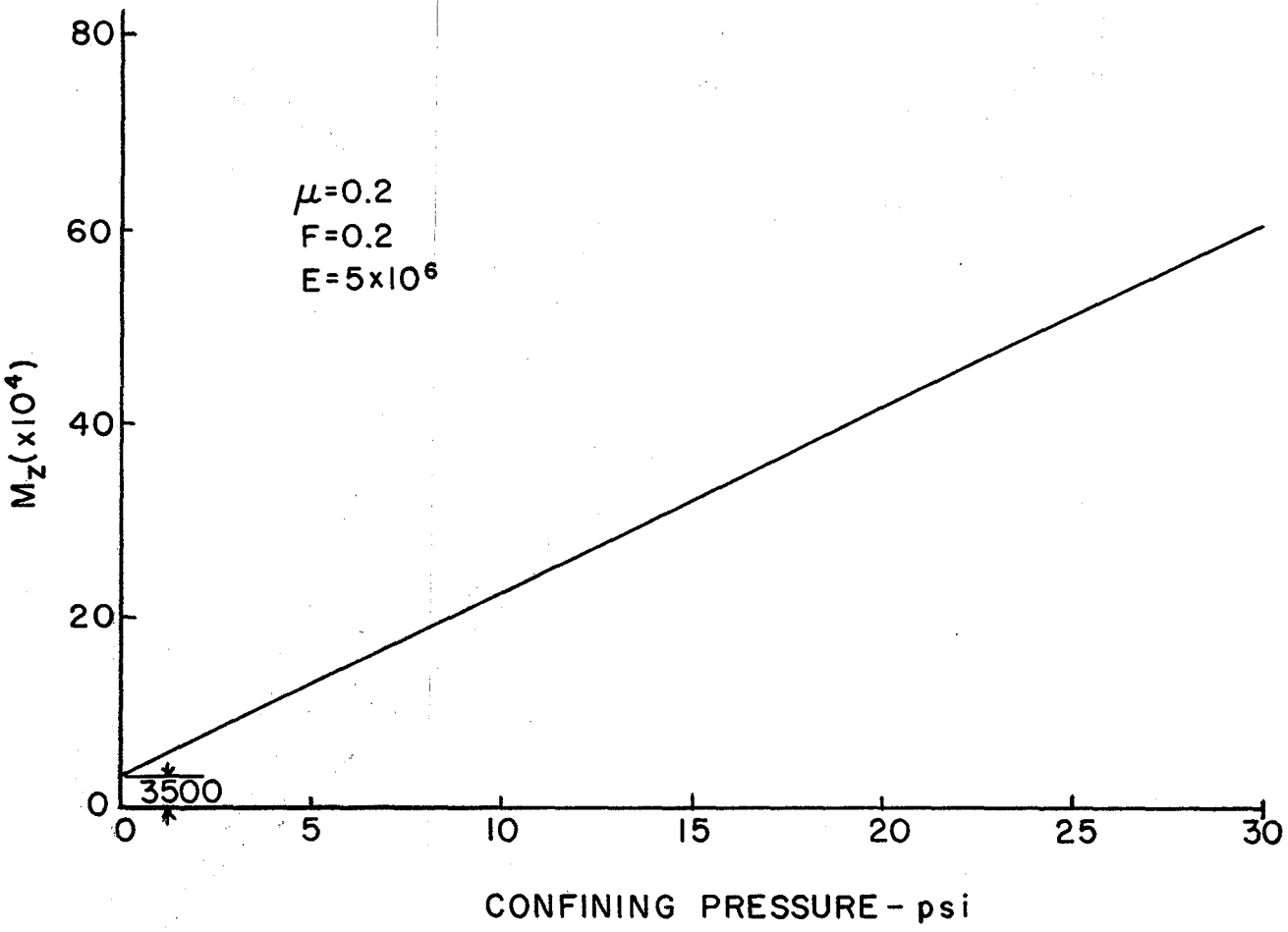

Figure 5.18 A plot of M_z versus confining pressure for the theoretical triaxial conditions.

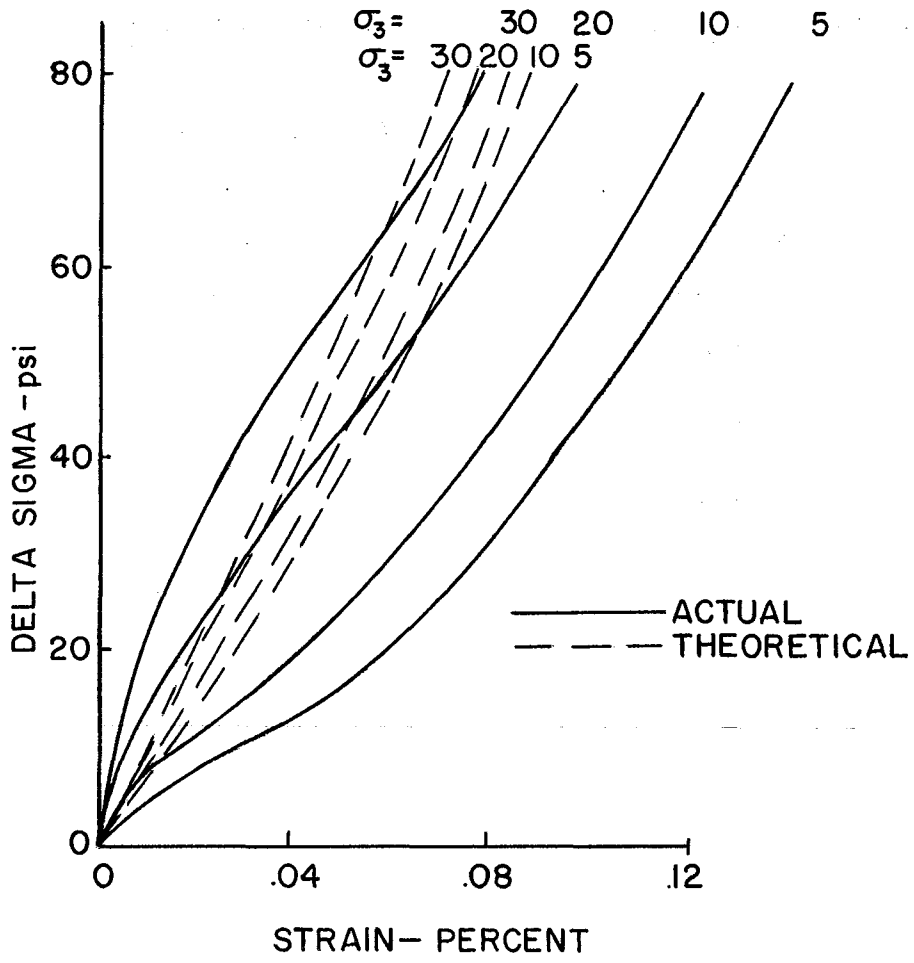

Figure 5.19 Actual stress-strain curves compared with stress-strain curves for three dimensional loose array under one dimensional compression.

TABLE V.2

Results of M_z Calculations for Triaxial Compression Conditions

$\mu = 0.2$ $F = 0.2$ $E = 5 \times 10^6$

ϵ	$\sigma_1 - \sigma_3$	σ_3	σ_1	M_z
0.00006	2.8	5	7.8	130,000
0.00006	4.05	10	14.05	234,167
0.00006	5.30	20	25.30	421,667
0.00006	6.10	30	36.10	601,667

One dimensional compression results were also compared to stress-strain curves of specimens of material other than those used in evaluating the other arrays (see Figures 5.20, through 5.23). These specimens had been subjected to several hundred thousand repetitions of load before the stress-strain curves were determined. In every case, the range of strains for the theoretical curves was too small, and they lacked the general shape of the experimental curves. The modulus of deformation was very high for the theoretical case. The reason for this becomes readily apparent upon examining the stress ratio, $\Delta\sigma_3/\Delta\sigma_1$, (see Table V.3). It increased up to a point and then remained constant thereafter. This indicated that the radial stress continued to increase as the vertical stress increased, thus causing the secant modulus to increase.

The high stiffness as well as the small range of strain values may be due to larger actual areas of contact between perfect equiradii spheres than between actual particles. If random sizes of spheres had been used, the contact areas would have varied from very small to quite large, and it may have been possible to gain a better fitting model.

There was an initial high tangent modulus which decreased after the first load increment and thereafter increased (Figure 5.25). This indicates that there was a slight reverse S-shaped curvature near the origin. It was not as evident in the three dimensional array as it was in Bratton's (10) two dimensional array, and the various parameters seemed to have little or no effect on the location of the inflection point.

Effect of Parameter Variation for Three Dimensional Array Subjected to One Dimensional Compression

The one dimensional compression calculations were made for the same parameters as in the triaxial compression condition, and the following observations were made:

A) An increase in Poisson's ratio had little effect on the shape of the stress-strain curve; however, it did increase the tangent modulus by a small amount (see Figure 5.25).

B) As the coefficient of friction increased, the shape of the curve did not change appreciably (see Figure 5.26).

C) As the modulus of elasticity increased the secant modulus increased markedly (see Figure 5.27).

D) As the initial confining pressure increased, the tangent modulus increased, but only a relatively small amount (see Figure 5.28).

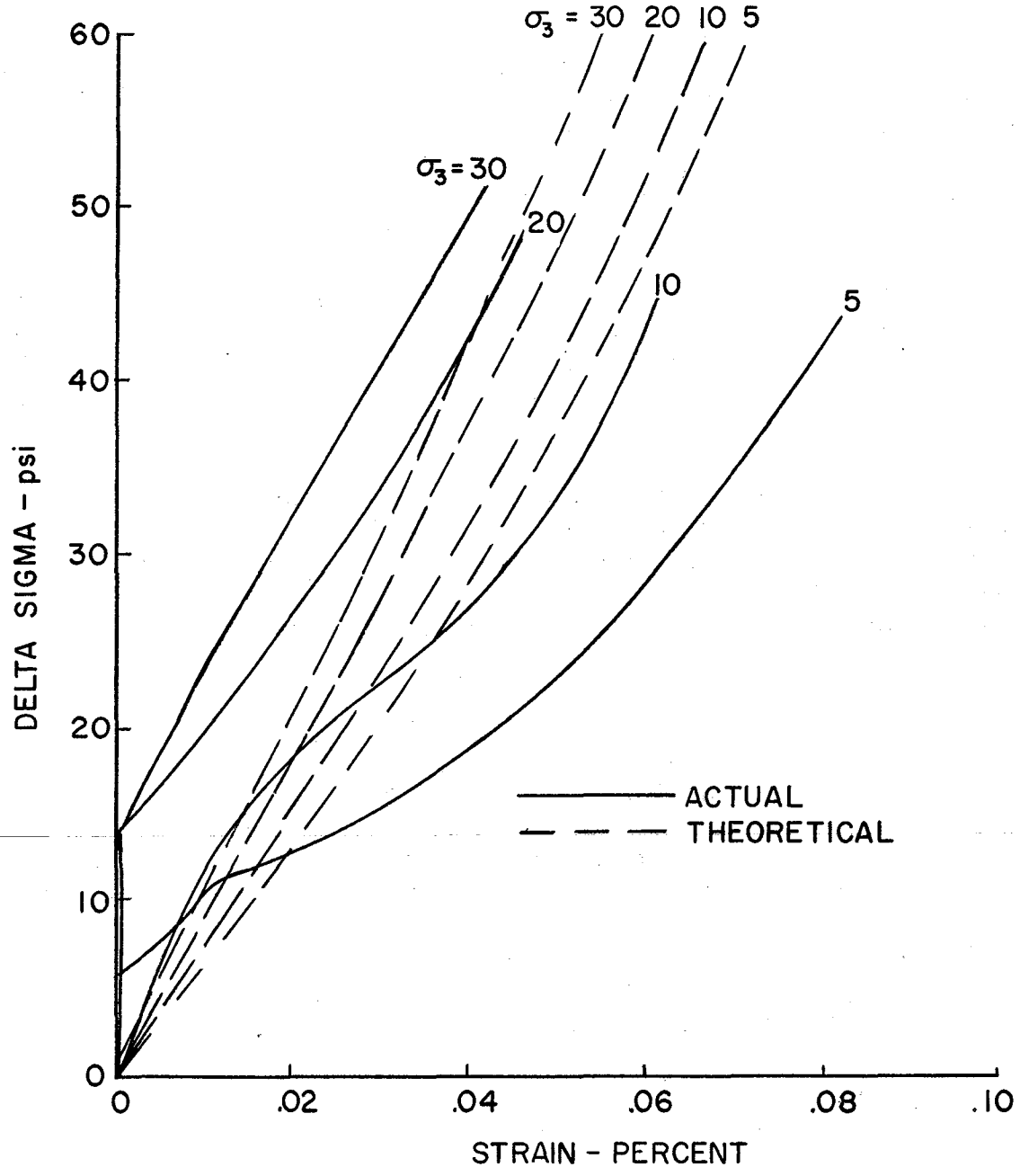

Figure 5.20 Stress-strain curves for a three dimensional loose array under one dimensional compression, compared with experimental stress-strain curves.

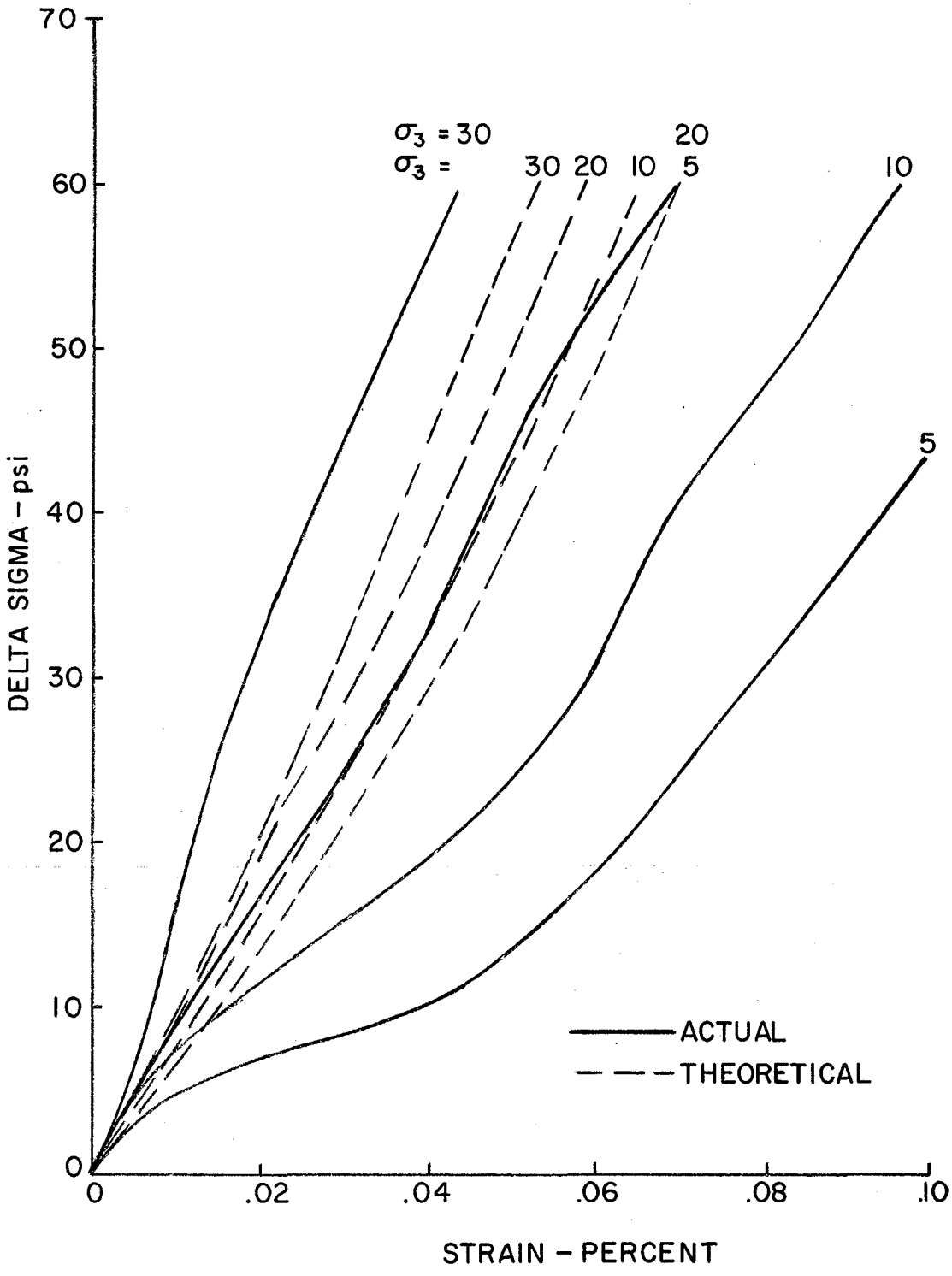

Figure 5.21 Stress-strain curves for a three dimensional loose array under one dimensional compression, compared with experimental stress-strain curves.

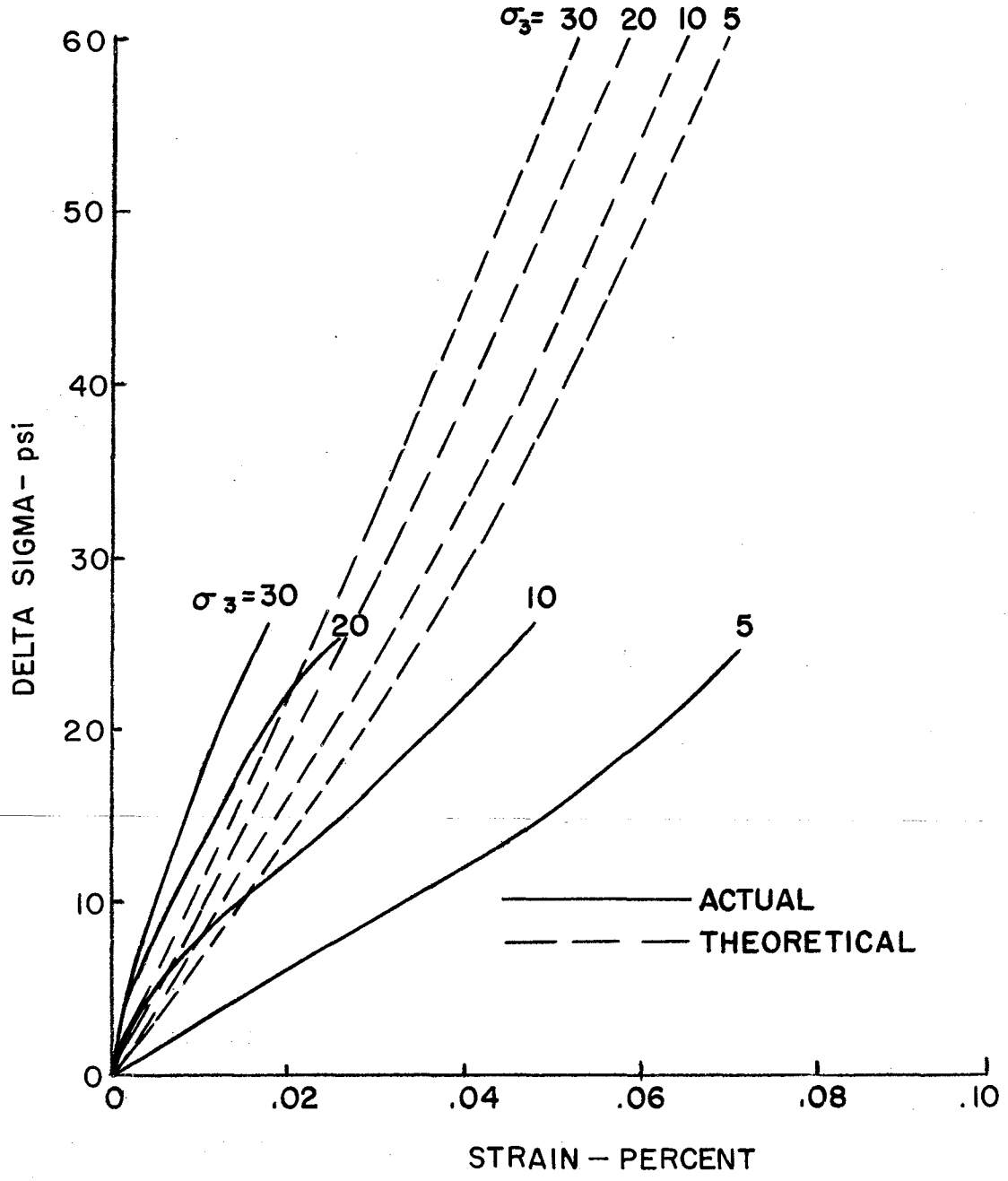

Figure 5.22 Stress-strain curves for a three dimensional loose array under one dimensional compression, compared with experimental stress-strain curves.

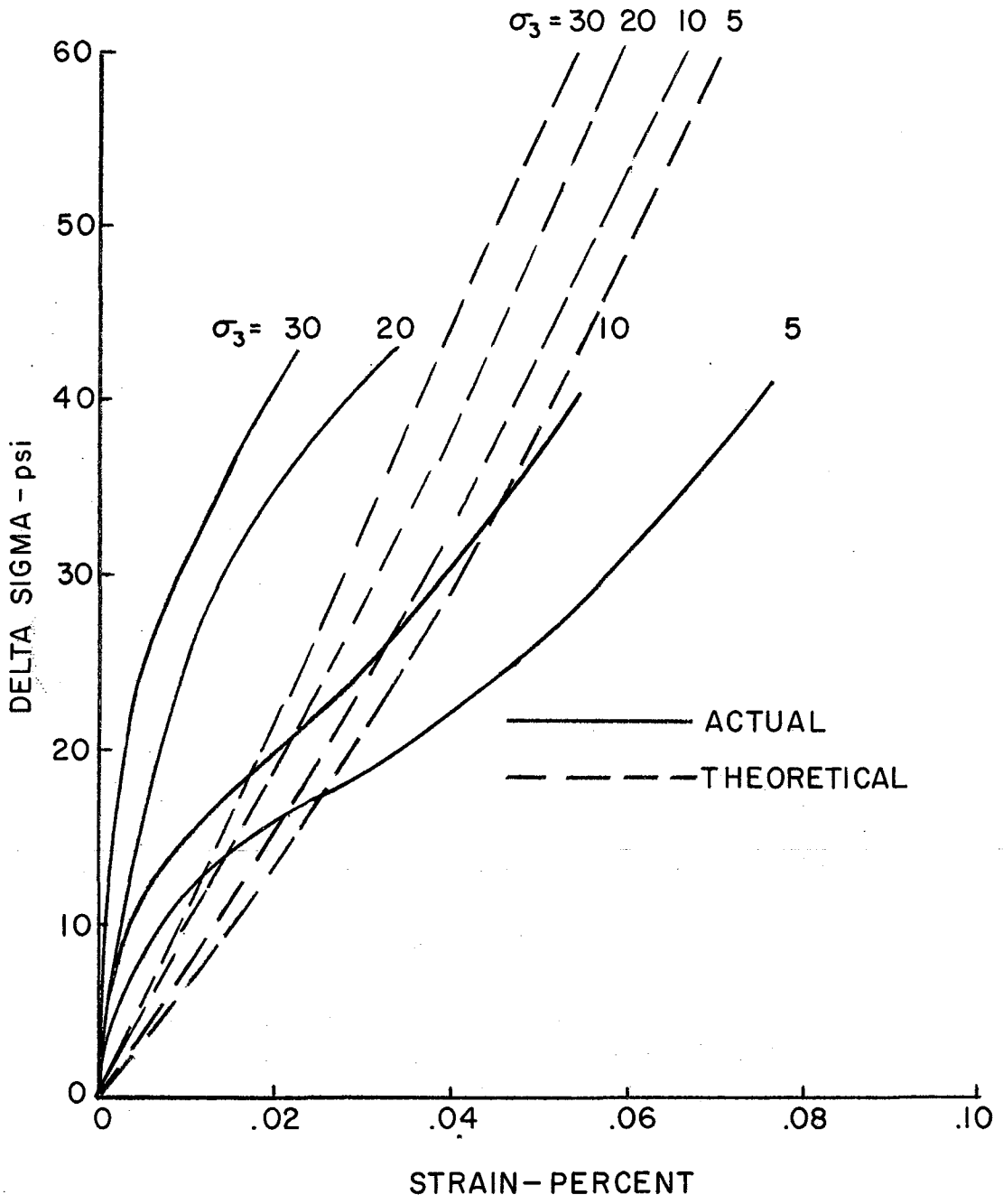

Figure 5.23 Stress-strain curves for a three dimensional loose array under one dimensional compression, compared with experimental stress-strain curves.

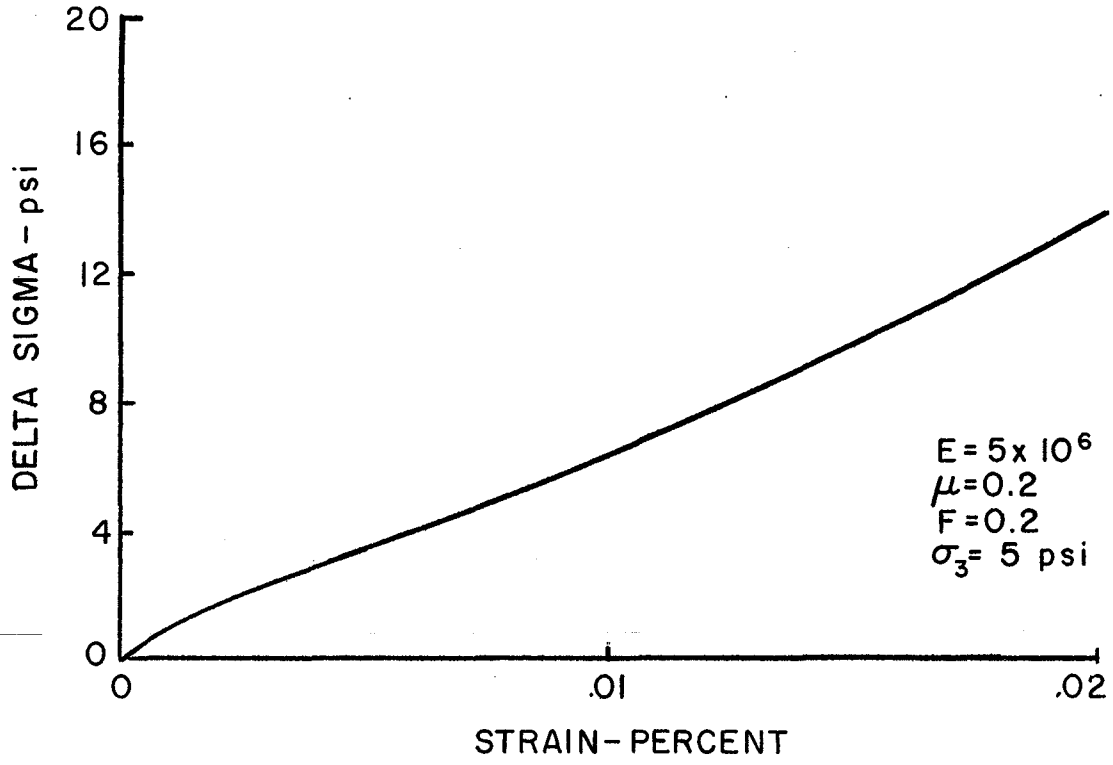

Figure 5.24 An indication of the reverse S-shape curvature near the origin for a three dimensional loose array under one dimensional compression.

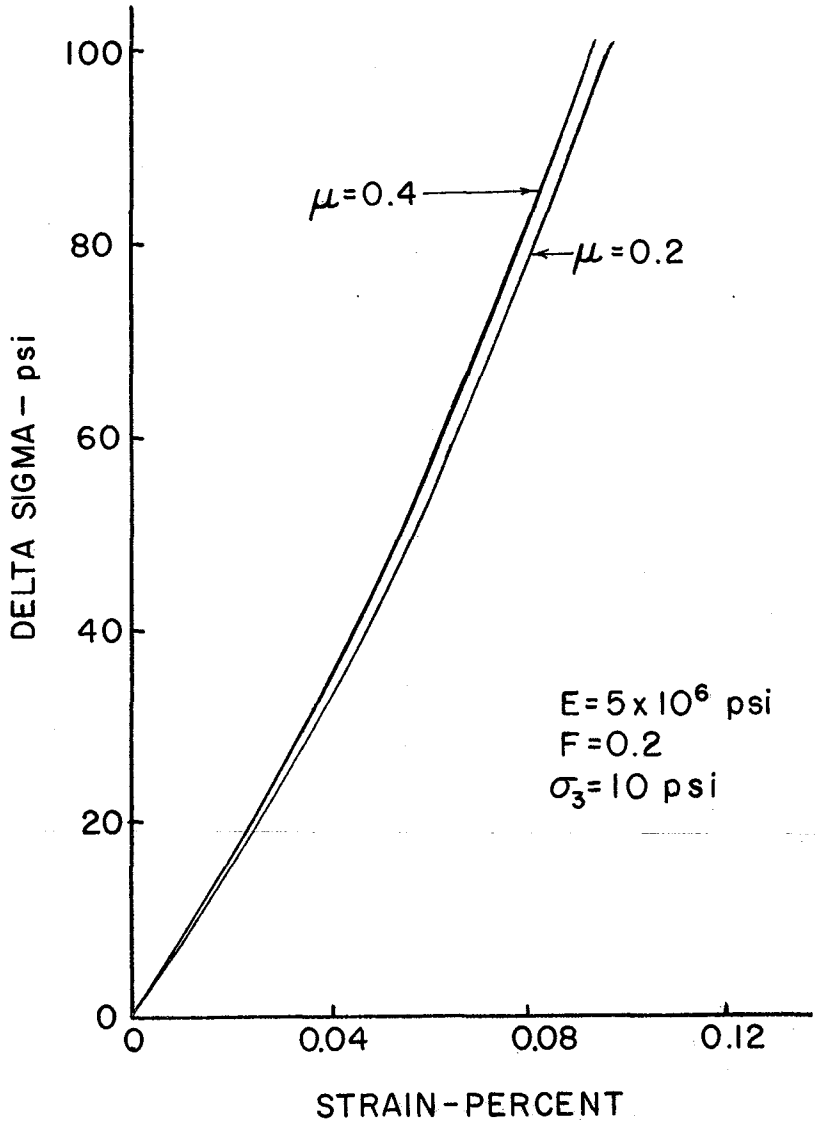

Figure 5.25 The effects of varying Poisson's ratio on stress-strain curves (three dimensional loose array under one dimensional compression).

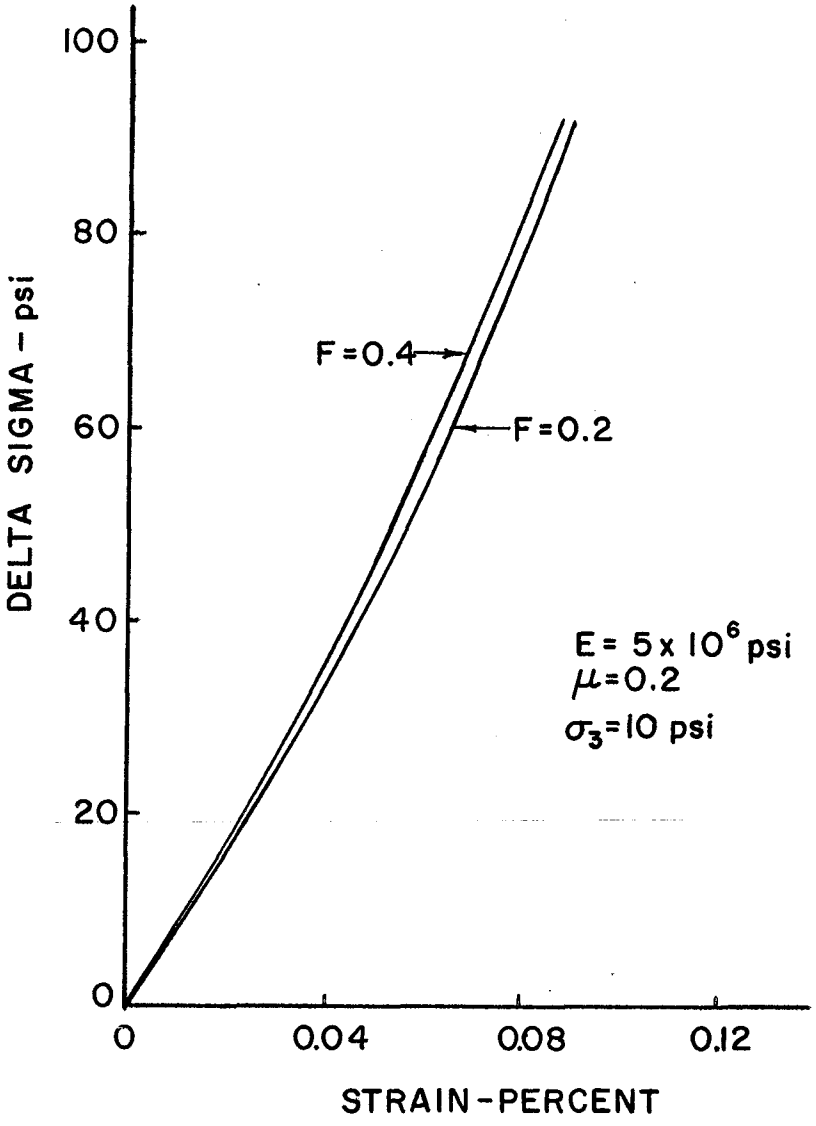

Figure 5.26 The effects of increasing the coefficient of friction on a stress-strain curve (three dimensional loose array under one dimensional compression).

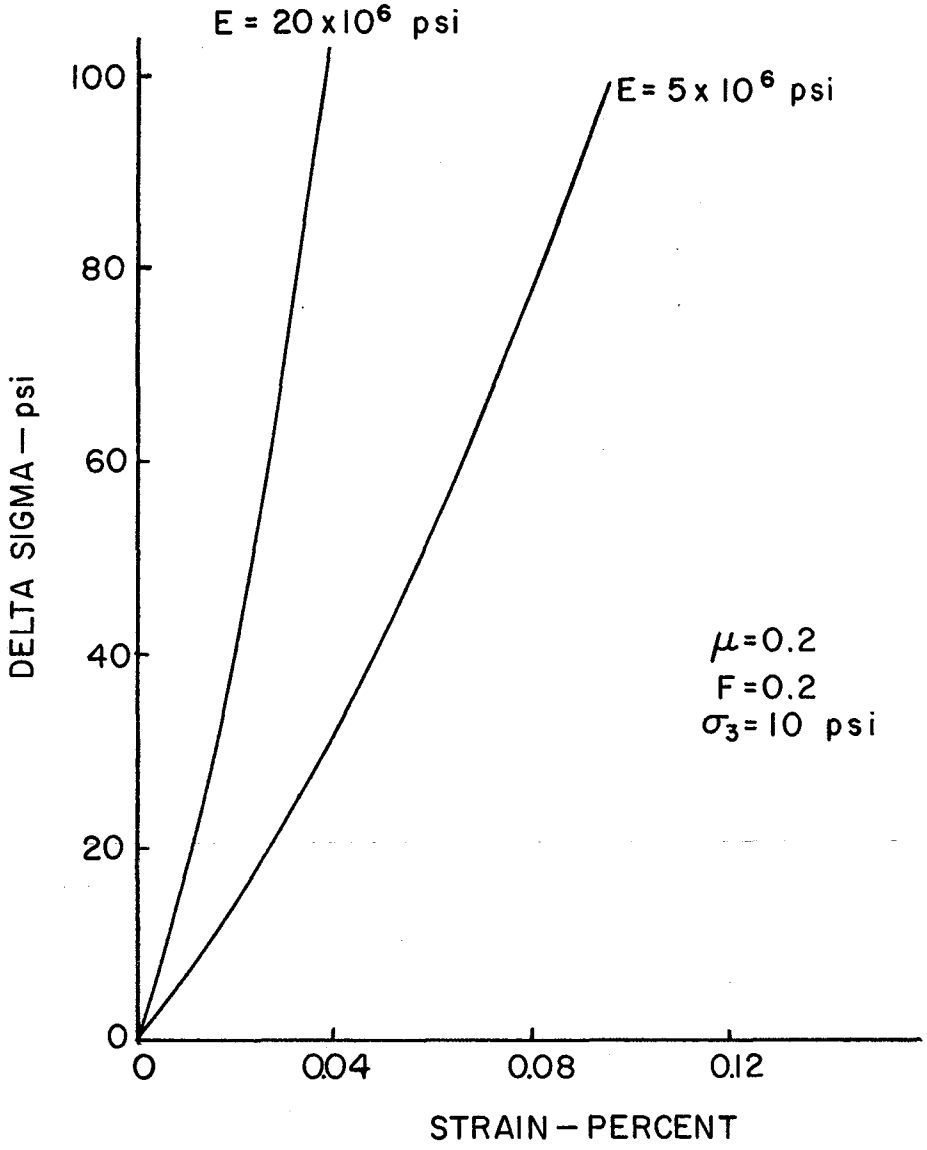

Figure 5.27 The effect of increasing the modulus of elasticity on a stress-strain curve (three dimensional loose array under one dimensional compression).

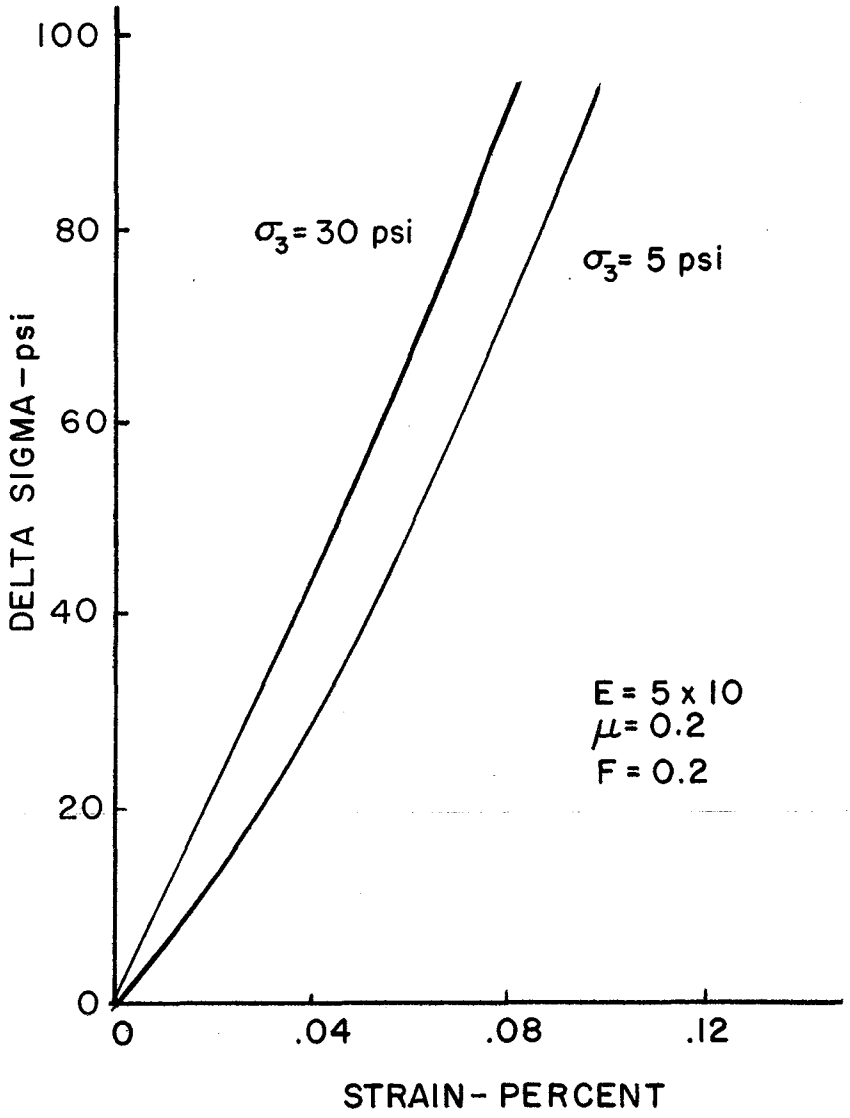

Figure 5.28 The effects of increasing the confining pressure on a stress-strain curve (three dimensional loose array under one dimensional compression).

TABLE V.3

Stress Ratio for One Dimensional Compression Conditions

μ	F	E	σ_3
0.2	0.2	5×10^6 psi	5.0 psi

DELTA SIGMA 1 (psi)	DELTA EPSILON 1 (in/in)	STRESS RATIO
5.32	0.8637×10^{-4}	0.4929
9.15	0.1463×10^{-3}	0.5196
12.88	0.2015×10^{-3}	0.5448
16.50	0.2526×10^{-3}	0.5730
19.97	0.2984×10^{-3}	0.6237
23.37	0.3385×10^{-3}	0.6237
27.76	0.3770×10^{-3}	0.6237
30.15	0.4142×10^{-3}	0.6237
33.54	0.4502×10^{-3}	0.6237
50.50	0.6165×10^{-3}	0.6237
80.46	0.8735×10^{-3}	0.6237

Comparison of One Dimensional Compression of the Three Dimensional Array With Variable Confining Pressure Tests

The one dimensional compression calculations produced curves which resemble experimental curves reported by O'Brien (20) for variable confining pressure triaxial tests. A constant ratio of σ_3 to σ_1 was maintained in these tests. Figures 5.29, 5.30 and 5.31 show theoretical curves compared to O'Brien's experimental curves. Although the strain depicted by the theoretical stress-strain curves was of the correct order of magnitude, in almost every case the experimental curves were not as steep as the theoretical ones. This may be due to the extremely slow rate of strain which O'Brien used (0.005 inches per minute). If facilities had permitted rapid loading, the experimental curves would undoubtedly have been much steeper, as indicated by Casagrande (31) and others.

Effects of Pore Pressures

The particulate theory as now set up does not consider pore pressures. However, these pressures do exist in actual soils subjected to rapid repetitive loading. The first few load repetitions cause considerable permanent deformation in a soil specimen, and during these repetitions -- since the permeability of the soil is relatively low -- the pore pressures may become quite high. The build up of positive pore pressures will cause the slope of the dynamic stress-strain curve to decrease. As the number of stress repetitions increase, the particles slide past each other into more favorable positions to carry the stress while water and air is extruded from the specimen. At times during the life of a specimen, the total and effective stresses may be nearly equal.

Bishop (29, 30) proposed the following relationship for the effective stress in soils:

$$\bar{\sigma} = \sigma - u_a + \chi (u_a - u_w) \qquad \text{Equation (5.1)}$$

where: $\bar{\sigma}$ = effective stress

σ = total applied stress

u_a = pore air pressure

u_w = pore water pressure

χ = a parameter which depends on the degree of saturation (Figure 5.32), cycle of wetting and drying or stress change.

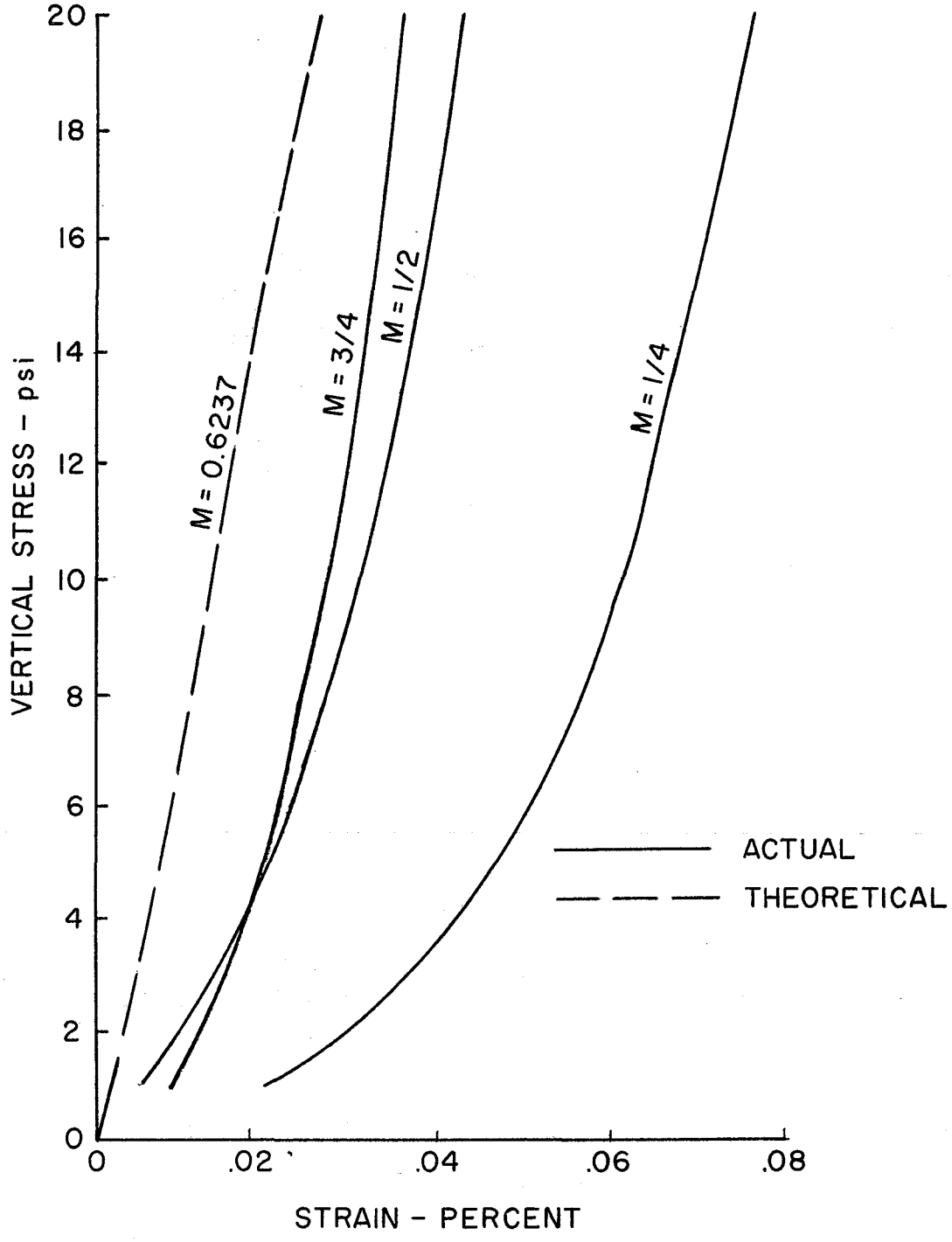

Figure 5.29 Stress-strain curves showing the effect of varying the confining pressure on material RP-23-1, compared with the stress-strain curve of a three dimensional loose array under one dimensional compression.

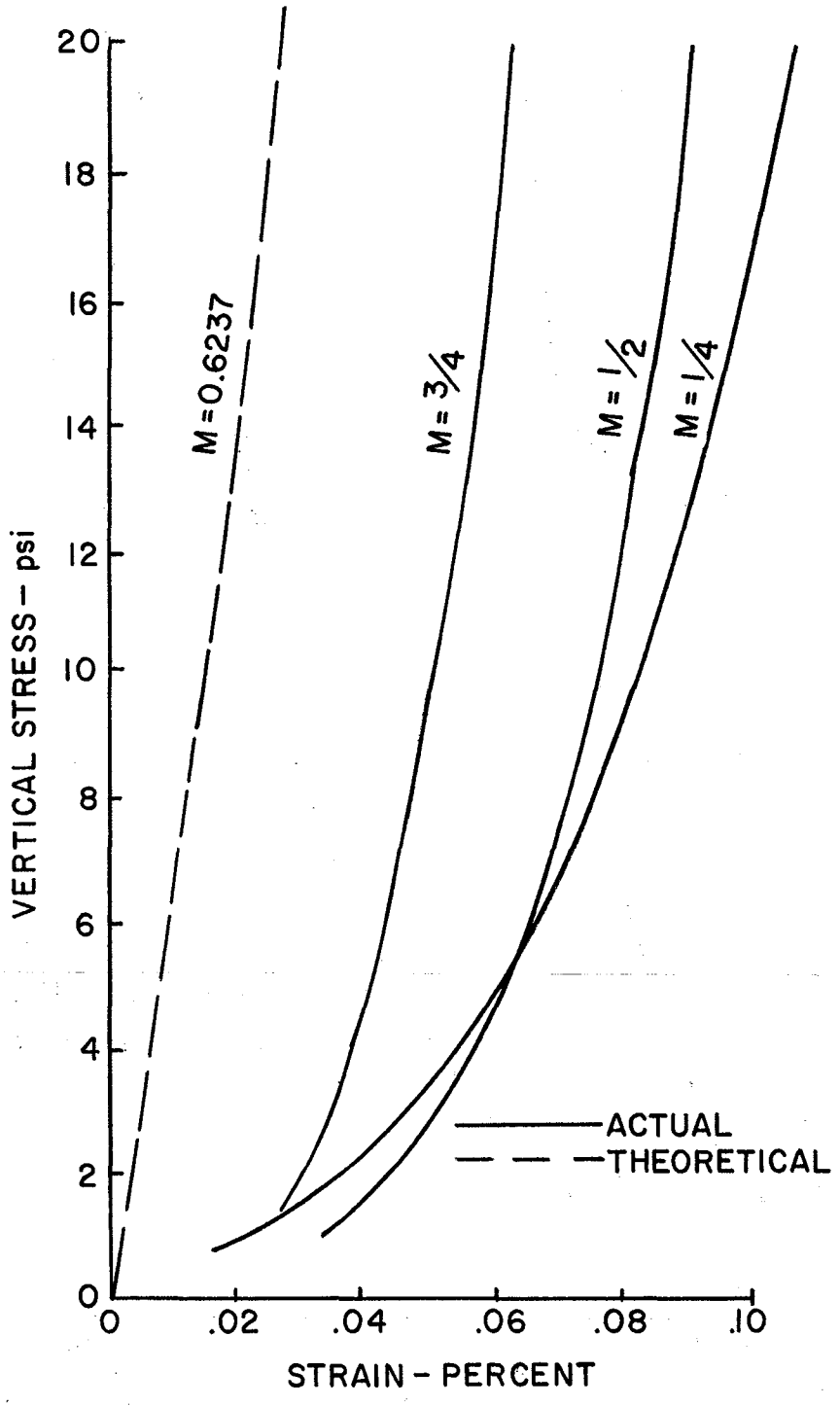

Figure 5.30 Stress-strain curves showing the effect of varying the confining pressure on material RP-23-2, compared with the stress-strain curve of a three dimensional loose array under one dimensional compression.

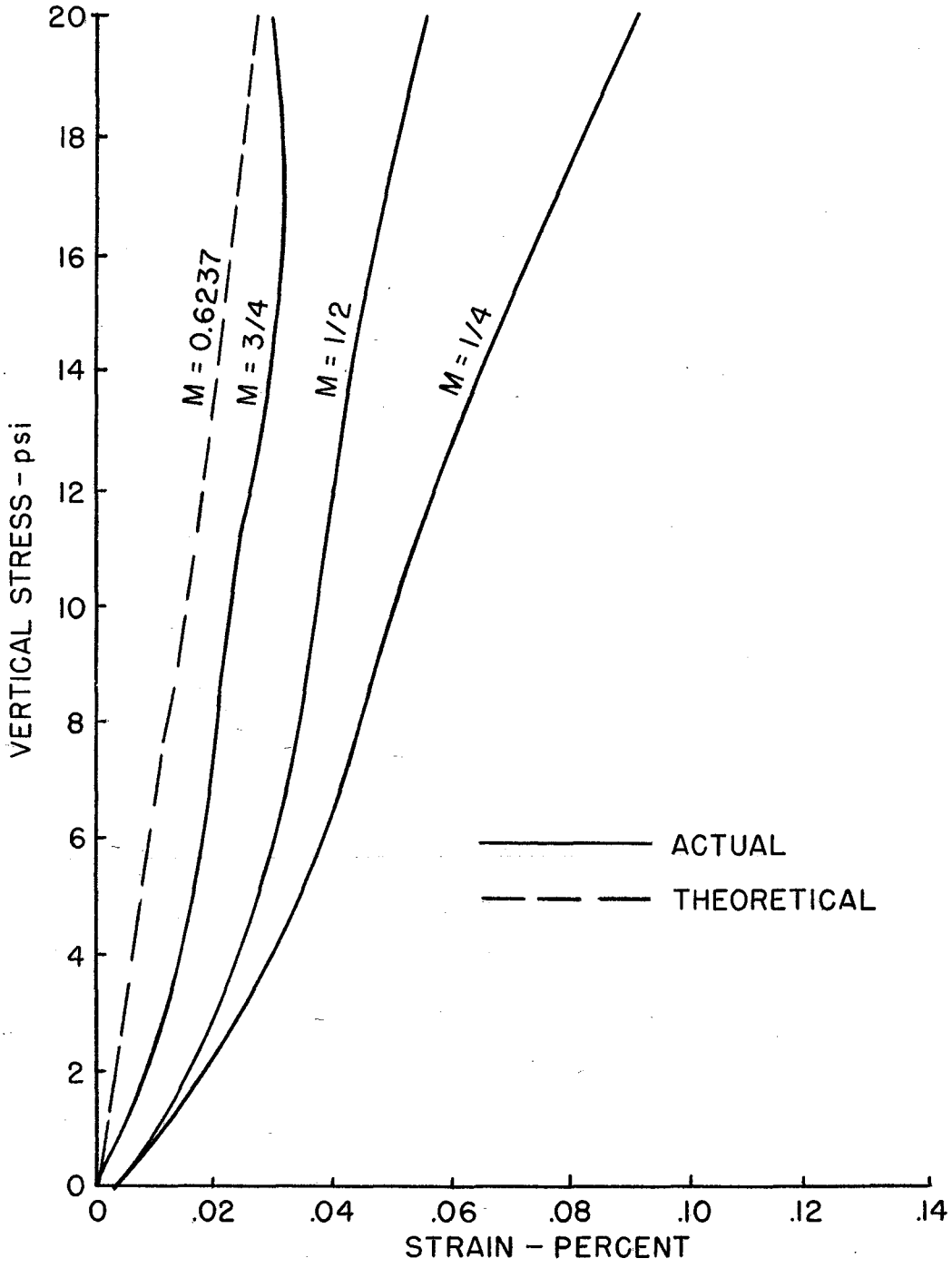

Figure 5.31 Stress-strain curves showing the effect of varying the confining pressure on material RP-23-3, compared with the stress-strain curve of a three dimensional loose array under a dimensional compression.

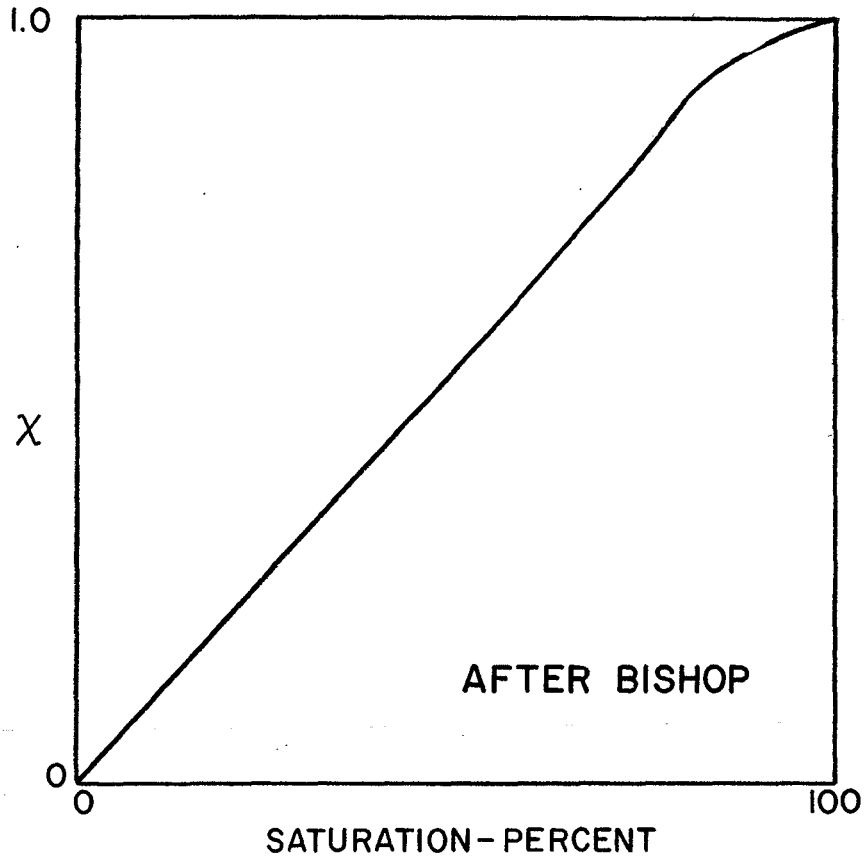

Figure 5.32 Probable distribution of the parameter x with degree of saturation.

As the number of load repetitions on a specimen increases, the degree of saturation, and thus χ, also increase. Depending on the corresponding changes in the pore air and water pressures, and effective stress -- which influences the shape of the stress-strain curve -- will either increase or decrease: if the effective stress decreases, the stress-strain curve will become flatter.

Figure 5.33 shows stress-strain curves of a typical repetitive test specimen at different numbers of repetitions. At 350 repetitions, the combination of χ, u_a and u_w apparently produces a lower effective stress than at 33,300 or 246,700 repetitions. And at 246,700 repetitions, and the effective stress appears to be generally less than it is at 33,300 repetitions.

The change in the degree of densification with the number of repetitions will also influence the shape of the stress-strain curves.

Thus, until dynamic pore pressures can be measured in repetitively loaded specimens little can be said about their influence except they do affect the shape of the stress-strain curves.

Effect of Degradation on the Frictional Resistance of the Soil

Dunlap (15) reported that degradation of the test material under repetitive loading was so insignificant that a detailed analysis was not required. However, the minute amount of degradation which occurred probably took place at the points of contact between particles. This could influence the frictional resistance between particles and cause the stress-strain characteristics to change with the number of repetitions.

To ascertain whether degradation influences the shape of the stress-strain curves, it would be necessary to perform a detailed study which would incorporate the measurement of degradation and dynamic pore pressures within the specimen to actually differentiate between the effect of wear on contact surfaces and the influence of pore pressure. Also, the original gradation would need to be more closely controlled. Until this time, the variation in frictional resistance with repetitions can only be assumed.

Elastic Strain in the Triaxial Cell

There is a certain amount of error induced into the experimental data as a result of elastic deformation in the triaxial cell. This deformation was determined under static load conditions substituting a concrete cylinder for a specimen. Although corrections were made, this static deformation may not be the same as that induced by dynamic loads. Also, the deformation in the cell using the concrete cylinder may not be the same as if soil were used.

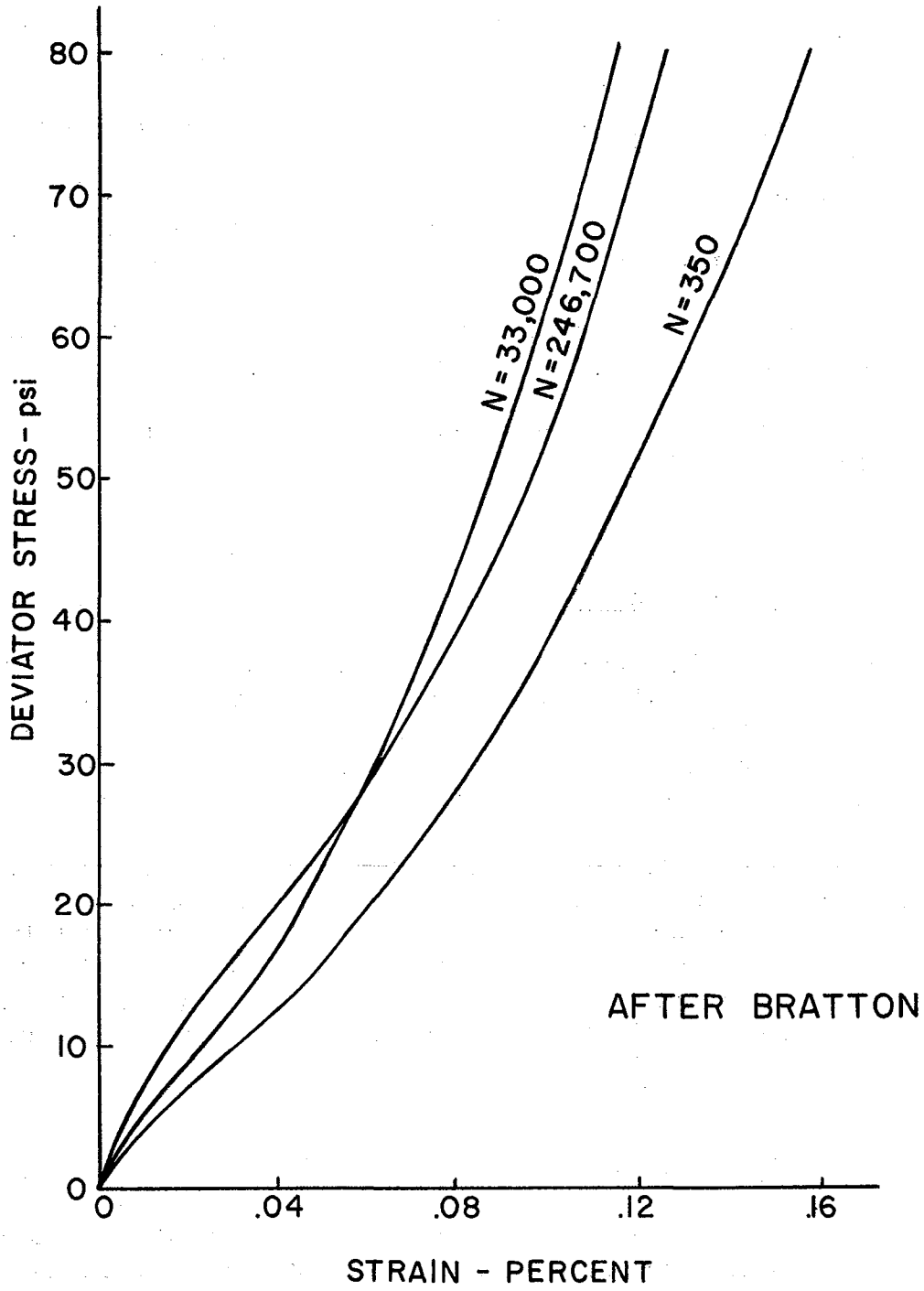

Figure 5.33 Variation in stress-strain curve with repetition of load.

To improve the accuracy of the strain calculations, it would be necessary to measure deformations within the central portion of the specimens. Facilities are now available for making these measurements. There are optical tracking devices which will lock onto any optical discontinuity in view and indicate the relative pisition of it by means of voltage output. There is a similar device which measures linear movement by measuring the amount of light reflected from a light source of known intensity. The use of instruments such as these can greatly enhance the probability of correlating theoretical with actual results.

CHAPTER IV

CONCLUSIONS

A theoretical analysis was conducted of the strains occurring in three different arrays. First, a two dimensional loose array was subjected to one dimensional compression; second, a two dimensional dense array was subjected to triaxial compression; and third, a three dimensional loose array was subjected to both triaxial and one dimensional compression conditions. The deformation equations for each of these arrays were developed, and a parametric study conducted for each of the above states. Finally, the computed theoretical stress-strain curves were compared to actual stress-strain curves of a cherty limestone gravel.

The following conclusions can be drawn from the loose planar array subjected to triaxial compression conditions:

1. A planar array of elastic spheres produces stress-strain curves which resemble granular materials subjected to rapid repetitive loading, though the effect of increasing the confining pressure was less than that observed for real soils.

2. To gain close agreement between theoretical and actual results, equations must be developed to allow slide and counter slide between particles.

When the dense planar array was considered the conclusions below were drawn:

1. The stress-strain curves, within the range of E, μ and F considered, did not have the reverse S-shape typically observed for real soils.

2. The stress-strain curves were always concave to the strain axis.

3. Increasing the coefficient of friction markedly increased the stress at which failure (sliding) occurred.

4. As for the planar array, the effect of increasing the confining pressure resembled the effect observed for real soils, but was less pronounced.

5. The stress-strain curves for the loose planar array subjected to one dimensional compression showed greater similarity to the actual curves.

The following conclusions can be drawn from the triaxial compression study of a three dimensional loose array of equiradii spheres:

1. There was not a close fit between theoretical stress-strain curves and actual stress-strain curves.

2. The computed triaxial compression curves, at least within the ranges of parameters studied, did not have the reverse S-shape typical of actual stress-strain curves.

3. The triaxial compression equations become indeterminate when the tangential stress equals the product of the normal stress and the coefficient of friction. Thereafter, the strain is strictly a function of the changing geometry of the array and cannot be explained with the present theory.

4. The three dimensional theory does predict the fan-shaped array typical of actual stress-strain curves, but to a lesser degree than usually observed.

5. The theoretical modulus of deformation versus radial stress curves resemble those obtained experimentally by Dunlap (27), but the theoretical modulus is too high by about one order of magnitude.

The conclusions below can be drawn from the analysis of the one dimensional compression conditions for the three dimensional loose array:

1. The stress-strain curves are generally concave to the stress axis. There is a very slight reverse curvature near the origin which is not noticeable on small scale representations of the stress-strain curves.

2. The theoretical curves resemble curves from variable confining pressure tests reported by O'Brien (20).

3. The secant moduli of the theoretical curves are too high to allow comparison with the family of experimental curves.

4. The one dimensional compression theory predicts the typical fan-shaped array of stress-strain curves observed in actual soils, but the range of strains in smaller than those observed in experimental soils.

5. The three dimensional model does not appear to give as good a correlation with experimental data as the loose planar array.

The following general comments are relevant:

1. It will be necessary to know the variations in pore pressures before changes in the coefficient of friction with increased stressing can be assessed.

2. The particulate theory seems to give results more consistent with experimental conditions than elastic theory applied to a continuous medium, but more study is needed before close correlations can be made with actual stress-strain curves.

CHAPTER VII

RECOMMENDATIONS

This research was exploratory in nature. Thus, relatively simple arrays of equiradii elastic spheres were chosen for the analyses. A number of refinements can be made which may enhance the chances of better agreement between theory and experimental results. A few suggestions for future consideration are as follows:

1. Vary the diameter of the spheres, calculate the number of contact points and relate these to experimental conditions.

2. Perform variable confining pressure tests on specimens of equiradii spheres with known elastic constants and relate these to theory.

3. Evaluate the effect of non-spherical particles in the array.

4. Develop equations or computer techniques which will permit computation of strains after sliding of the particles begins.

5. Determine the effects of one dimensional compression on a dense planar array.

6. Determine the effects of unloading and reloading on a three dimensional loose array.

7. Determine the actual frictional resistance in an experimental soil and compare these to values of solid block movement.

REFERENCES

1. Heierli, Werner, "Inelastic Wave Propagation in Soil Columns," Journal of Soil Mechanics and Foundation Division Proceedings of the American Society of Civil Engineers, Vol. 88, No. SM6, Dec., 1962.

2. Hendron, A. J., Jr., Fulton, R. E., and Mohraz, Bijan, "The Energy Absorption Capacity of Granular Materials in One-Dimensional Compression," Technical Documentary Report No. AFSWC - TDR - 62 - 91, Department of Civil Engineering, University of Illinois, Jan., 1963.

3. Whitman, Robert V., Miller, E. T. and Moore, P. J., "Yielding and Locking of Confined Sand," Journal of Soil Mechanics and Foundation Division Proceedings of the American Society of Civil Engineers, Vol. 90, no. SM4, July, 1964, pp. 57-84.

4. Timoskenko, S. and Goodier, J. N., "Theory of Elasticity," McGraw-Hill Book Company, Inc., 1951, pp. 372-373.

5. Cattaneo, C., "Sul Contatto di due Corpi Elastici," Accademi dei Lincei, Rendiconti, Series 6, Vol. 27, 1938, pp. 342-348, 434-436 and 474-478.

6. Mindlin, R. D., "Compliance of Elastic Bodies in Contact," Journal of Applied Mechanics, Trans. ASME, Vol. 71, Sept., 1949, pp. 259-268.

7. Mindlin, R. D. "Mechanics of Granular Media," Proceedings of the Second U. S. National Congress of Applied Mechanics, Ann Arbor, Mich., 1954, pp. 13-20.

8. Whitman, R. V., "Introduction of the Deformation of Particulate Systems," Unpublished Class Notes, November, 1962, pp. 1-19.

9. Miller, Edmond T., "Stresses and Strains in a Planar Array of Elastic Spheres," Massachusetts Institute of Technology, Report No. 19, August, 1963.

10. Bratton, J. L., "A Deformation Hypothesis for Granular Materials Subjected to Rapid Repetitive Loadings," Unpublished Master of Science Thesis, Texas A&M University, January, 1966.

11. Lynch, F. L., "Comparison of the Stress-Strain Relations of a Real Soil with Those of a Simulated Soil Under Triaxial Loading Conditions," Unpublished Master of Science Thesis, Texas A&M University, January, 1966.

12. Deresiewicz, H., "Stress-Strain Relations for a Simple Model of Granular Medium," Office of Naval Research Project Nr-064-388, Technical Report No. 18, April, 1957.

13. Hendron, A. J., Jr., "Behavior of Sand in One-Dimensional Compression," Technical Documentary Report No. RTD-TDR-63-3089, Department of Civil Engineering, University of Illinois, Urbana, Illinois, October, 1963.

14. Manual of Testing Procedures, Vol. I, Texas Highway Department, Undated.

15. Dunlap, W. A., "Deformation Characteristics of Granular Materials Subjected to Rapid Repetitive Loading," Research Report Number 27-4, Texas Transportation Institute, College Station, Texas, 1966.

16. Procedures For Testing Soils, American Society for Testing Materials, 1958.

17. Lambe, W. T., Soil Testing for Engineers, John Wiley and Sons, Inc., New York, 1951.

18. Dunlap, W. A., "A Repetitive Triaxial Loading Apparatus for Large Diameter Specimens of Granular Materials," Research Report Number 27-3, Texas Transportation Institute, College Station, Texas 1965.

19. Armstrong, James C., "A Study of the Effects of Rate and Frequency of Loading on the Stress-Strain Characteristics of Granular Soils," Texas Transportation Institute, College Station, Texas, 1962.

20. O'Brien, Thomas E., "Stress-Strain Characteristics of Soils in the Variable-Confining-Pressure Triaxial Test," Unpublished Master's Thesis, Texas A&M University, College Station, Texas, May, 1963.

21. Reynolds, H. R., Rock Mechanics, Ungar Publishing Co., New York, 1961.

22. Willis, T. F. and De Reus, M. E., "Thermal Volume Change and Modulus of Elasticity of Aggregate and Their Effect on Concrete," Proceedings ASTM, Vol. 39, 1939.

23. Hirsch, T. J., "Effects of the Elastic Moduli of the Cement Paste Matrix and Aggregate on the Modulus of Elasticity of Concrete," Unpublished Doctoral Dissertation, Texas A&M University, College Station, Texas, 1961.

24. Mantell, C. L., Engineering Materials Handbook, McGraw-Hill Book Company, Inc., New York, 1958.

25. Horn, H. M. and Deer, D. V., "Frictional Characteristics of Minerals," Geotechnique, Vol. XII, No. 4, Dec., 1962.

26. Wilson, S. D., and Sibley, E. A., "Ground Displacements Resulting from Air-Blast Loading," Preprint of Paper presented at the American Society of Civil Engineers' Houston Convention, Houston, Texas, February, 1962.

27. Dunalp, W. A., "A Report on a Mathematical Model Describing the Deformation Characteristics of Granular Materials," Research Report 27-1, Texas Transportation Institute, College Station, Texas, 1963.

28. Balmer, G. G., "Physical Properties of some Typcial Foundation Rocks," Concrete Laboratory Report No. SP-39, U.S. Bureau of Reclamation, Denver, Colorado, 1953.

29. Bishop, A. W., "The Principle of Effective Stress," Teknisk Ukeblad, Vol. 106, No. 39, 1959.

30. Bishop, A. W., "Measurement of Pore Pressure in the Triaxial Test," Pore Pressure and Suction of Soils, Butterworths, Inc., Washington D. C., 1961.

31. Casagrande, A. and Shannon, W. L., "Research on Stress-Deformation and Strength Characteristics of Soils and Soft Rocks Under Transient Loading," Graduate School of Engineering, Harvard University, Publication No. 447, June, 1948.

32. Whitman, R. V., and Healy, K. A., "Shearing Strength of Sands During Rapid Loadings," Journal of Soil Mechanics and Foundations Division Proceedings of the American Society of Civil Engineers, Volume 88, No. SM2, April, 1962.

33. Bowden, F. P., and Tabor, D., The Friction and Lubrication of Solids, Oxford University Press, London, 1950.

34. Scott, R. F., Principles of Soil Mechanics, Addison-Wesley Publishing Company, Inc., Massachusetts, 1963.

APPENDIX A

Basis for the Assumption $F_o = 0$

The dense planar array (Figure A.1) is subjected to an increasing vertical pressure and constant lateral pressure. The resultant movement of sphere 4 is vertically downward with relation to sphere 1. The centers of spheres 4 and 2, and 4 and 3 approach each other; simultaneously sphere 4 moves downward with respect to sphere centers 2 and 3. This down and outward forcing motion of 4 causes 2 and 3 to move apart resulting in a zero contact force between them. The assumption $F_o = 0$ is valid as long as these loading conditions occur.

Since the hydrostatic stress state exists initially in triaxial testing, the force relationship at F_o must also be considered (Figure 3.2). As the hydrostatic stress is incremented, 4 moves to the left with respect to 2 and right with respect to 3. Since 2 and 3 are in contact under these loading conditions some distortion on the contact plane does occur and $F_o \neq 0$. Further, sliding develops on the contact face between 4 and 2 and 4 and 3. If F_o is assumed = 0, more tangential force is developed between 4 and 2 and 4 and 3 than can be mobilized; therefore, $-T > FN$ occurs.

Without the restraint provided by F_o, failure would occur and the array collapse. Therefore, it is additionally assumed the excess tangential force is carried by F_o and the distortion in the array is that which would be produced by the forces mobilized on the faces between 4 and 2 and 4 and 3.

No further investigation of the strain between 2 and 3 was attempted. By ignoring the existance of F_o for this analysis, it was tacitly assumed that the relative approach of 2 and 3 due to F_o would equal the horizontal component of the deformation between 4 and 2 and 4 and 3.

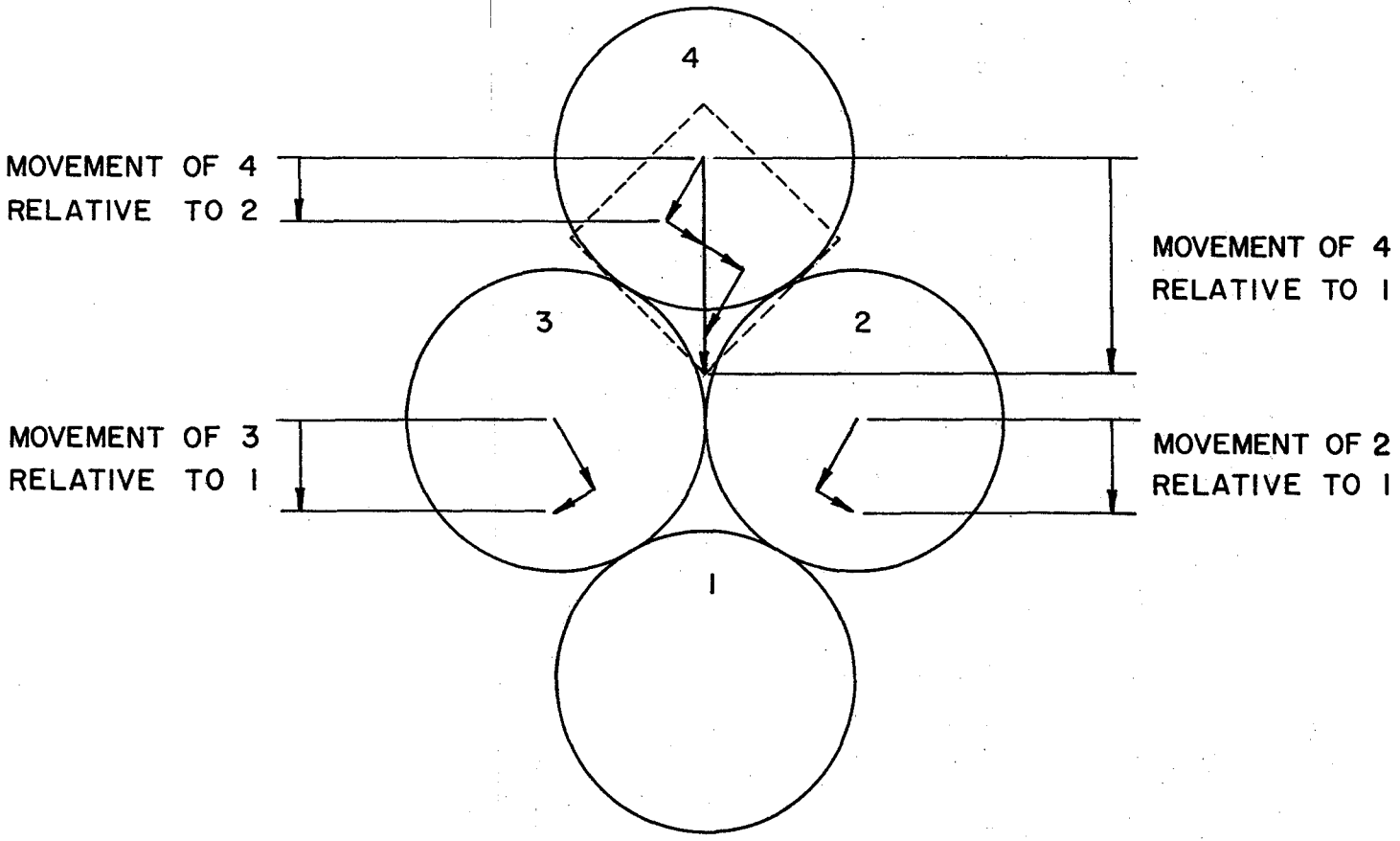

Figure A.1 Deformation in the sphere unit.